SDC-91-161

SDC
SOLENOIDAL DETECTOR NOTES

SDC MUON DETECTOR: OCTAGONAL TUBE OPTION

D. Carlsmith, R. Loveless, D. Reeder
University of Wisconsin

F. Feyzi
Physical Sciences Laboratory

A. Pitas
Pitas Instruments

December 12, 1991

SDC Note SDC-91-161
December 12, 1991

SDC Muon Detector: Octagonal Tube Option

D. Carlsmith, R. Loveless, D. Reeder
University of Wisconsin

F. Feyzi
Physical Sciences Laboratory

A. Pitas
Pitas Instruments

Contents

1 Introduction **5**

1.1 Overview 5

1.2 Design Concept and Goals 5

1.2.1 System Layout 5

1.2.2 Muon Trigger and Resolution 6

1.3 Octagonal Tube Option 7

1.3.1 Tubes 7

1.3.2 Modules 8

1.3.3 Supermodules 9

1.3.4 Production 10

1.3.5 Status of R&D 10

1.3.6 Channel Count and Cost 10

1.4 Comparison with other design options 11

1.5 Figure Captions 12

2 Drift Cell **14**

2.1 Electrostatics 14

2.2 Mechanical Stability 15

2.3 Signal Propagation 15

2.4 Gas Mixture 16

2.5 Gas Tolerances and Monitors 17

2.6 Figure Captions 17

3 Chamber Structure **18**

3.1 Extrusions 18

3.2 Wire, Wire Mount, and Crimp Tube 19

3.3 Endplug Design 19

3.4 Endplate 20

3.5 Prototype wire location achievements 20

3.6 Projectivity 21

3.7 Assembly 21

3.8 Thermal Properties 21

3.9 Figure Captions 22

4 Supermodule Layout and Support Concept **23**

4.1 Layout and Assembly 23

4.2 Barrel Truss Structure 23

4.3 Supermodule Mounting Options 24

4.3.1 Extrusion crush test 25

4.4 Gas Handling System 25

4.5 Electronics 26

4.6 Statistics 26

4.7 Figure Captions 28

5 Manufacturing Concepts **29**

5.1 Overview 29

5.2 Procurement 30

5.2.1 Aluminum extrusions 30

5.2.2 Plastics: endplugs, wire mounts, manifold plugs 30

5.2.3 Endplates 30

5.2.4 Cover plates 31

5.3 Chamber assembly 31

5.4 Chamber Testing 32

5.5 Muon Assembly Building 32

5.6 Schedule 33

Chapter 1

Introduction

1.1 Overview

This report presents the octagonal drift tube option for the SDC barrel and intermediate muon chambers. The use of extruded aluminum drift tubes without field shaping offers the advantages of simplicity, robustness and compactness while meeting the specifications for performance, cost, and schedule. The SDC muon system design goals and the distinguishing features of the drift tube option are described in this introductory chapter. Measurements, calculations, and other details of the ongoing R&D by the Wisconsin group are documented in what follows.

1.2 Design Concept and Goals

1.2.1 System Layout

The SDC central muon system (Figure 1.1 and Figure 1.2) provides:

- preliminary identification of prompt muons by penetration through the calorimeter and barrel toroid
- fast momentum analysis for triggering
- punchthrough rejection by momentum match with tracks in the central tracking device (CTD)
- improved muon momentum resolution at high energy

The number and distribution of wire planes have been selected for simple triggering and reasonably robust pattern recognition. Local clusters of 4 wire planes identify track stubs with ambiguity resolution. Measurements of θ (η) and ϕ as well as minimal stereo for pattern recognition are provided. Two scintillator layers for timing are arranged as projective paddles in the $\eta - \phi$ plane outside the toroid.

Table 1.1: Central Muon Modules

Module	θ	ϕ	Stereo	Scint
BW1	4	4	0	
BW2	4	0	2	1
BW3	4	4	0	1
IW2	4	0	2	1
IW3	4	4	0	1

The BW1 chambers inside the detector are cut back in two octants to allow access from the end of the detector between the forward and barrel toroids for servicing of calorimeter, muon and tracking electronics located between BW1 and the calorimeter. Major services (power, signal cables, gas, cryogenics, etc) are brought through this area and through a large hole in the top octant of the barrel toroid and chamber system. The toroid is supported from the floor and the calorimeter from the toroid of two near continuous legs at the boundaries of the bottom octant.

1.2.2 Muon Trigger and Resolution

A Level 1 trigger with a variable threshold near 20 GeV p_t is based on the toroid bend. The azimuth measurement is connected to CTD segments at Level 2 to confirm the muon identification and, for single muons, to place a higher trigger threshold with more precise momentum information. (The toroid system resolution is at best 16 percent, limited by multiple scattering.) The combination of θ and ϕ measurements serve to improve the CTD momentum measurement for muons above 1 TeV in a complete reconstruction. The inclusive muon trigger threshold is anticipated to between 100 and 200 GeV.

The 1.5 m toroid at 1.8 tesla provides a θ bend of .81 rad/p_t. A 20 GeV P_t muon bends approximately 40 mrad in the toroid. Multiple scattering in the calorimeter and toroid are comparable at $\eta = 0$ and contribute an error of about 10 mrad. The nominal vertex distribution implies a limiting uncertainty of about 6 mrad in the polar angle of a prompt muon exiting the toroid. A Level 1 trigger based solely on the difference between the θ angle from a projective ray as observed outside the toroid requires an angular resolution of approximately 10 mrad. A more robust trigger based on the angle difference between stubs on either side of the toroid is insensitive to the length of the vertex distribution and allows the threshold to be extended. For example, for $p_t = 40$ GeV, the bend is 20 mrad and the multiple scattering in the toroid about 3 mrad. A multiple scattering limited trigger requires about 2 mrad angular resolution.

Ten mrad angular resolution may be achieved locally by two drift cells separated by 15 cm with millimeter spatial resolution. Projective drift cells allow a simple trigger similar to that used in the CDF central muon system - the trigger circuit requires a coincidence of hits within a time window in pairs of projective cells within a module. A digital meantimer circuit can provide a direct angle measurement. Candidate chips are under development in the USA and Japan.

Two staggered pairs are required to reject low energy tracks which fake the signal via the left-right ambiguity. If ϕ cells are also arranged in projective geometry, a similar circuit identifies

track stubs projective in azimuth. A level 1 trigger may be formed as a coincidence of two or more θ trigger and matched with ϕ signals at either Level 1 or Level 2. The scintillator coincidence time identifies the crossing time and enables the transfer of signals from the detector to the surface counting house after the maximum drift time in synchronism with the accelerator.

At Level 2, the muon identification is verified by matching to stiff track segments in the CTD. If sufficient momentum resolution is available from the CTD trigger, the muon tracking system serves only to identify high P_t CTD tracks as muons and a only coarse ϕ resolution of approximately .2 degrees corresponding to the drift cell size is envisioned. In high luminosity operation, it is possible that only the outer two superlayers of the CTD are available. A high threshold trigger may be formed by combining the beam constraint, CTD stub and the ϕ location of the muon as observed in the muon system. The muon track must be known to approximately 1 mm in the ϕ system to implement a transverse momentum cut of 150 GeV.

The CTD momentum resolution is nominally 25 percent at 1 TeV. A resolution of about 250 micron per wire in the muon θ system allows comparable momentum resolution at 1 TeV if not limited by alignment. Below 1 TeV, the CTD provides superior resolution. Above 1 TeV, the independent measurement offers the potential of a factor of $\sqrt{2}$ improvement in the overall momentum determination. For momenta in excess of 1 TeV where multiple scattering is relatively unimportant, the combination of the muon ϕ measurements with the CTD can improve the solenoidal momentum. In a combined fit of CTD and muon measurements, an overall improvement of between 1.6 and 2.5 may be obtained at 2 TeV for muon wire resolutions between 350 and 1400 microns. In a scenario of high luminosity operation with more limited CTD capability, the muon system spatial resolution and alignment become more important in the performance of the SDC in measuring the momenta of TeV energy muons.

1.3 Octagonal Tube Option

1.3.1 Tubes

The octagonal tube option uses simple aluminum drift tubes as a uniform technology for all measurements. The design concept is illustrated in Figures 1.3-1.15 and features:

- simple drift tube with angle independent response
- projective geometry for simple triggering
- compact modular construction
- no wire supports or internal alignment mechanisms
- single high voltage, no field shaping elements
- precision endplates for wire location
- mechanical strength and robust operation
- nonflammable, nontoxic materials
- minimal dead area

Table 1.2: Drift Tube Option Parameters

Drift Length	36 mm
Wire	140 micron Au-W
Gas	Ar(90)/CO_2(5)/Methane(5)
Max Drift Time	1 μsec
Voltage	4000
Gain	$\sim 5 \times 10^5$

- uniform technology

The extrusions are made from 6063-T6 aluminum with two octagon-shaped profiles as shown in Figure 1.3. Thus each extrusion provides two wire cells. The inside width of each octagon is 71.8 mm x 70.9 mm, the wall thickness is 1.8 mm, and the total width of the extrusion is 149 mm. The octagon shape is an approximation to a circle which allows (1) a flat area for gluing to the adjacent extrusions to develop shear strength, and (2) locations for M5 screw bosses (outside the gas seal) so the extrusions can be firmly attached to endplates which locate the wires. The size represents a compromise - a smaller tube with shorter drift time and requires less radial space but an increased channel count.

The tubes operate at about +4000 Volts in proportional mode with a 140 micron diameter gold plated tungsten wire in a nonflammable gas mixture of $Ar(90)/CO_2(5)/Methane(5)$. The drift velocity is saturated over much of the cell volume. A uniform drift velocity may be assumed at the trigger level without significant degradation of the trigger performance. More precise time-to-distance calibration may be used offline. The maximum drift time is 1 microsecond, meeting the present requirements on the trigger pipeline length.

Electrostatic stability permits unsupported wire lengths sufficient to span an octant in the outermost layer. The wires are located solely from precision drilled endplates. The gravitational sag of the wire ($\leq$ 1.5 mm) does not substantially affect a local trigger or tube gain and may be corrected for offline. Complications and costs associated with providing and locating internal wire supports are thereby avoided. The cell response is also insensitive to extrusion and assembly tolerances in the location of the cell walls relative to the wires.

1.3.2 Modules

Extrusions stacked and glued together to form a half cell staggered, 4 layer, close packed rigid modules of dimensions up to about 9 m by 2.5 m containing about 120 wire cells. The assembly is illustrated in Figure 1.4 for the sealed tube option. Local projectivity is maintained by very small gaps between tubes which increase in size with depth into the module. Projectivity between wire clusters is not necessary in our trigger design. Chamber modules constructed in this fashion comfortably nest in monlithic layers so essentially no deadspace is associated with module boundaries along the tube direction. As illustrated in Figure 1.5 and Figure 1.9, gaps at appear at supermodule boundaries and at octant boundaries and may be further reduced by the introduction of single cell extrusions (not shown). Deadspace at the θ tube ends is minimized by a

stairstep endplate. As illustrated by the geometry details shown in Figures 1.16-1.18, at the ends of the barrel, more than four track measurements are typically made within a module.

Modules for θ and ϕ and small angle stereo measurements are of similar construction. For the intermediate region, θ modules are arranged as in the forward small drift tube system (Figure 1.11 and Figure 1.12). The simplest choice for orthogonal measurements in the intermediate region employs modules which are radial only at the center of the octant and at other azimuths only approximately radial (Figure 1.13). Radial tubes providing a true ϕ measurement arranged like the spokes of a bicycle wheel require additional thickness in the beam direction. We have not fully engineered either design nor attempted to determine the additional trigger complexity entailed by the nonprojective option.

We are pursuing two endplate options. In the baseline option shown in Figure 1.4, each extrusion is gas sealed with a plastic endcap. The wires are held by crimp tubes in wire mounts glued in the endcap. Wire locations are registered to precision holes in the endplates by locator plugs during module assembly and gas flow is accomplished through low tolerance holes in the endplate. This scheme in which each tube is fully assembled and tested prior to module assembly may have quality assurance advantages. We have demonstrated in prototypes wires may be precisely positioned with this endplug assembly.

The second option provides a more direct wire location method and may have advantages in assembly time. In this scheme, an endplug is glued into the tube to enforce a gas seal against the internal surface. The endplug bears an O-ring to seal against the endplate. Wires are supported in small diameter plastic wire mounts inserted directly into the endplate and strung after assembly of the cell wall structure. The robustness of the O-ring gas seal to tube length tolerances is under investigation. In both schemes, the tubes are attached rigidly to the endplate by screws passing through the endplate into 120 degree bosses in the extrusion. For the O-ring design, we can contemplate an extruded stairstep endplate which functions as a gas manifold, further simplifying the module.

1.3.3 Supermodules

A supermodule is a collection of chamber modules spanning an octant in azimuth and up to about 7.4 meters along the beam direction. Four supermodules make up the instrumentation for one octant along the barrel. The supermodule boundaries are nonprojective and coincide so that the relative alignment may be determined via wormholes through the barrel toroid. Supermodules are inserted from the end of the barrel onto two rails which run the length of each octant.

Space is at a premium inside the toroid and we propose to construct BW1 supermodules as a deck containing one monolithic layer (monolith)of several ϕ modules sandwiched between monoliths of θ modules. Monoliths may be bonded together by a variety of techniques. We have considered gluing and also a mechanical pinning arrangement illustrated in Figures 1.14 and 1.15. Registration of endplates is accomplished with a jig as illustrated in Figure 1.16. Our design requires of about 65 cm of radial thickness, minimizing the cost of the barrel toroid and outside chambers. The gravitational sag of a module simply supported at the ends is of order 2 millimeter. Much smaller sags are possible by supporting at the 20 percent points. The effect of less direct connection between the supermodule supports and the endplates which locate the wires is under study.

The outer barrel muon system is constructed from four supermodules which contain BW2

and BW3 modules as well as the two scintillator planes within a truss structure. The truss structure may be quite open and provides access to the photomultiplier tubes as well as space for power, gas and signal distribution and electronics crates. As of this writing, the configuration of the support structure for the intermediate region is not fixed. One option allows access for personnel and services between the intermediate and barrel regions and requires a support structure independent of the barrel. A second option under consideration is to provide this access between the intermediate and forward regions and to support intermediate modules and scintillators from the barrel toroid. As the lever arm is large, this option appears to requires the intermediate supermodules to be tied to the outboard barrel supermodules to form L shaped supermodules which wrap around the end. There are also cost advantages to locating the ϕ layers in BW2. In Figures 1.5, 1.11, 1.12 and 1.13, we have arbitrarily left the barrel ϕ cells in BW3 and shown the intermediate ϕ cells in IW2 leaving a ϕ gap. The precise layout requires further simulation of the pattern recognition capability differences between the several options. The layout of a barrel supertower is shown in Figure 1.17.

1.3.4 Production

Our baseline production model is predicated on distributed module production and centralized supermodule assembly in the muon surface facility. For the sealed tube design, distributed tube production and central module and supermodule may be contemplated. The baseline model is expected to take best advantage of existing university personnel and infrastructure and to dovetail with the surface facility construction and detector installation schedule.

1.3.5 Status of R&D

Octagonal extrusions have been obtained from industry. Several 1 meter length modules containing 16 cells and one 9 meter 32 cell module have been constructed.

1.3.6 Channel Count and Cost

A summary of estimated wire counts appears in Table 1.3. There are about 61,300 wires in the barrel region and 11,600 in the intermediate. The electronics channel count remains to be specified. Aside from the possibility of connecting ϕ wires along the barrel, it is possible to logic OR these signals or signals from adjacent octants. The addition of further electronics for higher luminosity operation could be implemented as an upgrade. The total BW1 particle rate at $L = 10^3 3$ is estimated to be 100 kHz corresponding to a 50 Hz rate per tube.

The cost the chamber production has been estimated from vender quotes where available and estimates of assembly time. Updated numbers reflect our experience in constructing a full length prototype partial module. The results are summarized in a work breakdown structure spreadsheet by Martin Marietta for purposes of comparison of chamber technologies. For details, the reader is referred to their report.

Table 1.3: Estimated Cell Counts

Module	θ	ϕ	Stereo
BW1	8176	7176	0
BW2	11840	0	0
BW3	12672	14848	6656
IW2	1728	4736	0
IW3	5120	0	0

1.4 Comparison with other design options

The octagonal tube option is perhaps the simplest and least inovative of designs presently under consideration. Other designs include

- 1) Round 3 inch tubes without field shaping (Washington)
- 2) Round 3 inch tubes with single electrode shaping (Washington)
- 3) Oval 16 cm drift tubes with multielectrode shaping (Boston)
- 4) Projective jet cell chambers (KEK)

The octagonal tube option is most similar to option 1 in which single cylindrical tubes are glued to patchwork sheets in a projective layered structure to form modules or entire monoliths. A cylindrical tube without field shaping measures the impact parameter of a track relative to the wire - no special arrangements must be made to orient field shaping elements to be nearly perpendicular to projective tracks, an important concern for θ measurements near the end of the barrel. The attainable spatial resolution as determined from the arrival of the first few drifting electrons is in principle as good as might be obtained in a field shaped cell. We feel the octagonal shape has advantages in assembly and rigidity and lends itself to nesting modular construction.

The no field shaping option is expected to have limited multihit capability relative to field shaped options. However, simulations of pattern recognition by Y. Asano suggest that the effective resolution of the toroid system as a function momentum is unaffected by two hit resolution - events are either sufficiently simple that the pattern recognition succeeds, or so complex that it fails no matter what. The hit rates in the barrel are also so low that deadtime is no an issue. Field shaping allows a relatively constant drift field for linear response but the trigger does not appear to require good linearity. There may be some advantage in handling systematic drift velocity variations with pressure and temperature but the gas parameters must be highly constrained in any event to ensure proper amplification.

While it is possible to insert field shaping elements within octagonal drift tubes, we have concentrated on the no field shaping option to minimize piece count and assembly time, simplify high voltage distribution, and avoid potential thermal incompatibility and tolerance issues. The second round tube option includes a simple continuous electrode on either side of the wire within

a round tube. The round shape allows the electrode support to be incorporated into the extrusion shaping and the individual tubes to be oriented.

Field shaping may be used to extend the drift length for reduced channel count. A larger version of the round tube option 2 could be contemplated but would be bulky. The oval tube option addresses this issue through the use of oriented near rectagular cells arranged more compactly in a loose geometry. For this, one pays the price of internal wire supports for electrostatic stability and individual tube supports (wineracks) since single tubes are not self supporting. The design requires an additional support and alignment system for each module. A CF_4 based "fast" gas mix is probably required for operation with long drift lengths.

Lower mass is obtained in the jet cell option which incorporates thin plate and wire electrodes to form many cells within in a single gas enclosure. Each cell includes 3 or 4 slightly staggered wires sampling the ionization signal of a track. This kind of design has been used in many colliding beam and fixed target high resolution tracking devices and may offer superior pattern recognition over tube designs since multiple scattering of soft particles internal to a module is reduced. Fine sampling in a compact cell requires wire supports and internal alignment monitoring and compensation (?) mechanisms.

1.5 Figure Captions

Figure 1.1 Elevation view of one quarter of the SDC showing the location of the BW1, BW2, BW3 and intermediate chamber modules.

Figure 1.2 Section of the SDC.

Figure 1.3 Section of the octagonal extrusion.

Figure 1.4 Illustration of module assembly for the sealed tube option showing endplugs, precision endplates, and gas distribution.

Figure 1.5 Elevation view of octagonal tube option. There are four supermodules along the barrel in each octant. Circles indicate locations of details.

Figure 1.6 Detail A of Figure 1.5.

Figure 1.7 Detail B of Figure 1.5.

Figure 1.8 Detail C of Figure 1.5.

Figure 1.9 Section of barrel octant for octagonal tube option. Location of detail is indicated by circle.

Figure 1.10 Detail of Figure 1.9

Figure 1.11 Layout of IW3 θ chambers.

Figure 1.12 Layout of IW2 θ chambers.

Figure 1.13 Layout of IW2 ϕ chambers.

Figure 1.14 Illustration of stringer option for BW1 monolith and supermodule assembly.

Figure 1.15 Illustration of stringer option for BW3 monolith and supermodule assembly.

Figure 1.16 Supermodule assembly jig.

Figure 1.17 Supertower layout.

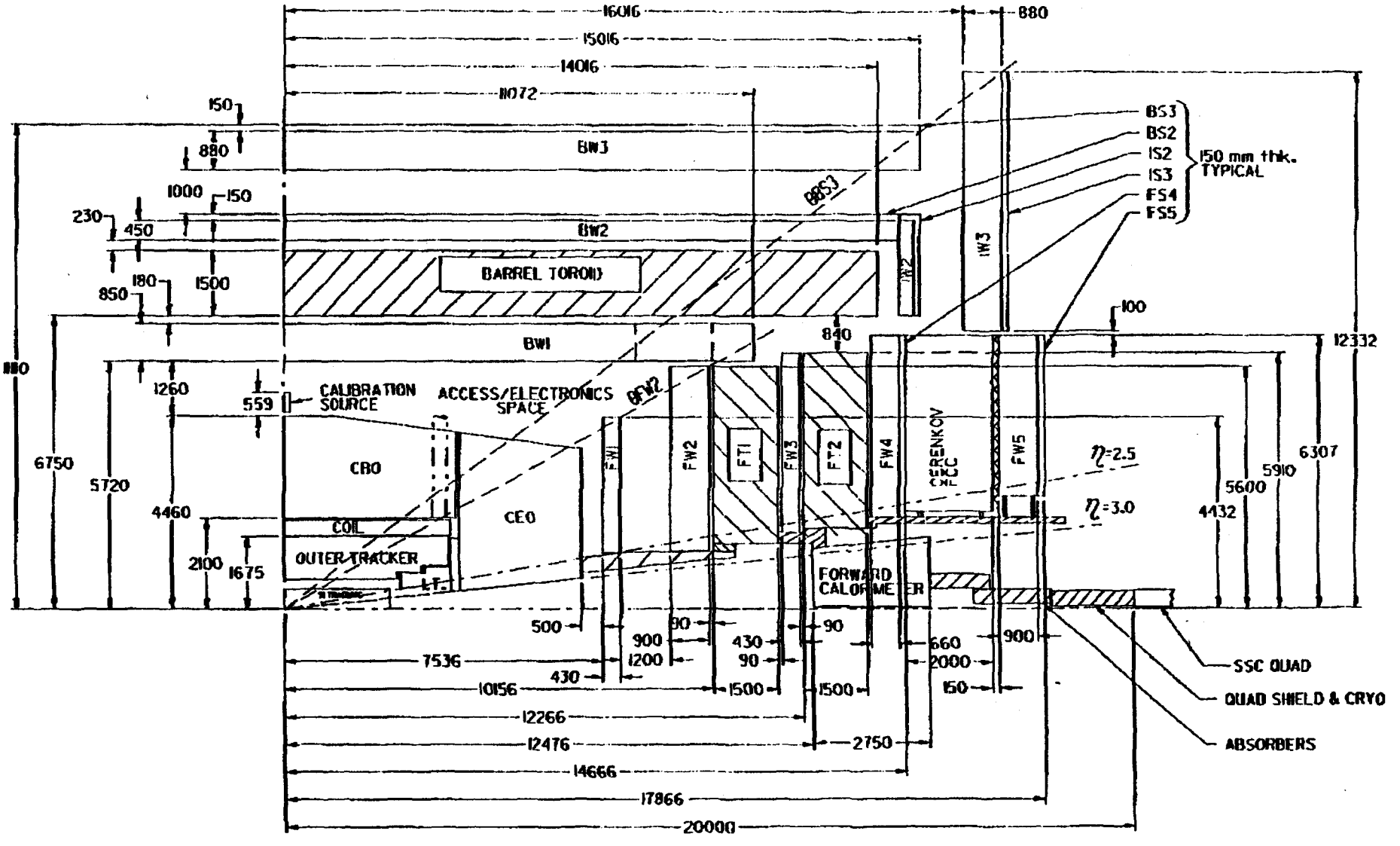

SDC DETECTOR
TECHNICAL PROPOSAL DIMENSIONS

SSC DRAWING sdd000081 11-25-91

0 1 2 4 5M

NOTE: DIMENSIONS ARE IN MILLIMETERS

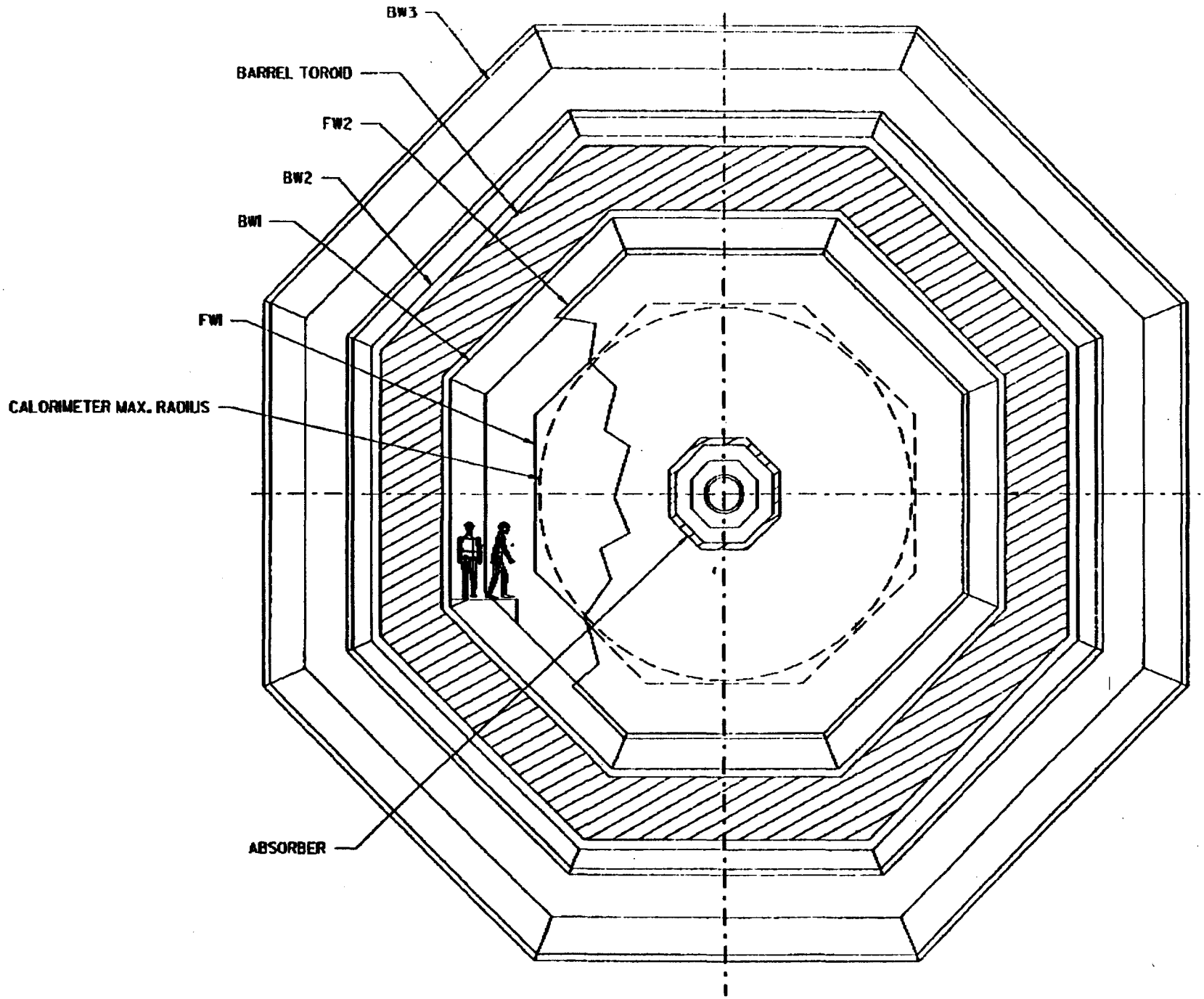

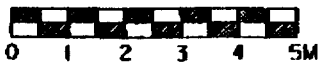

SECTION THRU FW2

SSC DRAWING *sdd000081 11-25-91

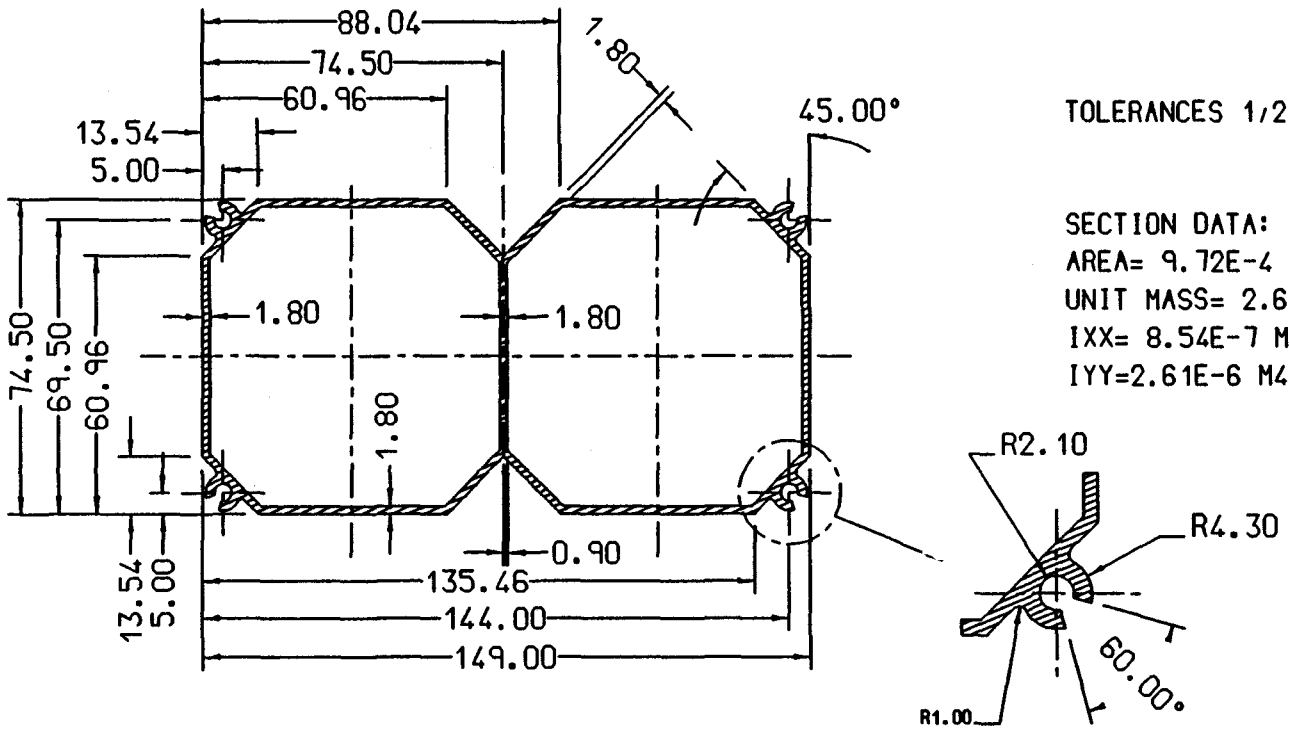

TOLERANCES 1/2 ALUM ASSOC STANDARD

SECTION DATA:
AREA= 9.72E-4 M2
UNIT MASS= 2.625 KG/M (1.764 LB/FT)
IXX= 8.54E-7 M4
IYY=2.61E-6 M4

ALL DIMENSIONS IN MILLIMETERS

SCREW BOSS FOR M5X0.8 THREAD
2X SCALE

KEY	Q'TY	PART NO.	DESCRIPTION

DR. FF
MAT'L 6063-T6 ALUMINUM
CHK'D
SDC MUON SYSTEM DEVELOPMENT
APPR'D
MUON CHAMBER PROTOTYPE
NO. REQ.
DOUBLE CELL EXTRUSION PROTOTYPE

UNITS ARE INCHES UNLESS OTHERWISE SPECIFIED. ANSI STANDARD Y14.5 APPLIES.

SURFACE FINISH EXCEPT AS NOTED:

TOLERANCES UNLESS OTHERWISE SPECIFIED:
3 PLACE DECIMAL
2 PLACE DECIMAL
1 PLACE DEC., FRAC.

CHANGE LETTER	CHKD. BY	DWN BY	DATE	CHANGE

PHYSICAL SCIENCES LABORATORY
UNIVERSITY OF WISCONSIN (608)873-6851

SCALE FULL
DATE 5/14/91
USED ON
DWG. NO. 4626B022

DRAWN BY PHYSC BOSS CAD V3.2060

PRODUCED BY FF
11/22/91 AT 17:10

DRAWING FILENAME R4626022B
PLOTTED AT SCALE 1/1

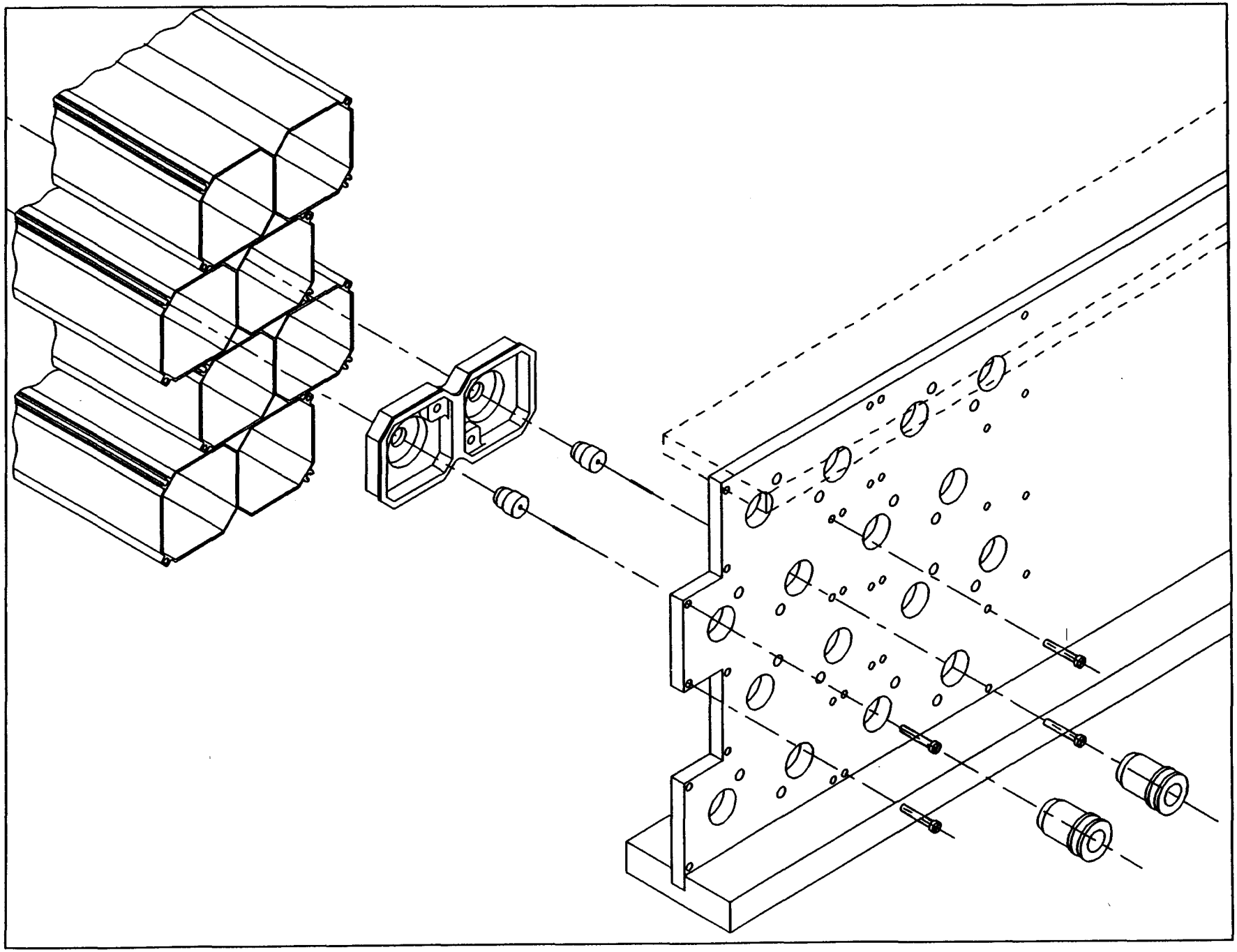

PRODUCED BY FF
ON 12 / 12 / 91 AT 11 : 59

DRAWING FILENAME SAT002B
PLOTTED AT SCALE 1/1

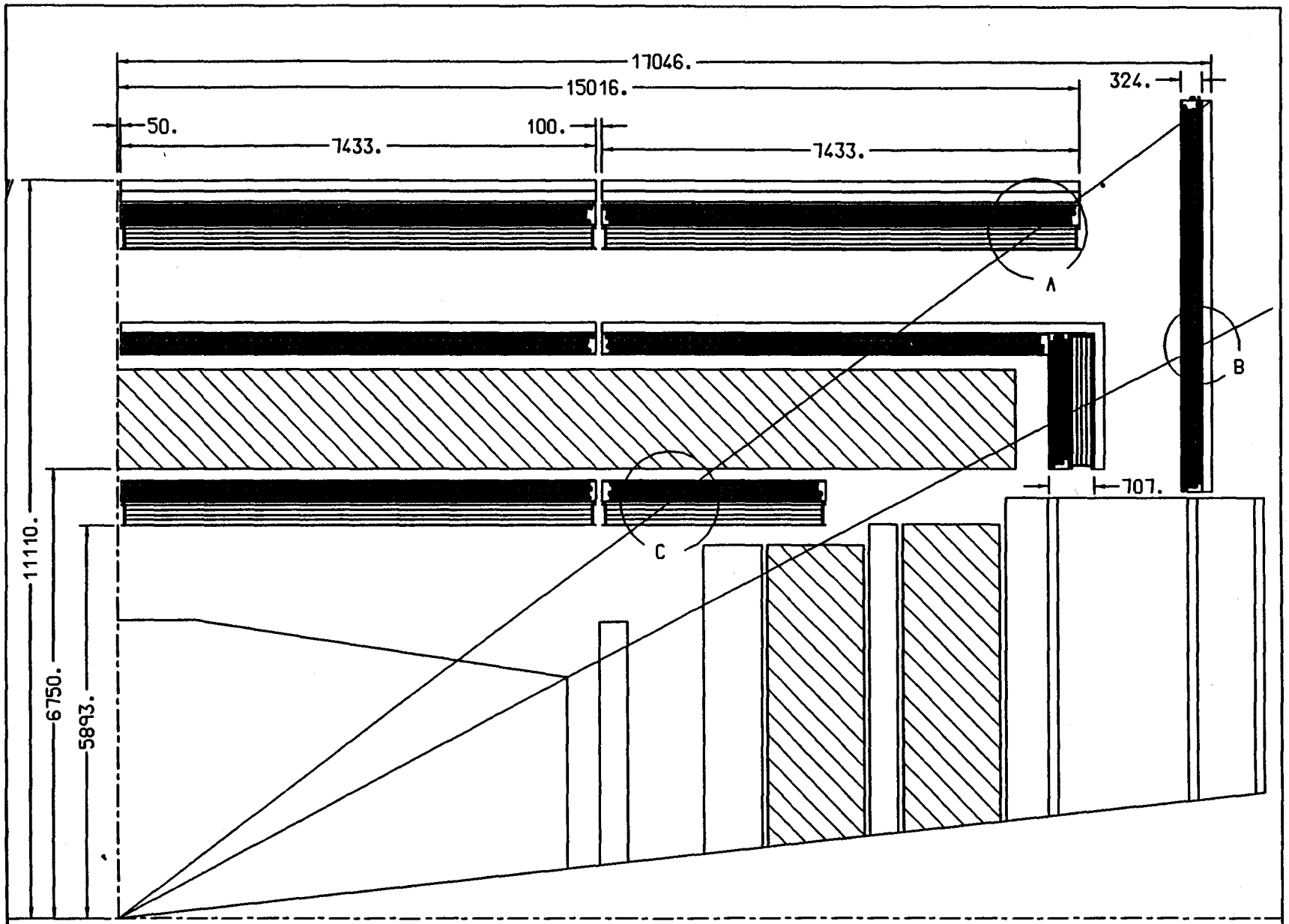

DERIVED FROM SSC DWG# SDD000081

PRODUCED BY FF
12 / 10 / 91 AT 09 : 37

DRAWING FILENAME Z051E
PLOTTED AT SCALE 1/1

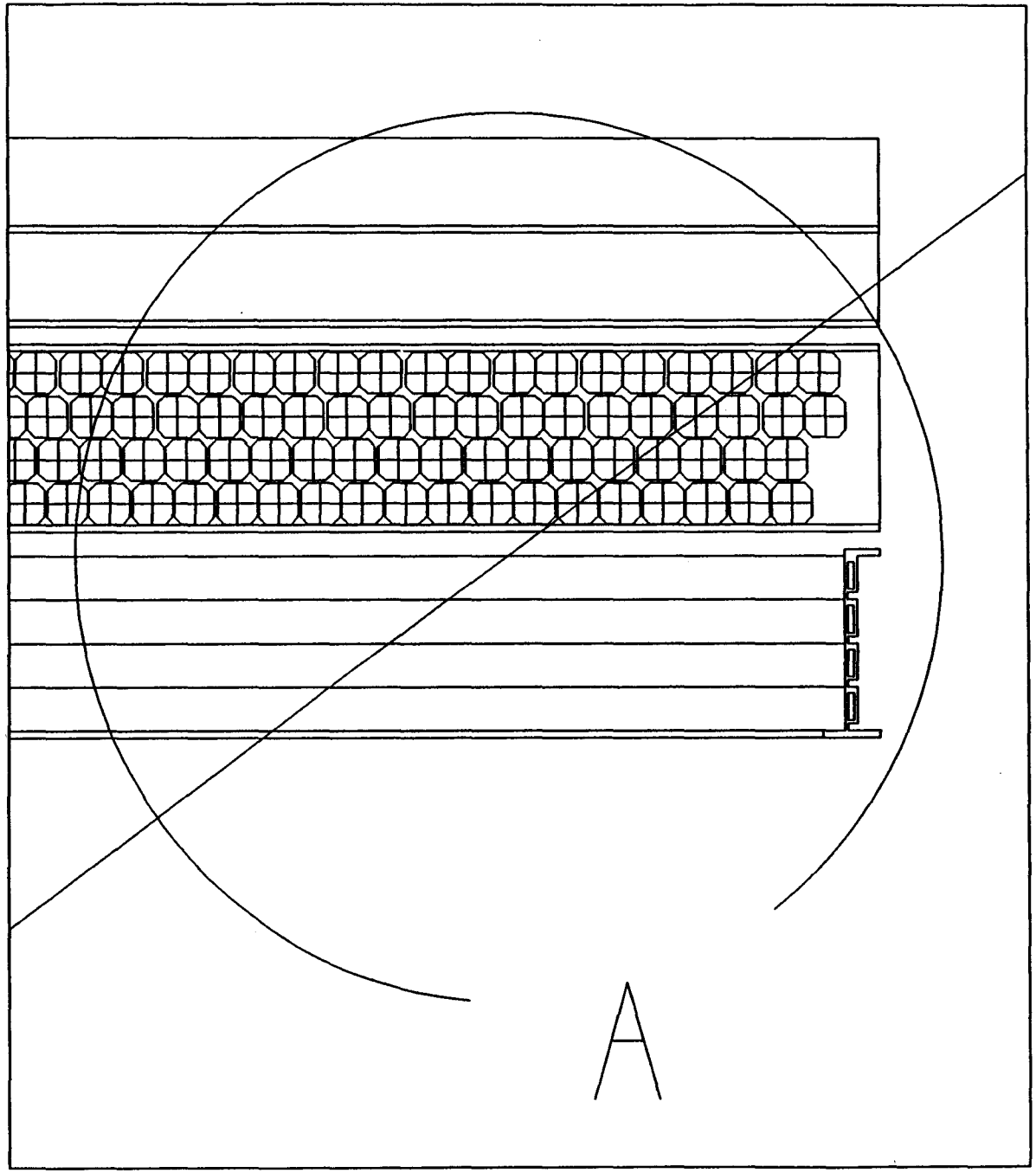

PRODUCED BY FF
ON 12 / 10 / 91 AT 09 : 39

DRAWING FILENAME Z051E
PLOTTED AT SCALE 5/1

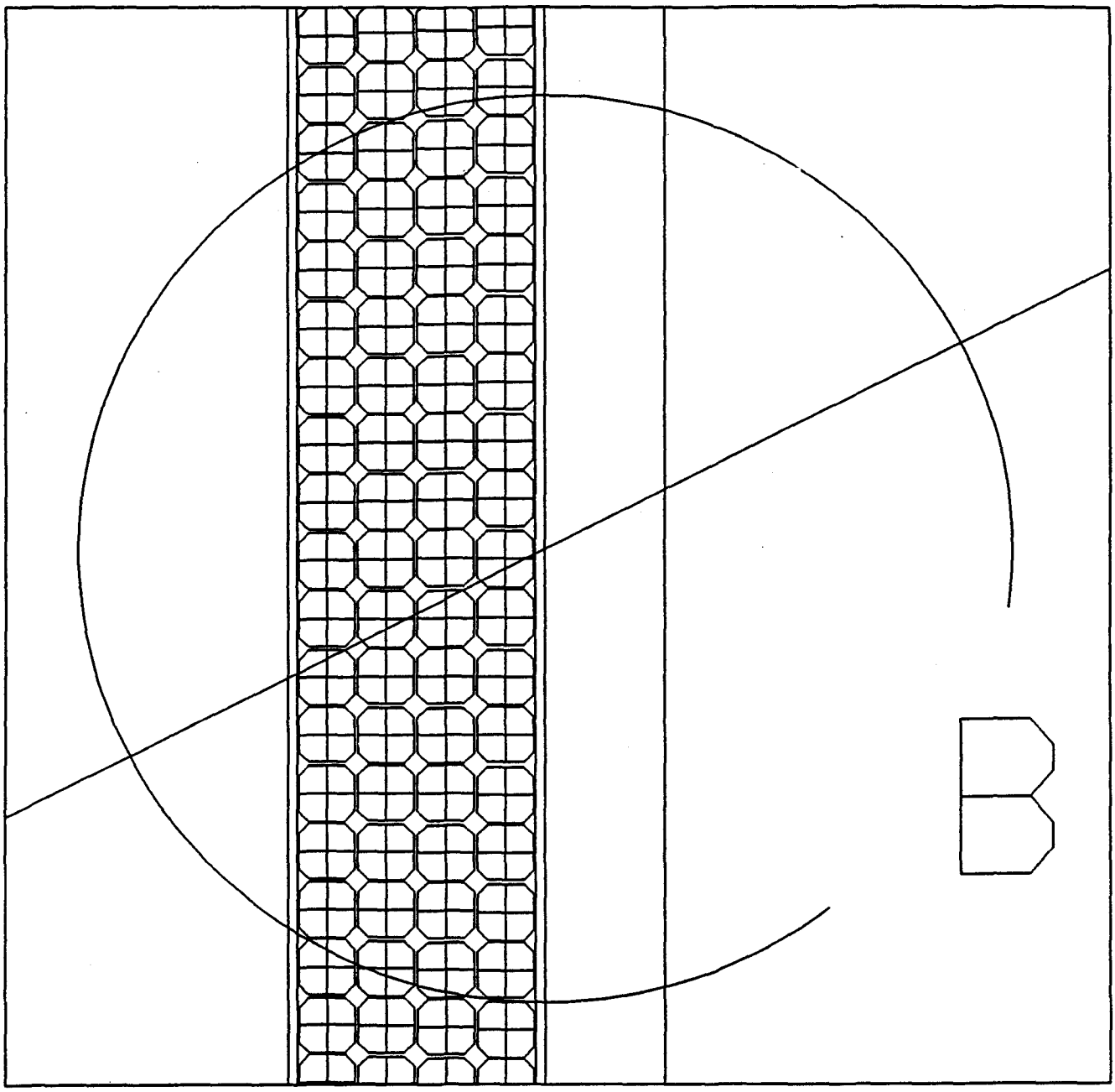

PRODUCED BY FF
ON 12 / 10 / 91 AT 09 : 40

DRAWING FILENAME Z051E
PLOTTED AT SCALE 5/1

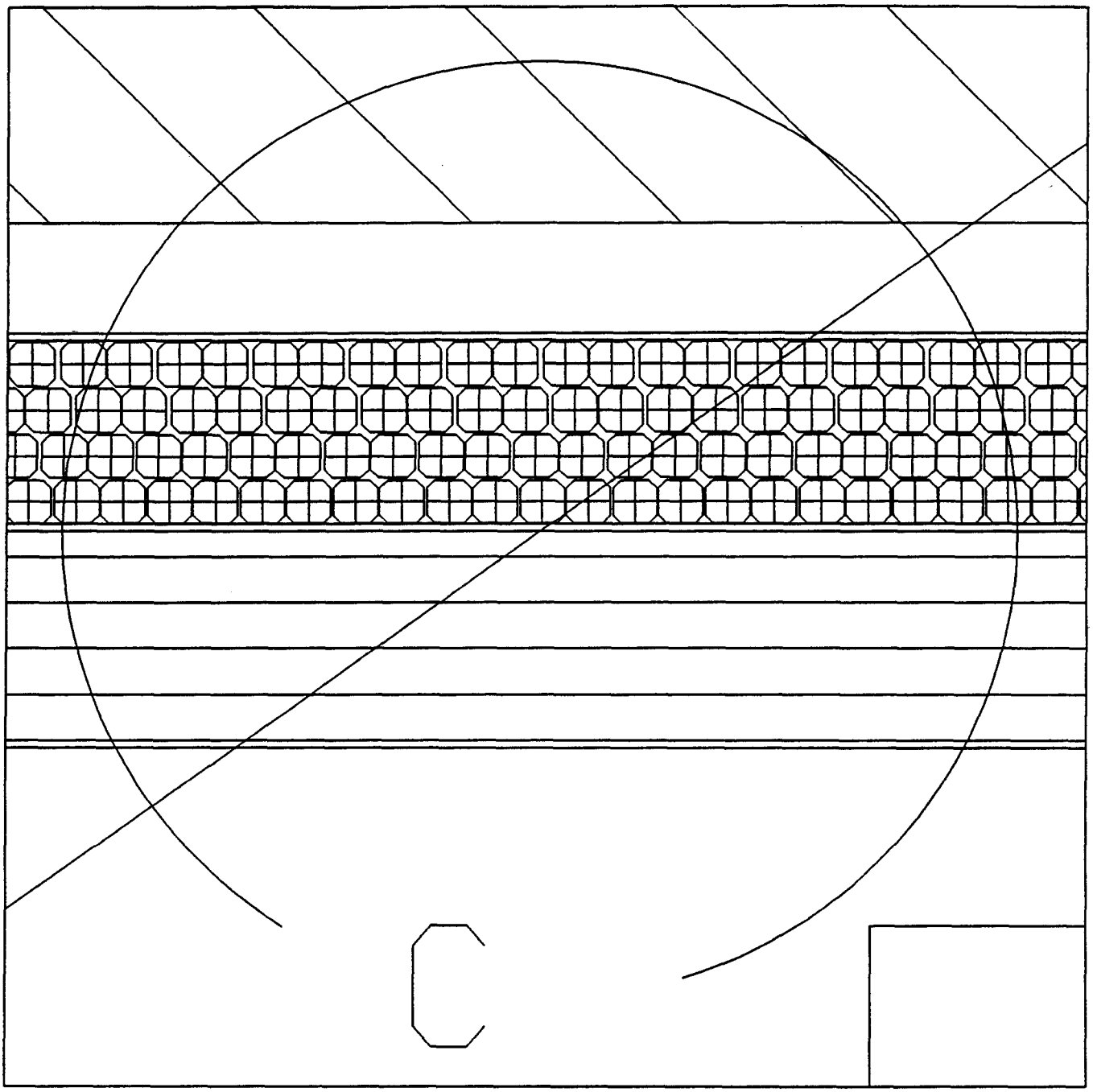

PRODUCED BY FF DRAWING FILENAME Z051E
ON 12 / 10 / 91 AT 09 : 41 PLOTTED AT SCALE 5/1

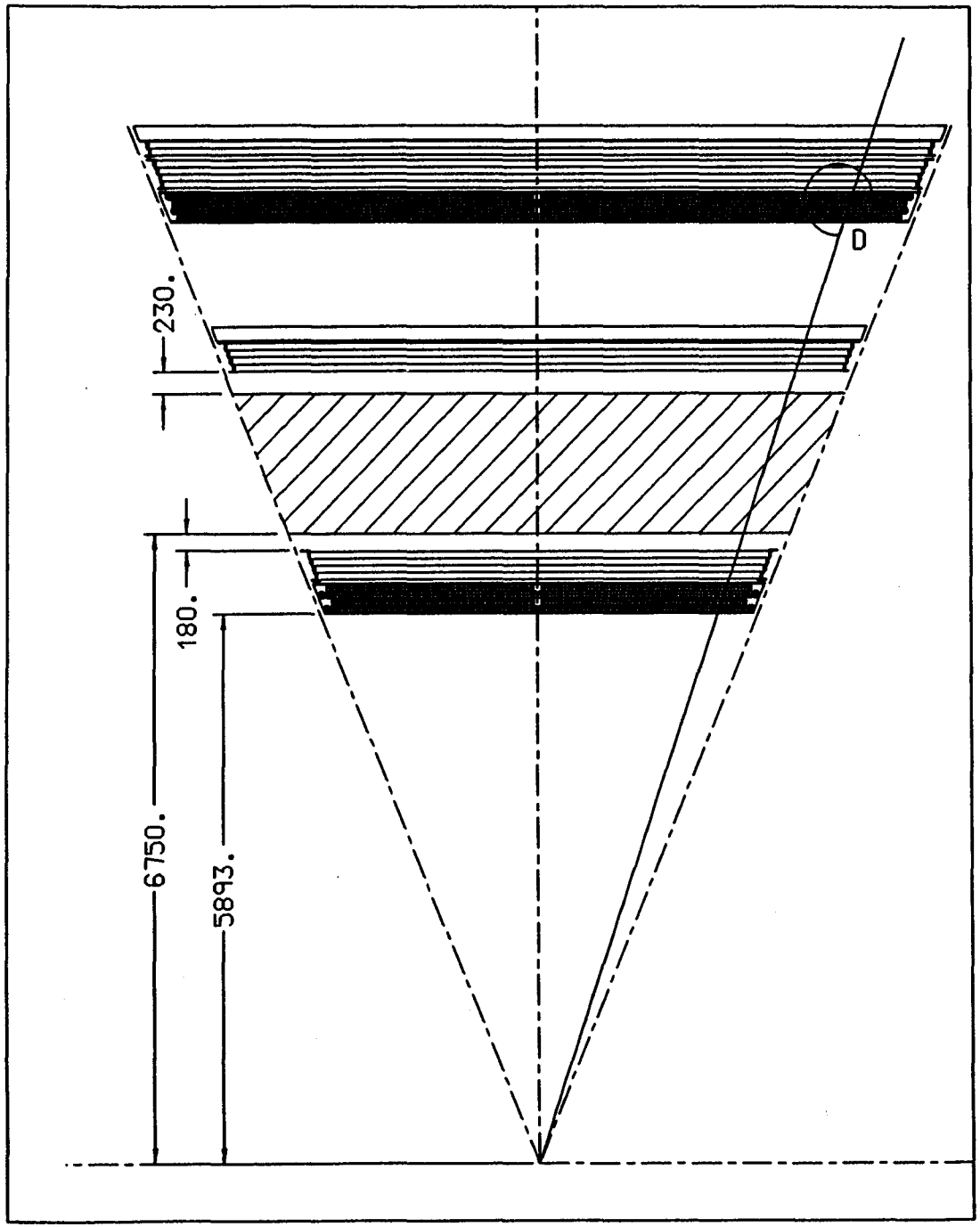

PRODUCED BY FF
12 / 10 / 91 AT 09 : 49

DRAWING FILENAME Z051E
PLOTTED AT SCALE 1/1

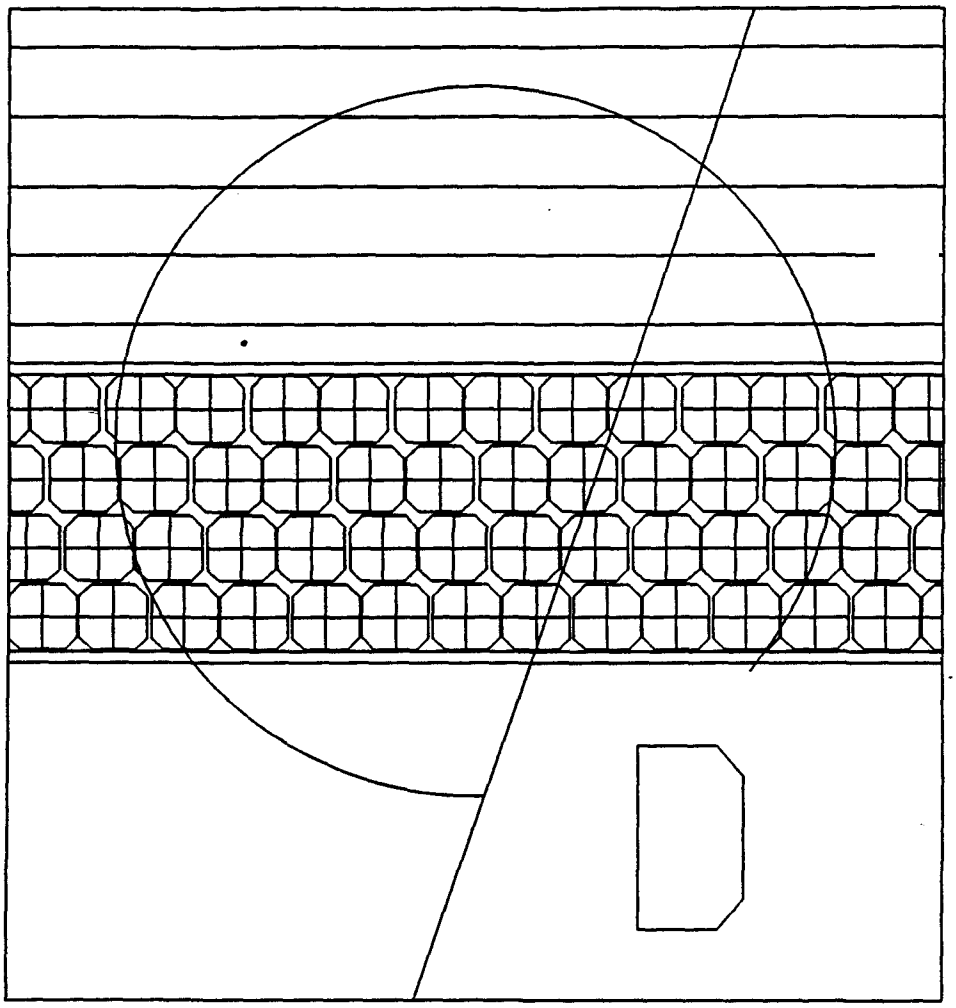

PRODUCED BY FF DRAWING FILENAME Z051E
ON 12 / 10 / 91 AT 09 : 50 PLOTTED AT SCALE 5/1

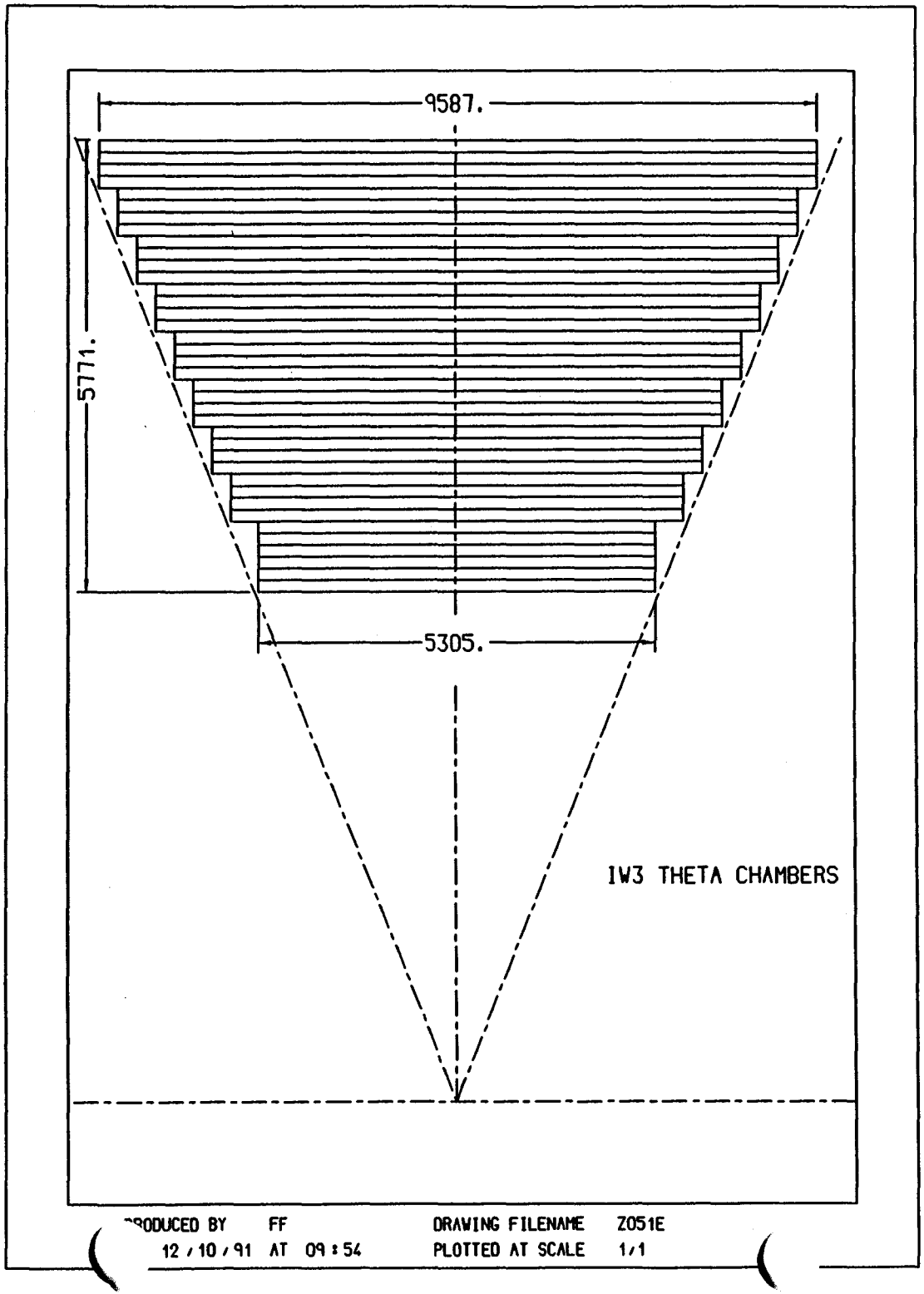
9587.
5771.
5305.
IW3 THETA CHAMBERS
PRODUCED BY FF
12 / 10 / 91 AT 09 : 54
DRAWING FILENAME Z051E
PLOTTED AT SCALE 1/1

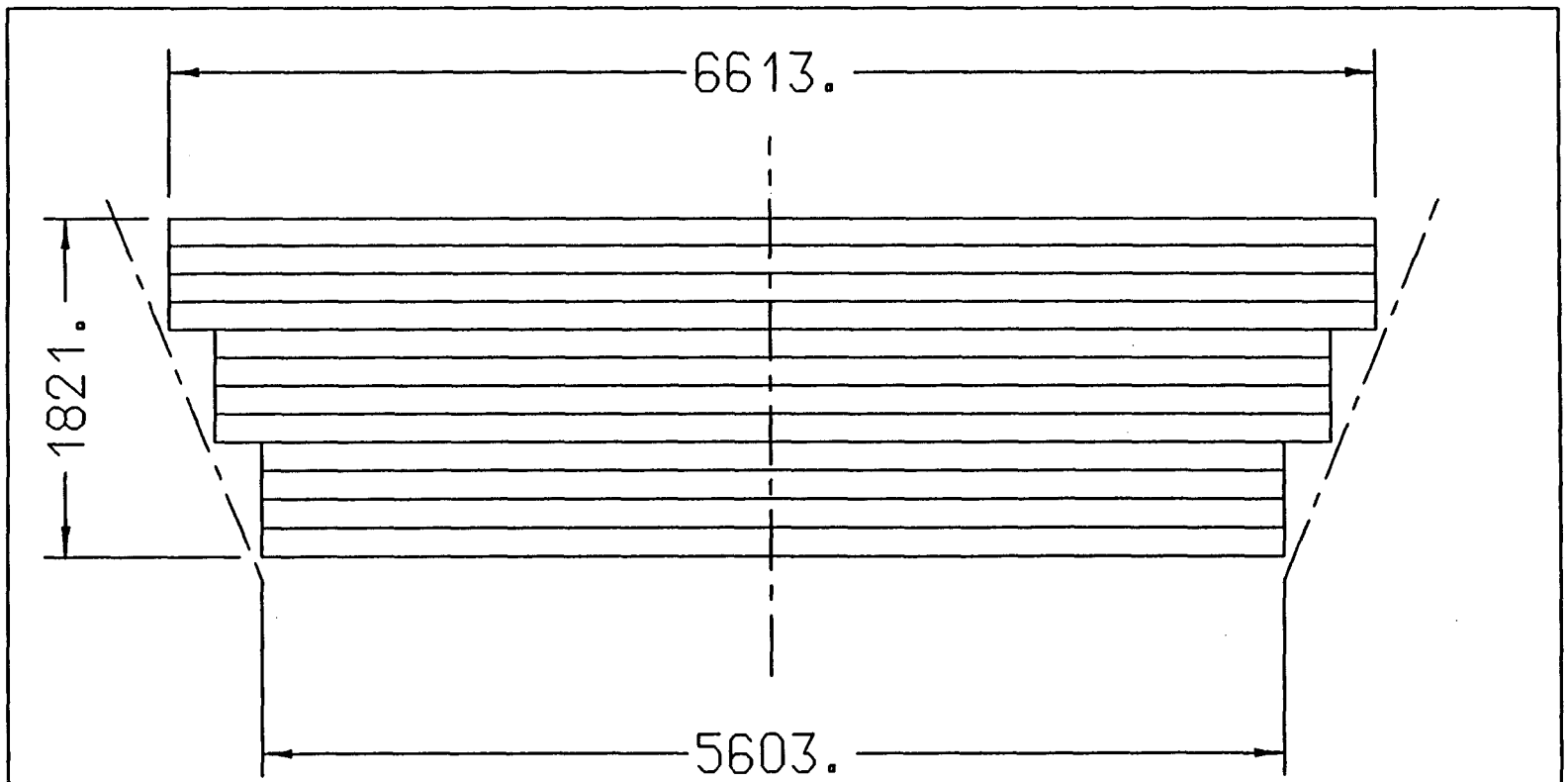

IW2 THETA CHAMBERS

PRODUCED BY FF
ON 12 / 10 / 91 AT 09 : 56

DRAWING FILENAME Z051E
PLOTTED AT SCALE 1/1

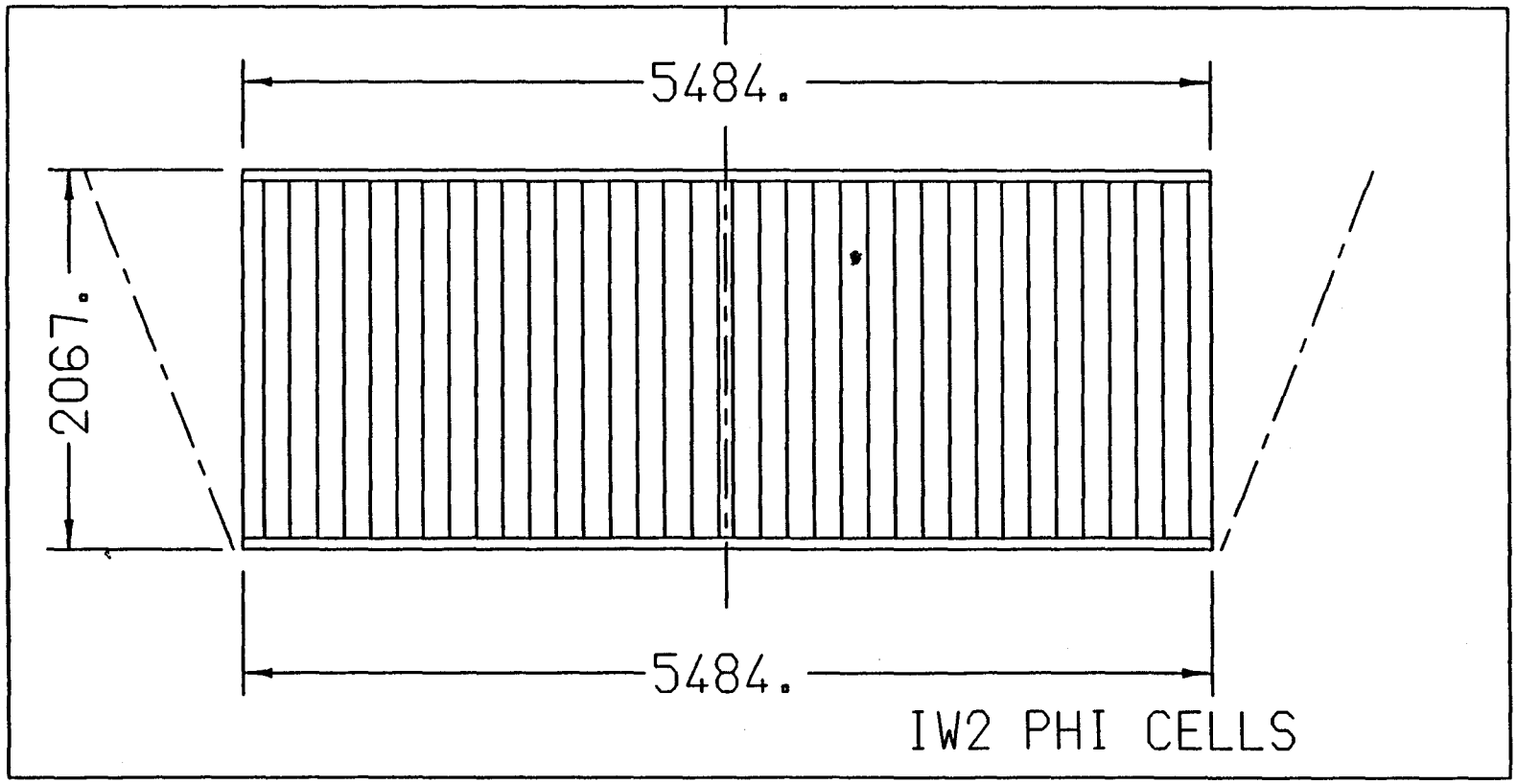

PRODUCED BY FF DRAWING FILENAME Z051E
12 / 10 / 91 AT 09 : 57 PLOTTED AT SCALE 1/1

MODULES MANUFACTURED AT DISTRIBUTED FACILITIES

ASSEMBLED AT SSCL

SUPERMODULE TO BE ASSEBLED ONTO TRUSS

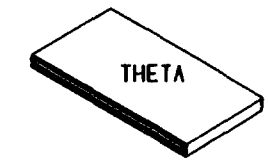

48 UNITS

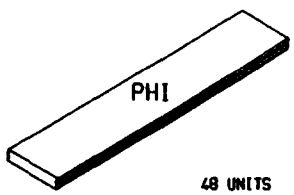

48 UNITS

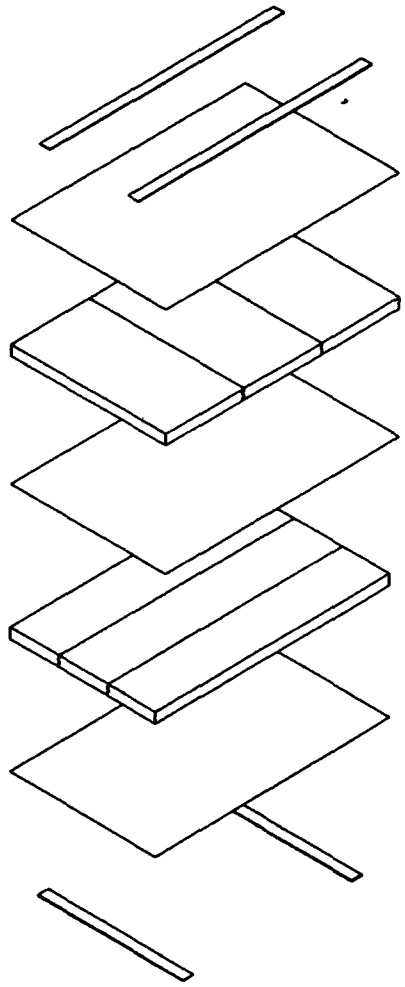

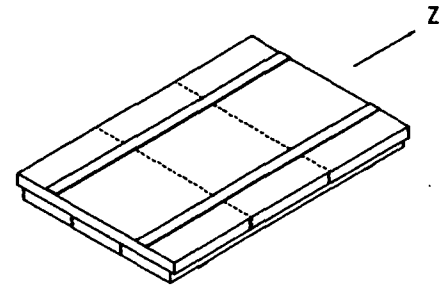

16 UNITS

5.44M X 7.51M X 0.7 M

6,600 KG

BW1 SUPERMODULE ASSEMBLY LAYOUT

PHYSICAL SCIENCES LABORATORY

PRODUCED BY GP_JDP DRAWING FILENAME SAT005E

ON 12 / 11 / 91 AT 09 : 59 PLOTTED AT SCALE 1/1

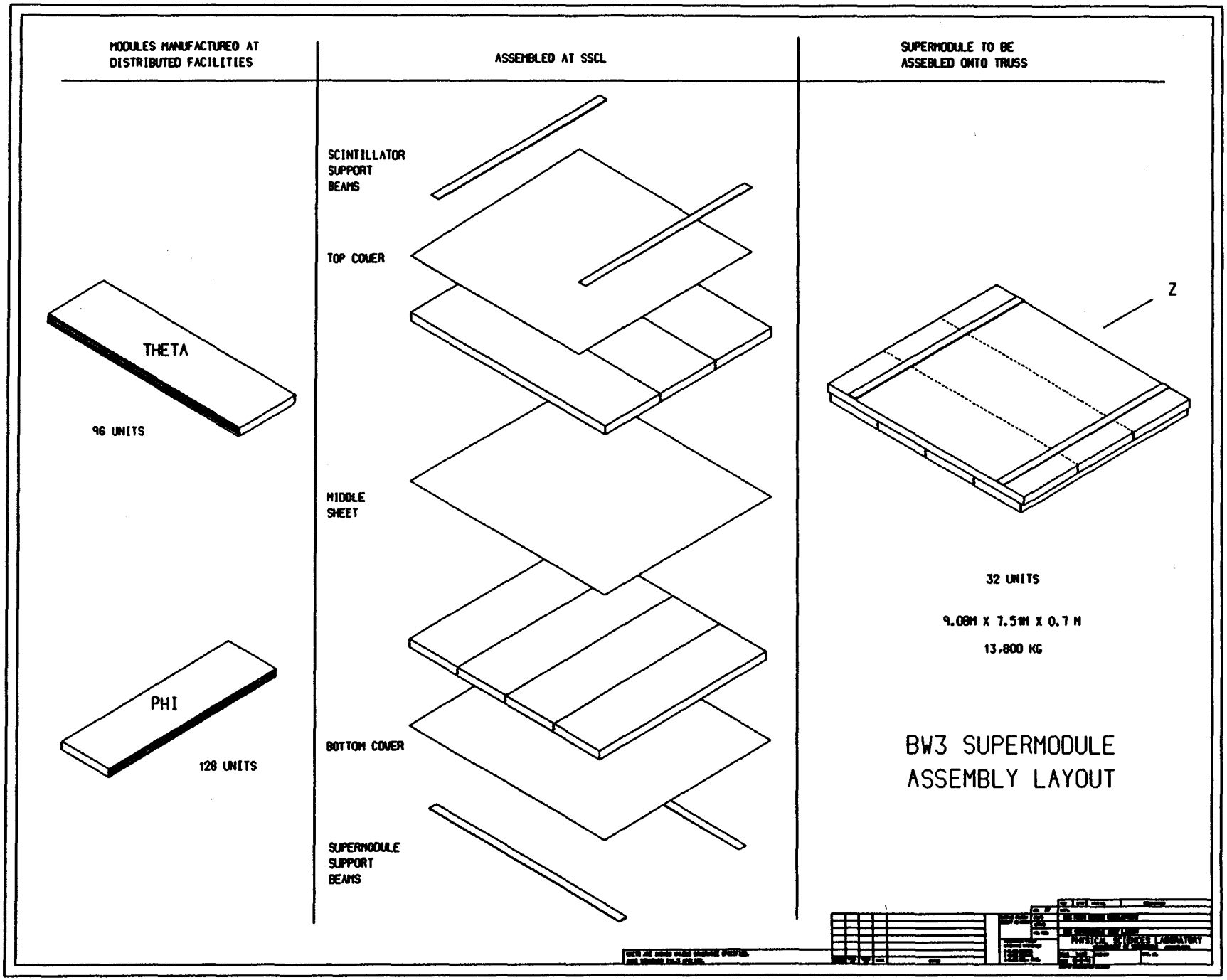

PRODUCED BY GP_JDP
12 / 11 / 91 AT 09 : 59

DRAWING FILENAME SAT006E
PLOTTED AT SCALE 1/1

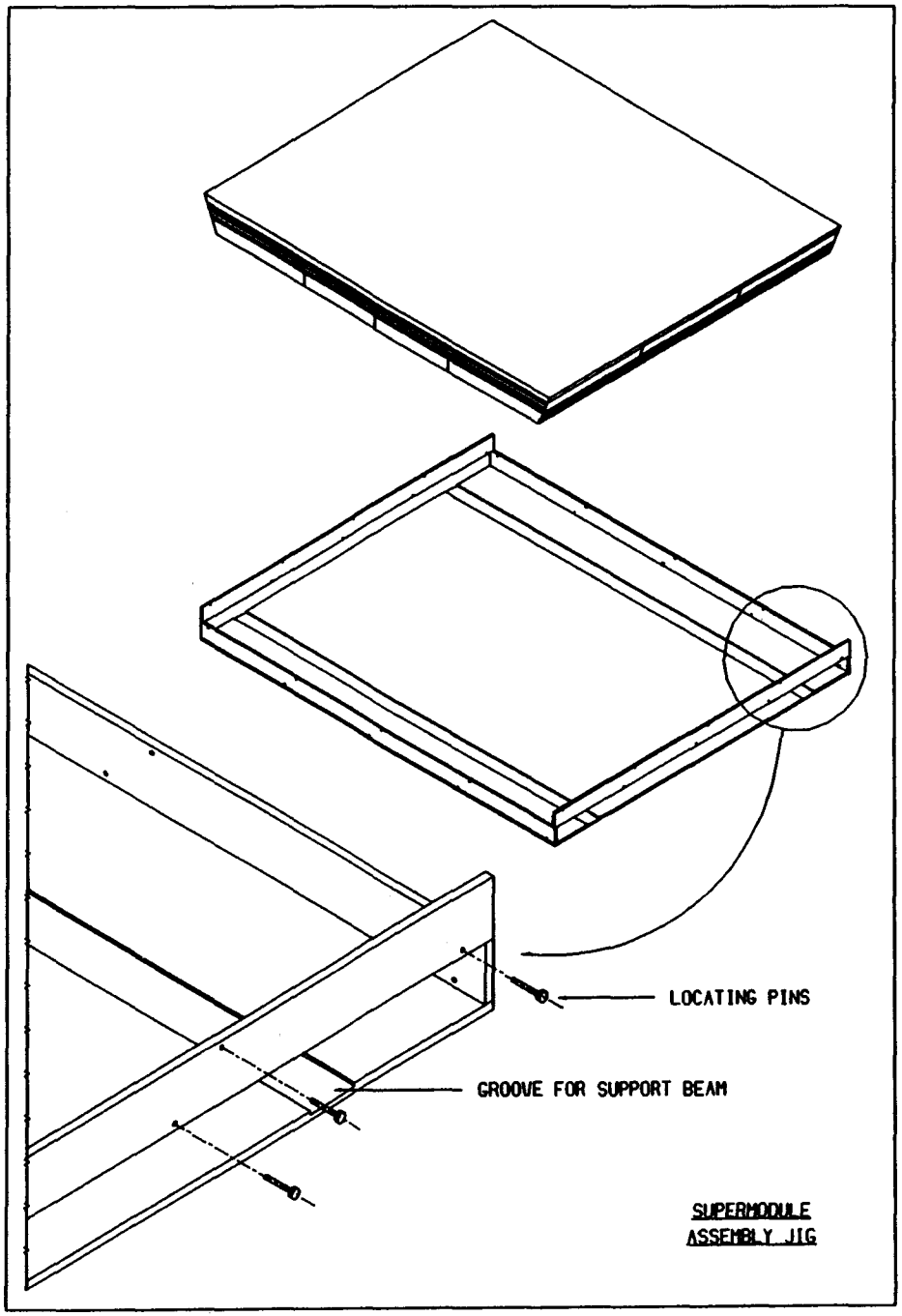

PRODUCED BY PIP DRAWING FILENAME SAT009E
ON 12 / 12 / 91 AT 14 : 05 PLOTTED AT SCALE 1/1

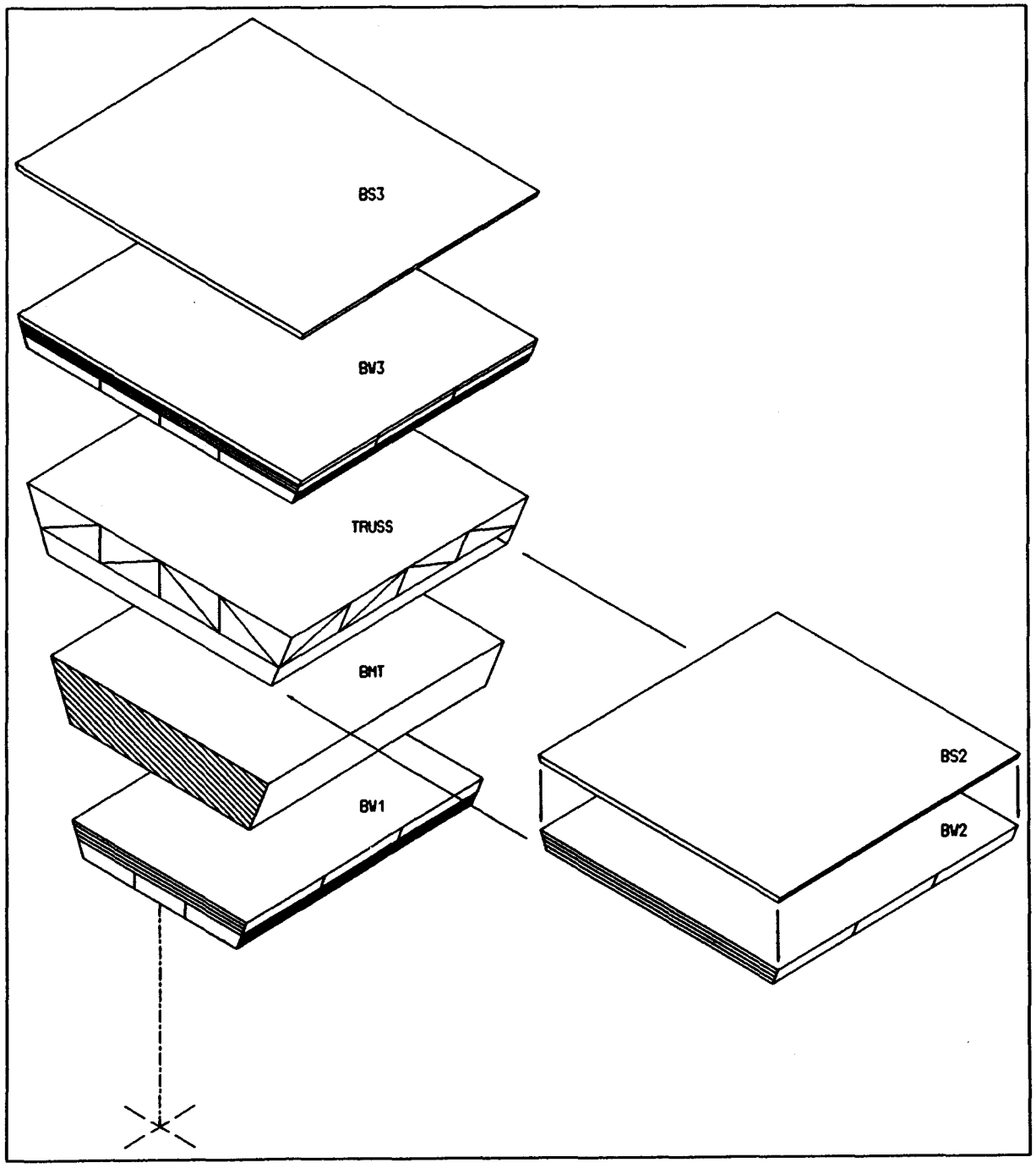

PRODUCED BY PIP
12 / 12 / 91 AT 12 : 55

DRAWING FILENAME SAT008E
PLOTTED AT SCALE 1/1

Chapter 2

Drift Cell

2.1 Electrostatics

The electrostatic field in the octagonal cell is essentially that of a cylindrical tube. For a tube of radius R and wire of radius r_w, the capacitance, charge per unit length, and electric field are

$$C = \frac{2\pi\epsilon_0}{ln(R/r_w)} \; ; \; \lambda = CV \; ; \; E(r) = \frac{\lambda}{2\pi\epsilon_0 r} = \frac{V}{ln(R/r_w)r}$$

For prototyping, we chose the values R = 36 mm and r_w = 63 micron and V = 4 kV for which

$$C \; = \; 8.8 \; pF/m \; ; \; \lambda \; = \; 35 \; nC/m$$

The electric field strengths at the wire surface and at the interior surface of the tube are

$$E_w \; = \; 100kV/cm \; ; \; E_{min} \; = \; 175 \; V/cm$$

The results of a numerical calculation of the potential and electric fields are shown in Figures 2.1 - 2.4. For radii larger than about 2 cm, the electric field deviates somewhat from cylindrical symmetry. Figure 2.5 illustrates the isochrones expected for a simple model of the drift velocity, namely that the velocity is linear in field strength up to 300 V/cm where it saturates at 4 cm/μs.

For a given gas mix, wire radius and tube radius, the operating voltage is determined by the choice of gas gain. Proportional mode multiplication may be parameterized as

$$ln(M) = \frac{\lambda}{2\pi\epsilon_0\epsilon^{thres}} \exp[-2\pi\epsilon_0\epsilon^{thres} N\sigma r_w/\lambda]$$

where N is the number density of molecules, ϵ^{thres} is the ionization threshold and σ is the cross section. The limit of the proportional regime corresponds to $M \simeq 10^6$. where the avalanche linear charge density becomes comparable λ. The operating point would typically be selected as between 10^5 and 10^6. The exponential dependence of multiplication on voltage implies a relatively small voltage variation covers this range.

A large value of E_{min} is desirable to maintain the drift velocity roughly saturated. Larger drift fields may be supported if a larger wire radius and voltage are selected. We have not optimized our selection. It is likely that voltages in excess of 6 kV could be used without risk of corona in the high voltage distribution, allowing somewhat higher drift fields and improved linearity.

2.2 Mechanical Stability

The sensitivity of the tube operation to wire sag may be judged from the expression for the capacitance of a cylindrical tube of radius R with a wire of radius r_w displaced a distance x from the tube center:

$$C(x) = \frac{2\pi\epsilon_0}{\cosh^{-1}[(r_w^2 + R^2 - x^2)/2r_wR]} \simeq \frac{2\pi\epsilon_0}{ln[\frac{R}{r_w} - \frac{x^2}{Rr_w}]}$$

As illustrated in Figure 2.6, the capacitance has a very shallow minimum about the symmetry point. To reach a one percent change in capacitance requires a wire sag equal to a quarter of the tube radius or about 1 cm for our tube. At fixed voltage, the capacitance determines the charge per length on the wire and hence the surface field and gain. A one percent capacitance change produces a gain change of order 30 percent depending on the operating point and is deemed acceptable. The effect on the drift velocity is expected to be negligible.

The electrostatic force per unit length on the wire for fixed potential is

$$F = \frac{1}{2}\frac{d^2C}{dx^2}\,|_{x=0}\,V^2x \simeq \frac{1}{2}\frac{C^2(0)}{\pi\epsilon_0(R-r_w)^2}V^2x \equiv kx$$

The image force is counteracted by the tension. The critical length for mechanical stability under electrostatic forces alone is given by

$$L_{crit} = \pi\sqrt{T/k}$$

where T is the tension and k the force constant defined by the preceding expression. For our tube parameters, the critical length is long compared to the SDC. Gravitational sag in the absence of electrostatic forces has a maximum amplitude given by

$$\delta h_0 = g\frac{\lambda}{T}\frac{L^2}{8}$$

where g is the acceleration of gravity, λ is the mass per unit length, and L is the wire length. As the tension of each wire is supported by a a strong tube, for any wire radius, the tension may be picked close to the elastic limit and scales with wire mass. The sag therefore depends only on strength to mass ratio and the length. With electrostatic forces included, the sag is

$$\delta h_{max} = \frac{g\lambda}{k}(\frac{1}{\cos(\sqrt{kl^2/2T})} - 1) = \delta h_0\frac{2}{x^2}(\frac{1}{\cos(x)} - 1)$$

where $x = \pi L/2L_{crit}$. Enhancement of gravitational sag by electrostatic forces occurs only at a sensible fraction of the critical length and is unimportant.

2.3 Signal Propagation

The characteristic impedance of the drift tube is

$$Z_0 = \frac{1}{cC} \approx 383\ \Omega$$

We anticipate quite small signal attenuation. For a coaxial transmission line, neglecting dielectric losses in the gas, the signal attenuation length is given perturbatively by

$$L = 2ln(R/r_w)/(\Sigma_w/r_w + \Sigma_R/R)$$

In this expression, Σ_w and Σ_R characterize the loss in the skin depth of the wire and wall respectively and are given by

$$\Sigma = (\pi f \rho \epsilon)^{1/2}$$

where f is the frequency, ϵ the permittivity, and ρ the resistivity of the material. If the wall and wire have similar resistivities, the loss is dominated by the wire loss and the attenuation length is proportional to the wire radius (until b/a = 3.6). Handbook values for resistivities in microOhm-cm are: Cu (drawn) 1.77, Gold 2.44, Aluminum 2.8, Tungsten (drawn) 5.6, Steel 10. The Seattle Group has measured an attenuation length for Fe source signals of 47 m for 100 micron W-Re wire and we anticipate an even smaller attenuation.For a 70 micron radius gold wire in a 36 mm radius tube at f = 100 Hz, the attenuation length is predicted to be 106 m.

The long attenuation length implies that wire ORing of analog signals of ϕ wires along the barrel may be contemplated. However, reflection of the signal at the interface of two tubes is a potential source of difficulty. Preliminary tests with short wires connecting two 9 meter long prototype tubes indicate reflection coefficients of several percent. These effects may result from the impedance mismatch caused by the dielectric endplug. Further study is required.

2.4 Gas Mixture

The gas mixture we have used in prototype work is a commercial premix of $Ar(90)/CO_2(5)/Methane(5)$. This mix was selected for a combination of low value of electric field at which the drift velocity saturates, relatively large saturated drift velocity, and relatively large range of field over which the drift velocity remain saturated. These qualities provide a near linear time to distance relationship within the cell and a maximum drift time of approximately one microsecond. The small hydrocarbon content meets Department of Transportation specifications for nonflammability. Figure 2.7 shows the voltage dependence of ^{55}Fe X-ray signals in short tubes with 50 micron and 140 micron wire diameters with both this gas mix and Ar(50)-Ethane(50). The proportional mode X-ray signal is observed as a sharply defined pulse is all cases. The $Ar(90)/CO_2(5)/Methane(5)$ mix is found to have higher intrinsic gain than Ar(50)-Ethane(50).

The time-to-distance relationship for a 1 meter length octagonal tube operating at 4350 Volts with a 5.5 mil wire and $Ar(90)/CO_2(5)/Methane(5)$ was obtained by extrapolating cosmic ray tracks from a 16 cell chamber. The 16 cell chamber used for this study has essentially the structure proposed for the forward muon system. It was constructed from 1.5 inch square tubes and operated with 5.5 mil wire and $Ar(50) - Ethane(50)$. A typical event is shown in Figure 2.8. The time-to-distance relationship for the SDC tube is shown in Figure 2.9. The width of the distribution is a reflection of resolution and scattering effects within both chambers and of extrapolation error. The SDC tube spatial resolution has no yet been determined.

The drift velocity versus drift field relationship for a variety of gas mixes of slightly different composition have been measured by the Washington group. As the additive content is reduced, the drift velocity developes a peak at a progressively lower field value (implying faster drift at the outer radius) but the "saturation" value at large field strengths decreases (implying slower drift closer to the wire). The nonlinearities in the time-to-distance relationship and also the maximum drift time can hence be manipulated. With $Ar(95)/CO_2(2.5)/CH_4(2.5)$ and a 100 micron wire, the Washington group has calculated a 1 microsecond drift for 36 mm radius. Nonlinearity does not affect the trigger operation for high momentum tracks which appear at roughly equal distances

from projective wires. Simulations by the Washington group show no appreciable difference in the trigger response functions with and without nonlinearities of the size contemplated.

2.5 Gas Tolerances and Monitors

The drift velocity generally varies inversely and the gain exponentially with gas density and hence with the product of temperature and pressure. Gain stability at fixed voltage requires the density variation not exceed about 1 percent which implies a temperature variation of about 2 degrees absolute and a drift distance systematic error of 360 micron at the edge of the cell. It is likely that temperature and pressure gradients will require voltage compensation on a supermodule basis.

Variations in the gas composition must be kept below of order 1 percent to maintain the time-to-distance relationship. The exact specification requires detailed measurements with gas mixtures differing slightly in composition. Gas sampling on a supermodule basis may be implemented to verify gas quality, as well as gas flow monitors. The specification of the requirements will be based on experience with the first prototype supermodule.

2.6 Figure Captions

Figure 2.1 Electrostatic potential in the octagonal tube.

Figure 2.2 Equipotential contours in the octagonal tube.

Figure 2.3 Drift trajectories in the octagonal tube.

Figure 2.4 Electric field strength versus radius for various angles within the tube.

Figure 2.5 Isochrones (50 ns intervals) for model gas.

Figure 2.6 Tube capacitance versus wire displacement from the center of a cylindrical tube.

Figure 2.7 Fe source signal sizes for various tubes, wires and gases. 10 mV corresponds to a gain of $\sim 10^6$.

Figure 2.8 Event display for cosmic ray test of octagonal tube.

Figure 2.9 Time-to-distance relationship for octagonal tube with $Ar(90)/CO_2(5)/Methane(5)$, 5.5 mil wire, 4350 Volts as measured by extrapolation.

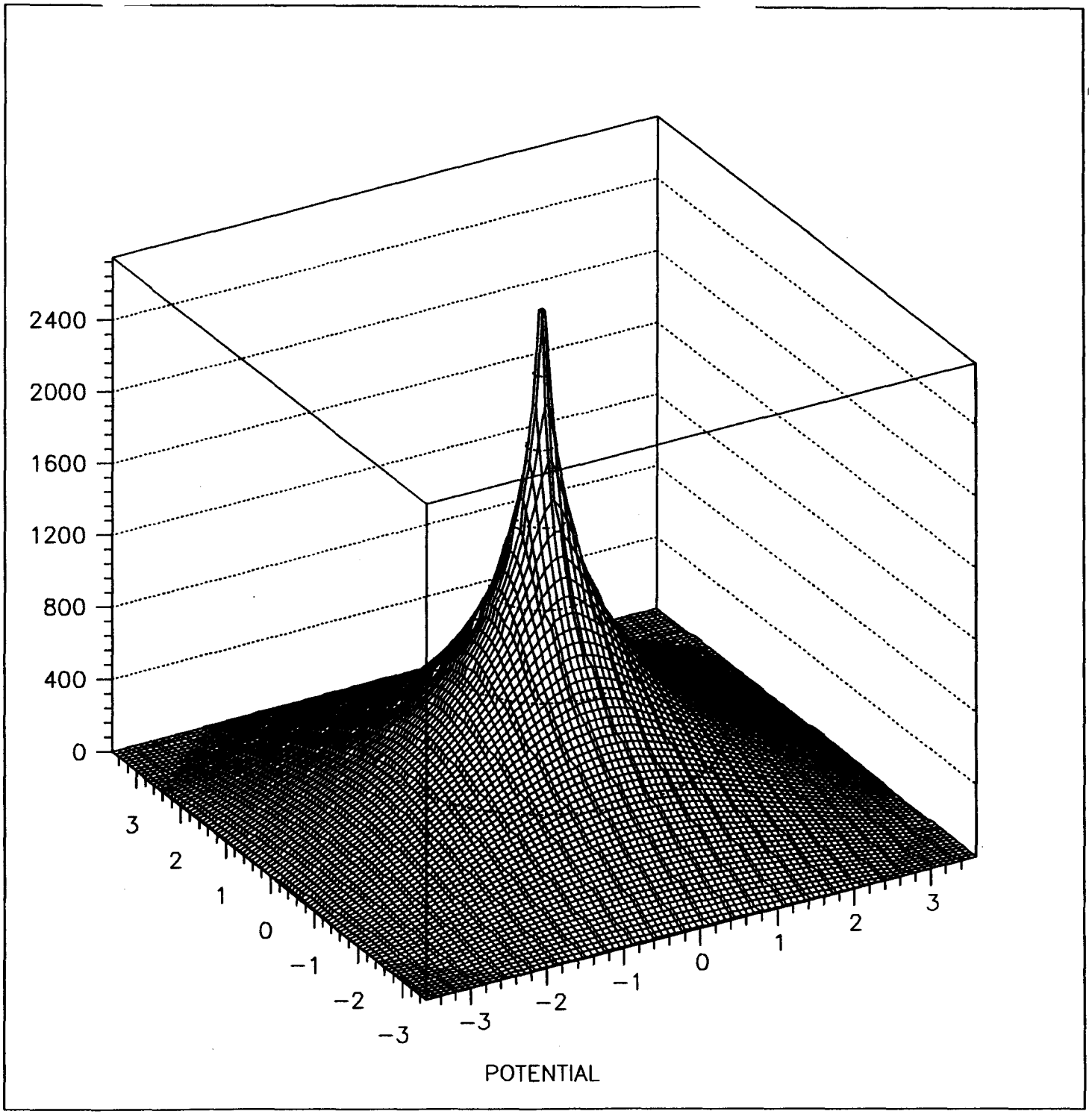
2400
2000
1600
1200
800
400
0
3
2
1
0
−1
−2
−3
−3
−2
−1
0
1
2
3
POTENTIAL

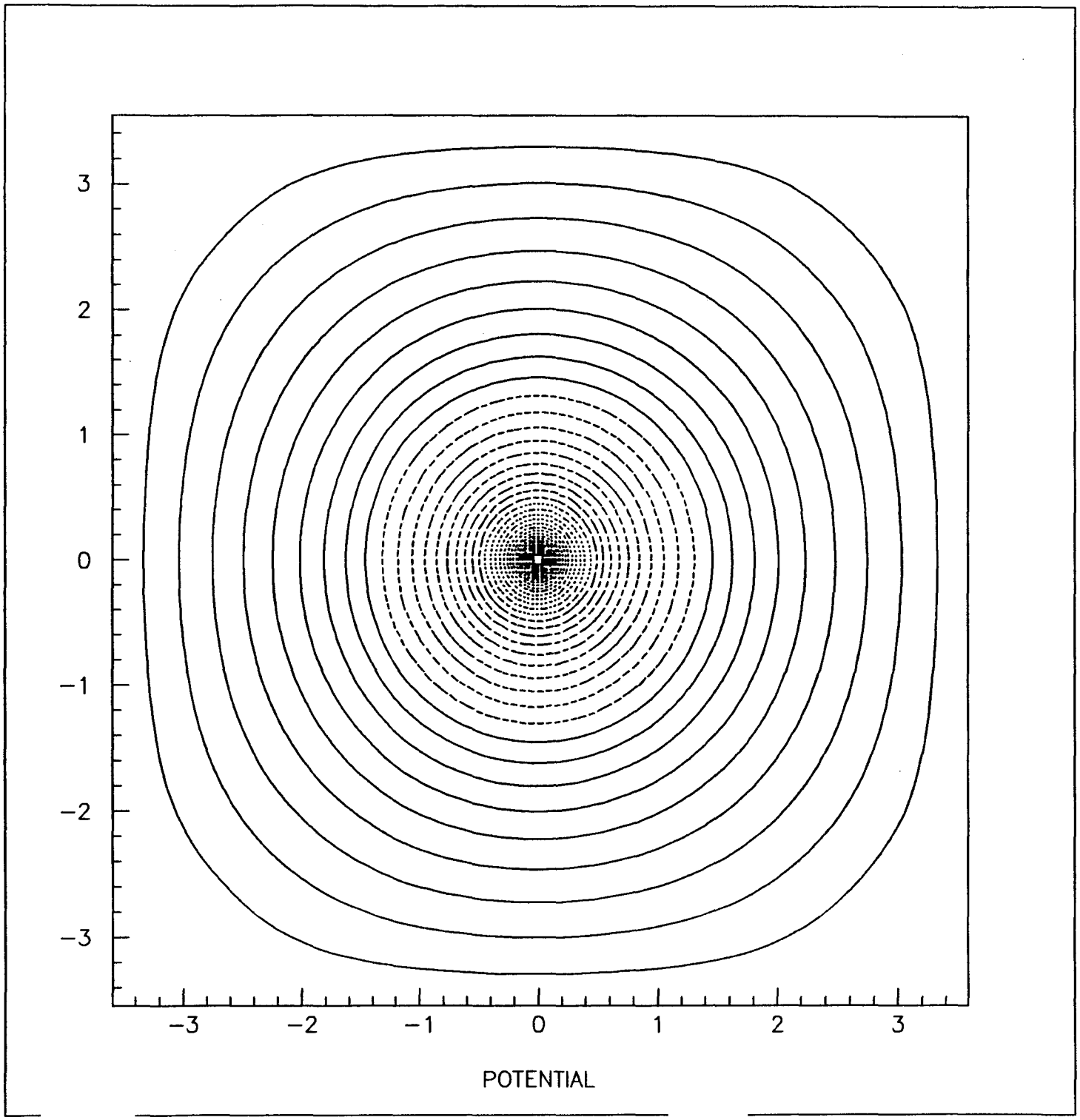
3
2
1
0
−1
−2
−3
−3
−2
−1
0
1
2
3
POTENTIAL

Drift Trajectories

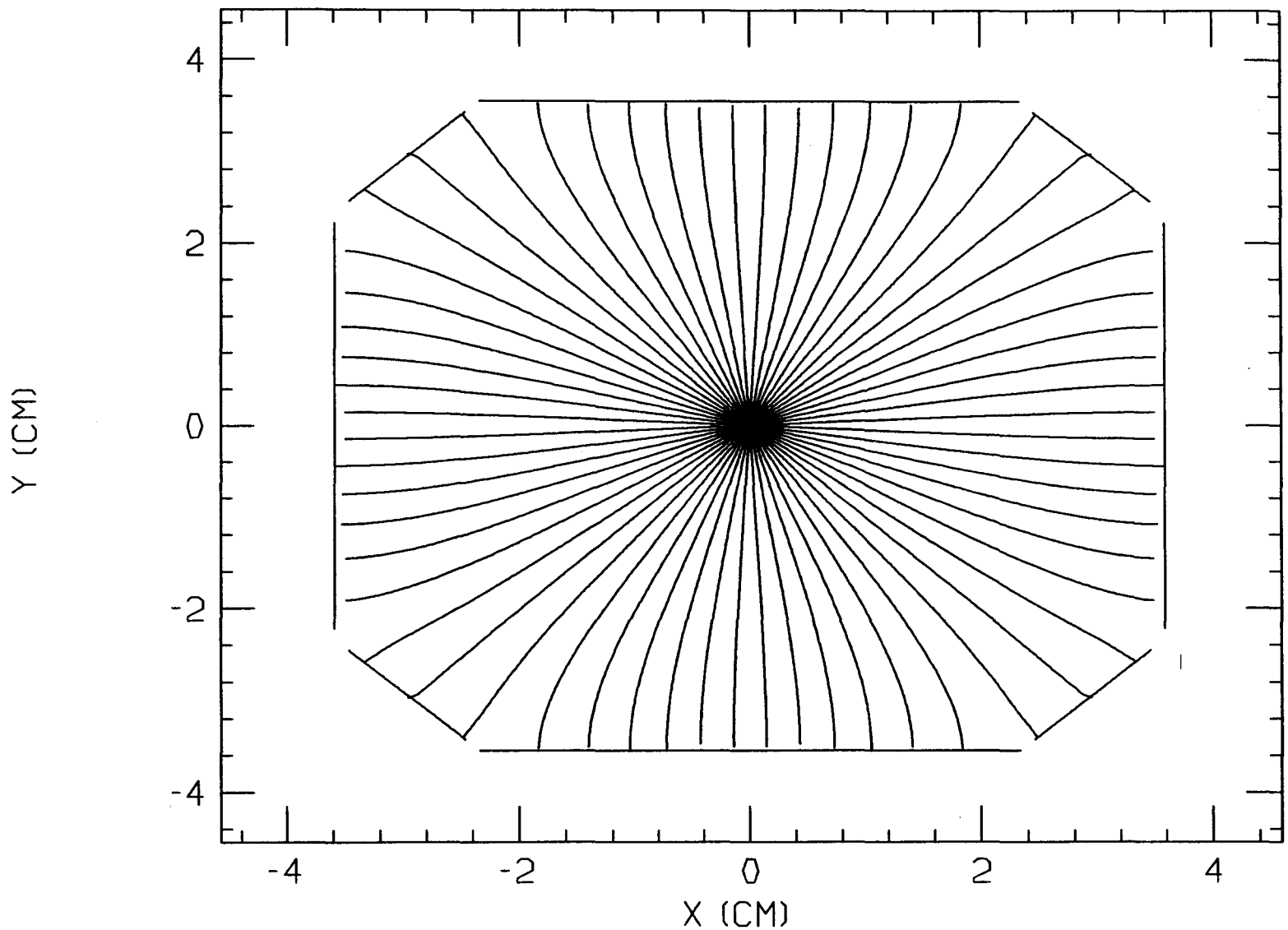

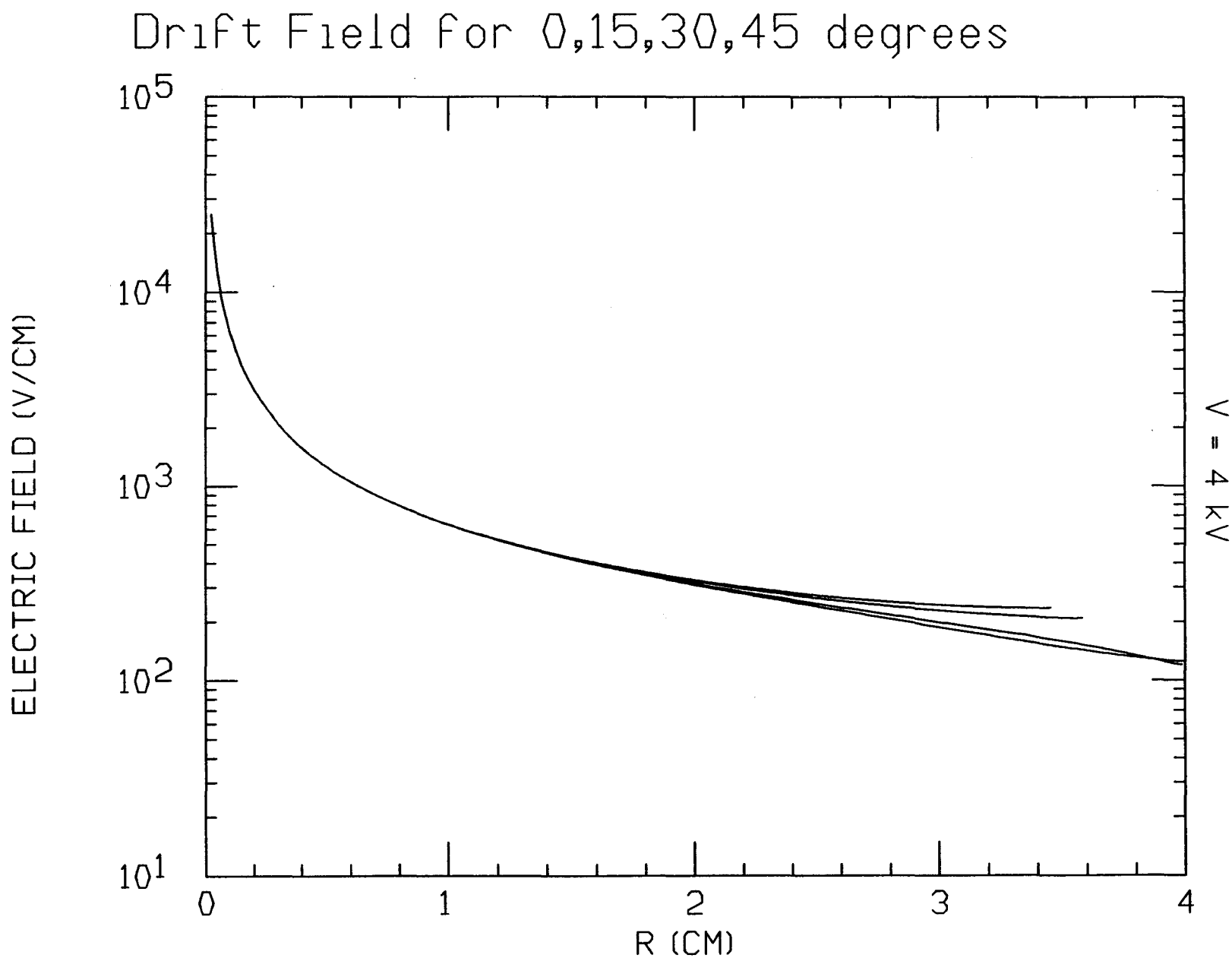
Drift Field for 0,15,30,45 degrees
ELECTRIC FIELD (V/CM)
10^5
10^4
10^3
10^2
10^1
0
1
2
3
4
R (CM)
V = 4 kV

Model 50 ns Isochrones

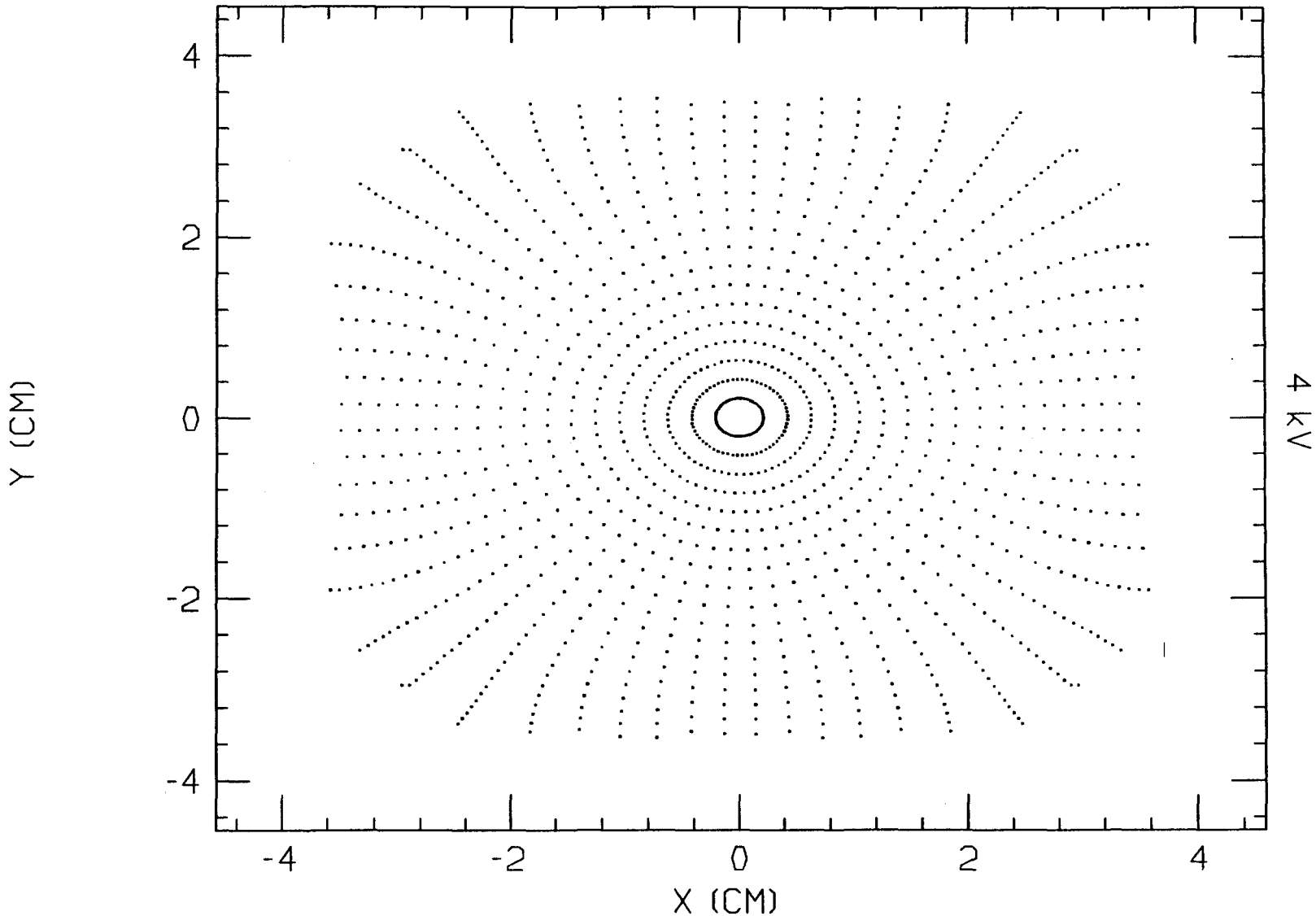

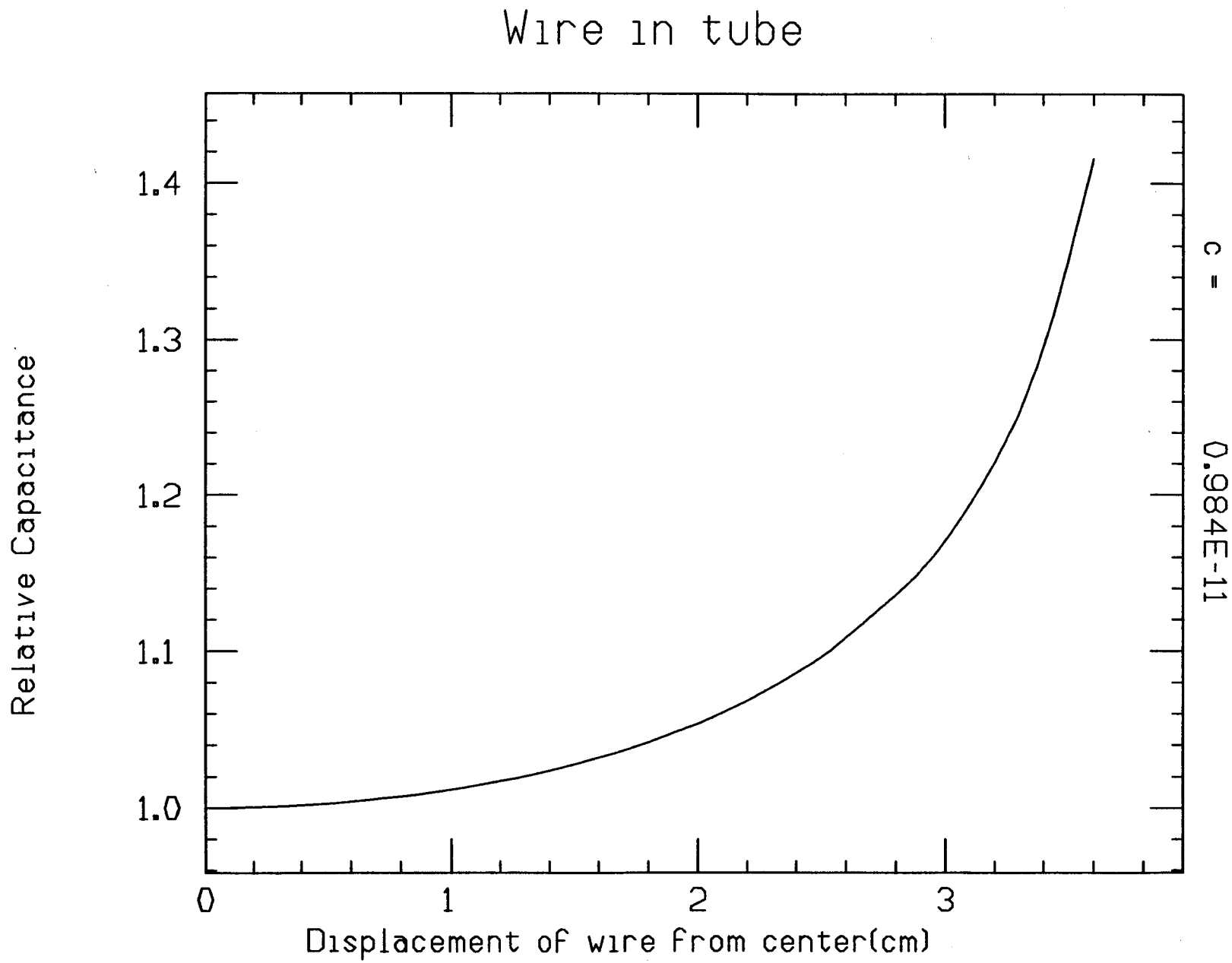
Wire in tube
Relative Capacitance
1.4
1.3
1.2
1.1
1.0
0
1
2
3
Displacement of wire from center(cm)
c = 0.984E-11

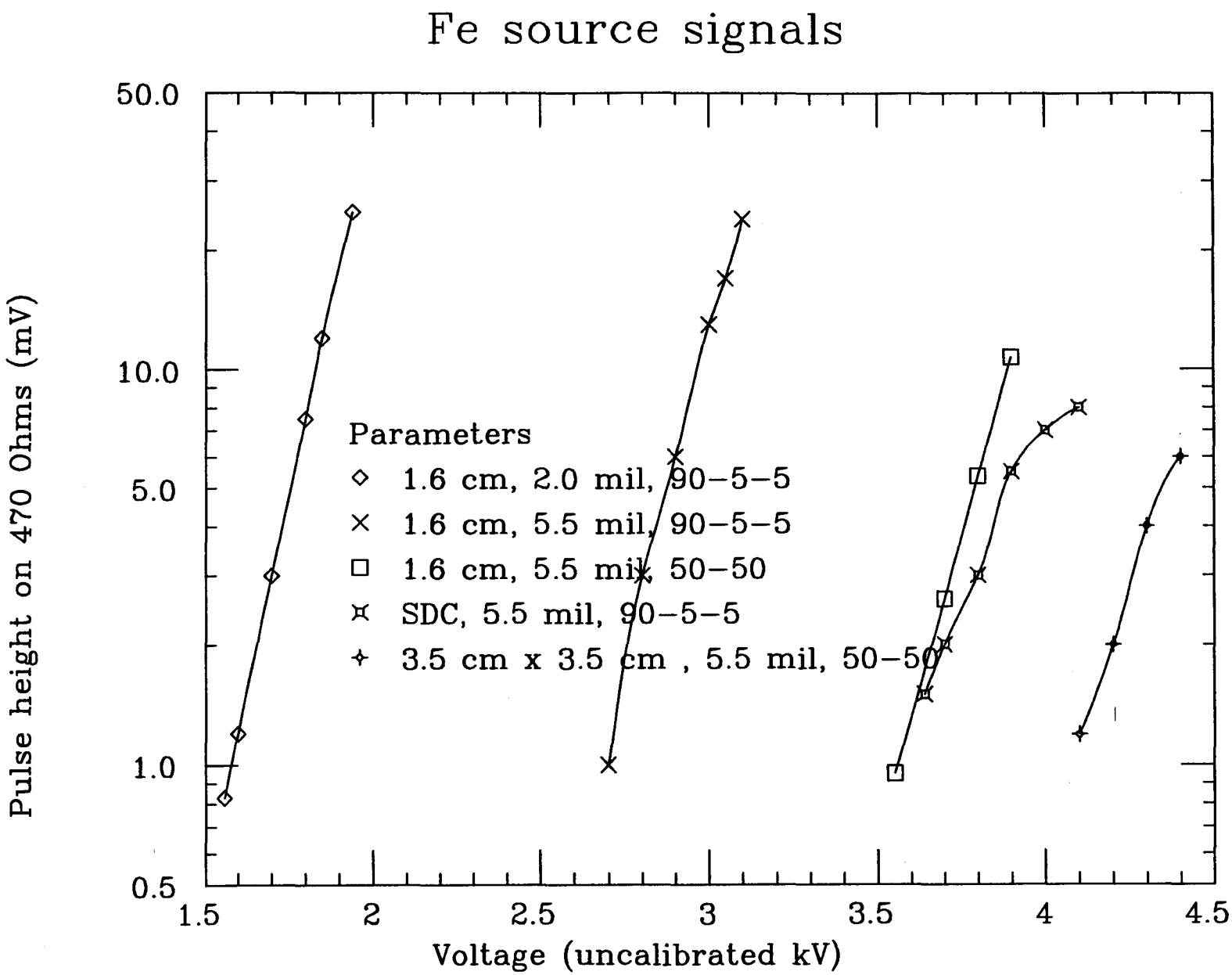
Fe source signals
Pulse height on 470 Ohms (mV)
50.0
10.0
5.0
1.0
0.5
1.5
2
2.5
3
3.5
4
4.5
Voltage (uncalibrated kV)
Parameters
1.6 cm, 2.0 mil, 90–5–5
1.6 cm, 5.5 mil, 90–5–5
1.6 cm, 5.5 mil, 50–50
SDC, 5.5 mil, 90–5–5
3.5 cm x 3.5 cm , 5.5 mil, 50–50

University of Wisconsin

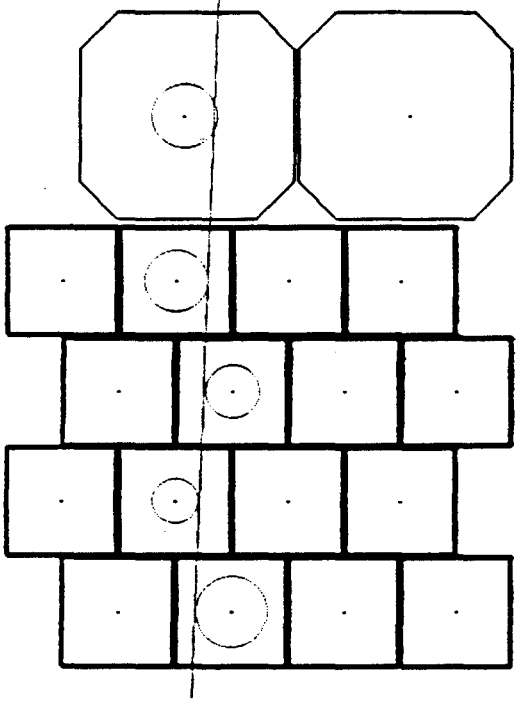

DISVSTIME

HBOOK ID = 101 DATE 20/09/91 NO

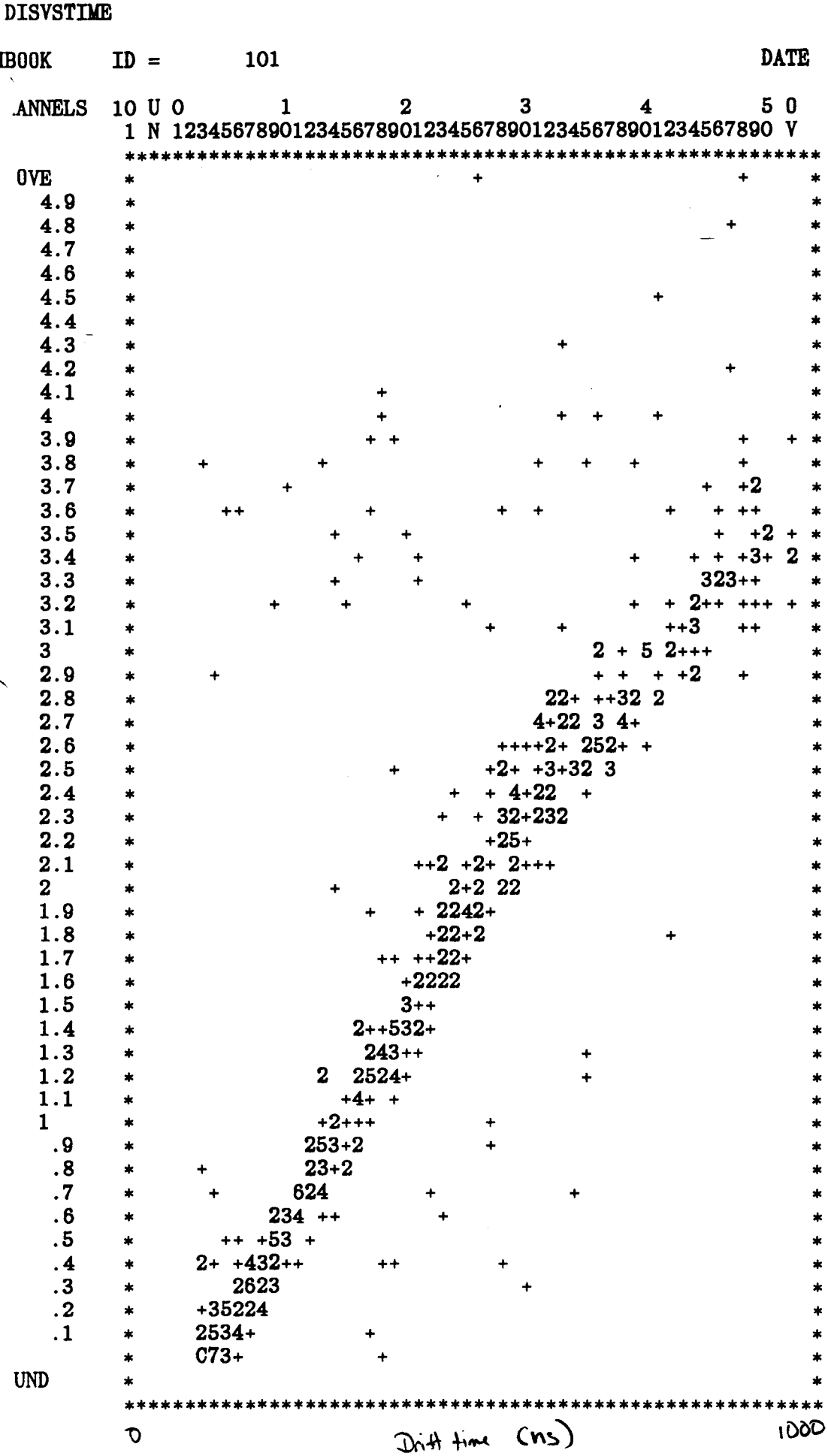

Chapter 3

Chamber Structure

3.1 Extrusions

The choice of aluminum as opposed to lighter resistive plastic as the base material was dictated by consideration of flammability and strength to mass ratio. The cost of an extrusion is proportional to the raw material mass and to the speed at which the extrusion process occurs. Smaller wall thicknesses and larger extrusions demand a slower extrusion for given tolerances. The tube doublet eliminates one interior wall thickness and appears to be most cost effective. Octagonal singlet tubes will be obtained to minimize deadspace at supermodule boundaries.

A simple analysis indicates that the stiffness of the tube against gravitational sag is largely independent of wall thickness as the linear mass and area inertial moment scale linearly with wall thickness. GEANT simulations of delta ray production in aluminum walls (Figure 3.1) indicate a significant decrease for wall thicknesses below one millimeter. Unfortunately, no vendor was prepared to provide such a low mass chamber at a competitive cost. The 1.8 millimeter wall thickness appears to represent the minimum cost.

While a square tube provides the maximal surface for adhesion, the electric field essentially vanishes in the corners. Concern over possible stale ionization and minimization of material led to the octagonal design. From the point of view of electrostatics, the octagonal cell is very nearly cylindrical. The omitted corner provides a space for the introduction of screw bosses which are located outside the region of the gas seal. Thus the design facilitates a robust tube endplate connection without complicating the pressure integrity.

Several options are available for surface finish and samples of different processes were examined. Stabilization and cleansing of the exterior surface by anodization leads to a nonconductive interior surface to a significant depth from the end of the tube and was rejected. A proprietary "allodyning" process as well as a simple caustic etch produce stable conductive interior and exterior surfaces. The less expensive etch process was selected for prototyping but the proprietary finish in costing. Evaluation of the relative merits of the two processes for glue adhesion and potential Maltier effect are required for a final choice.

3.2 Wire, Wire Mount, and Crimp Tube

We have selected gold plated tungsten wire for prototype development. Although relatively expensive, this wire has a high tensile strength and good surface quality, and has been used successfully in many drift chambers. The wire is crimped in a 1 mm O.D. stainless steel crimp tube with inner diameter 20-50 micron larger than the wire. A manual crimp tool has been used for initial tests and is observed by microscope to produce a flow of the crimp tube around the wire leading to near uniform contact with the surface. The wire mount is a Delrin plug with a .969 mm diameter hole machined in the center in which the crimp tube is inserted. Insertion molded mounts could be developed. Wires may be rapidly strung with a simple insertion tool (expanding poker) developed by PSL.

We have performed preliminary studies of the effectiveness of the crimp procedure and of wire deformation under tension. The experimental arrangement consisted of a 3 inch sample of extrusion containing the endcap, wire mount and crimp tube for the sealed tube option. A wire length of approximately 1 meter under variable tension was suspended vertically in a stainless steel jig and the motions of tape at the top and bottom of the wire were monitored with microscopes mounted on microstages. The elastic modulus and yield point are consistent with handbook values and there is no indication of slippage in the crimp tube or of the crimp tube within the endplug. Hysteresis is observed for tensions in excess of 1700 grams. A tension of 1650 gm or so is similar to the value obtained by scaling tensions used in CDF chambers by the wire cross sectional area. A tension precision of 1 percent was reported in the construction of the CDF central drift tubes and 2 percent was reported for the VENUS 7.6 m tubes. We anticipate comparable precision and, as the worst case sag is approximately 1.5 mm, offline correction should be straight forward. Further measurements of wire mechanical properties are underway.

3.3 Endplug Design

A Delrin endcap is glued into the ends of each double cell tube to provide a gas seal. We are pursuing two designs: a) the sealed tube option in which the tubes are strung and tested prior to assembly into modules and b) an O-ring option in which wire stringing is performed after assembly of the modules.

The prototype sealed tube endcap design shown in Figure 3.5 provides a gas seal against the interior tube walls. Two 14 mm holes in the endcap support wire mounts recessed within the tube to allow stacking of the tubes without interference with the crimp tubes. The wire mount/endcap interface completes the gas seal of the tube. The endcap/wire mount assembly is registered to the endplate by two plastic locator plugs (outside diameter 26 mm, inside diameter 16 mm). Gas is distributed by threaded tubes which pass from a chamber gas manifold through M6 holes in the endplate into threaded holes in the endplug.

The O-ring design shown in Figure 3.8 has a single 8 mm diameter wire mount seated directly in the endplate. The endcap, consisting of a large (50 mm) hole and an O-ring groove (3/16"), is glued into the extrusion and provides an O-ring seal between the endcap and the endplate. The wire mount is seated directly in the endplate. In this option the entire chamber is built, and then the wires are strung. The disadvantage of this option is the difficulty of fixing any gas leaks discovered after the chamber structure has been built. More stringent tube length tolerances are required in this design to ensure a reliable gas seal and determine the size of the O-ring. A 16-cell

prototype has been constructed using this design and tests are in progress.

3.4 Endplate

The endplate for a module is typically 2.4 m long and 4 layers (300 mm) high. Holes (26 or 8 mm diameter) are machined into the endplate for locating the wire, either using a locator plug (sealed tube option) or a wire mount (O-ring option). In the sealed tube option the endplate must also contain clearance holes (8 mm) for the gas manifolding. The wire positions are projective so as the wire location gets farther from the beam line the spacing between wires increases. This means that each endplate is designed for a specific θ region. The endplate for a 32-cell prototype is illustrated in Figure 3.9.

To minimize dead space the edges of the endplate are crenellated to accept the corresponding endplate from the next chamber. During the monolith assembly at the SSCL, monolith endplates will be pinned to a precise jig using dowel holes machined in the endplates. In this way the accuracy of wire position can be maintained over the 4 chambers that make up a complete monolith.

Prototype endplates were machined from 1/2" aluminum plate. However, the production endplates will be extruded from 6063-T6 aluminum. For the θ chambers the endplate will be extruded in a stairstep design to minimize the dead space at the intersection of supertowers while straight endplates are used for ϕ modules. The extruded endplate for the O-ring option may provide an enclosed volume for the gas manifolding for each layer, as illustrated in Figure 3.10. The inner hole of the extrusion is larger than the wire mount outer diameter and can be designed to provide a uniform gas flow for each cell (size of hole may depend on the distance from the input or output). This endplate option remains to be developed.

In Figure 3.11, measured hole location deviations are shown for two prototype endplates of 1/2 inch aluminim plate drilled on a Hermle CNC machine at PSL. The rms deviations from design values are found to distributed with rms values of order 2 micron about mean values shifted by of order 10 micron from 0. Temperature control in the drilling process is essential to maintain fine tolerances. The small systematic effects may result from a 1 degree F temperature difference between production and measurement and are presently under investigation.

3.5 Prototype wire location achievements

The wire positions have been measured for a 16-cell 1 meter long sealed-tube prototype. The endplate design is the first half of the 32-cell endplate shown in Figure 3.9. Holes (2 cm diameter) were cut in the sides of each extrusion about 3 cm from each end. After the chamber was completely assembled it was placed on a flat table and the actual y positions of each wire were surveyed optically by sighting through these holes. The telescope was mounted on a height gauge which had a readout accuracy of 1 micron and a range of 1 meter. Repeated measurements of the same point indicate an accuracy of $\sim$6 microns. The y position of each wire was measured and compared to the design value. The differences are plotted in Figure 3.12 and fitted to a gaussian. The sigma of this distribution is 85 microns and the mean value is 7 microns. This accuracy reflects the accumulated tolerances in milling the endplates, the Delrin endcap, the Delrin wire mounts, and the Delrin locator plugs.

3.6 Projectivity

For single tubes of diameter R close packed in a four layers, projectivity between wires in layers 0 and 2 requires the wire spacing be related by

$$\frac{\Delta Z(2)}{\Delta Z(0)} = 1 + \frac{2\Delta Z(0)}{\rho(0)}$$

where $\rho(0)$ is the radius of layer 0. For a cell size $\Delta Z(0) = 75$ mm at a radii of 5720 mm, 8500 mm and 10080 corresponding to the inner surfaces of BW1, BW2 and BW3, the gaps required for projectivity are .026, .0176 and .014 units of cell size or about 2 mm, 1.3 mm, and 1 mm. In practice, there is a gap of about 1 mm between tubes in the first layer to allow for extrusion tolerances and, since there are two cells to an extrusion, the wires in two projective tubes form one exactly projective pair and one parallel pair. It may also be noted that the tube walls are not exactly projective but parallel to the wires and hence project to a point displaced by one cell size along the beam direction, ie about 1 σ in the vertex distribution. Another geometrical effect applies to BW3. A track deflected by the toroid at radius ρ_T by polar angle by $\delta\theta$ arrives at BW3 at radius ρ_3 displaced along the beam direction by

$$\Delta Z = \rho_T(1 - \frac{\rho_3}{\rho_T})\frac{\delta\theta}{\sin^2(\theta)}$$

At 20 GeV near the end of the barrel, this amounts to about 1 cell size. Truly projective response would require the drift velocity and cell size increase with depth into the module.

3.7 Assembly

Modules are constructed on a flat assembly table on which the endplates are first precisely located. The first layer of tubes are positioned using the endplates. In prototype production, beads of 2 component 3M DP-460 Epoxy Adhesive are applied with a Duo-Pak gun applicator prior to positioning of the next layer of tubes. Uniform application of adhesive is not required - most of the shear stress is developed near the ends of the module. The chosen adhesive requires 4 hours at 75 degree F to set. The 9 meter 32-cell prototype is found to readily support 2 men. Supported from the endplates, the sag is 5 mm. With inboard supports, the sag is less than 1 mm. Further mechanical tests are in progress.

3.8 Thermal Properties

Within the SDC detector large quantities of heat will be produced by the electronics. In the latest integration plan many electronics racks for the tracker and the calorimeter will be located directly in front of the BW1 supertowers. While these racks will probably be water-cooled, it is likely that the inner surface of BW1 will have some heat input. It is also likely that heat sources will cause thermal gradients in other supertowers as well.

What effect will this heat have on the distribution of temperatures in the muon system? To answer this question we have measured the flow of heat through a 100 mm long section of a typical 4-layer chamber of octagon tubes, As shown in Figure 3.13, two inches of fiberglass insulate on the

bottom, sides, front, and back. There is no insulation at the top, so heat can escape only at the top of the chamber. Fastened to the bottom of the test unit is a copper plate with an electrical heating element. The input energy to the heating coils is controlled by a Variac, and both current and voltage are measured. Temperature measurements are taken with thermocouples at 4 points inside the chamber section.

Figure 3.14 shows the temperature distribution over a period of 500 minutes for a heat input of 35 watts. Steady state conditions are reached after ~300 min. At the steady state we calculate that a heat input of 17 watts/m^2 results in a temperature difference of 1° C over the 4 layers of the chamber. Because of the differential expansion of the aluminum this 1° C difference causes the 9 m chamber to curl up with a sagitta of 1 mm. This effect is likely to be similar for any of the options we are considering.

The conclusion is that we need to ensure that the temperature difference across the chambers remains less than 1° C. It may be possible to achieve this by flowing gas, since the time to reach equilibrium (5 hours) is roughly the same as the time to change completely the volume of gas within the chambers.

3.9 Figure Captions

Figure 3.1 GEANT simulations of δ yield vs aluminum wall thickness.

Figure 3.2 Elongation of 1 m lengths of 5 mil Au-W wire.

Figure 3.3 Hysteresis in elongation of Au-W wire indicating yield point.

Figure 3.4 Endplug assembly for the sealed tube option.

Figure 3.5 Prototype endcap.

Figure 3.6 Prototype locator plug.

Figure 3.7 Prototype wire mount and crimp tube.

Figure 3.8 O-ring endplug option with flat endplate.

Figure 3.9 Endplate for 32-cell prototype.

Figure 3.10 O-ring endplate with internal gas manifolding.

Figure 3.11 Measured hole locations for 16-cell prototype endplates.

Figure 3.12 Distribution of residuals to wire locations for 16-cell sealed tube prototype.

Figure 3.13 Module thermal test setup indicating locations of thermocouples.

Figure 3.14 Thermal response for Octagonal tube module.

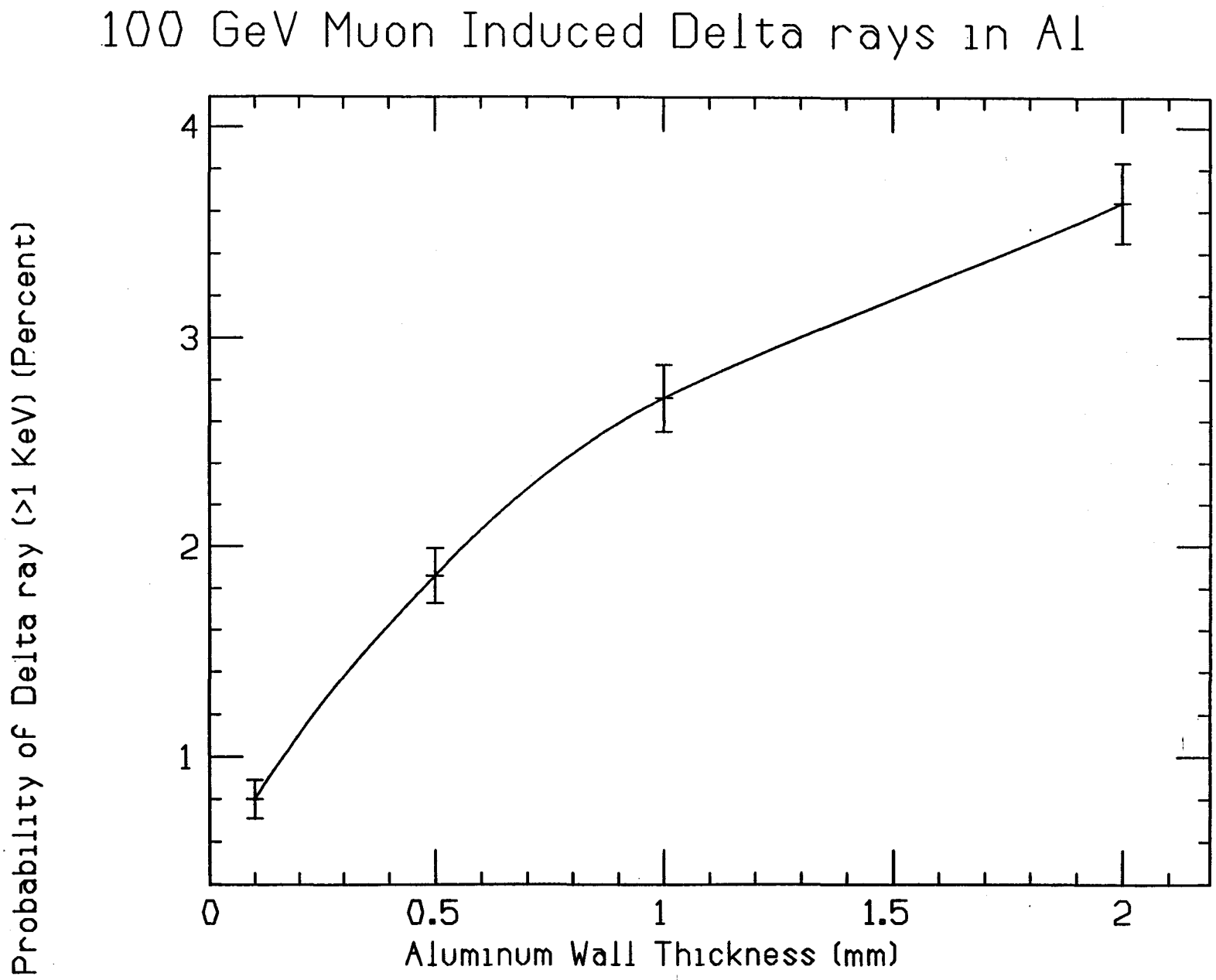
100 GeV Muon Induced Delta rays in Al
Probability of Delta ray (>1 KeV) (Percent)
4
3
2
1
0
0.5
1
1.5
2
Aluminum Wall Thickness (mm)

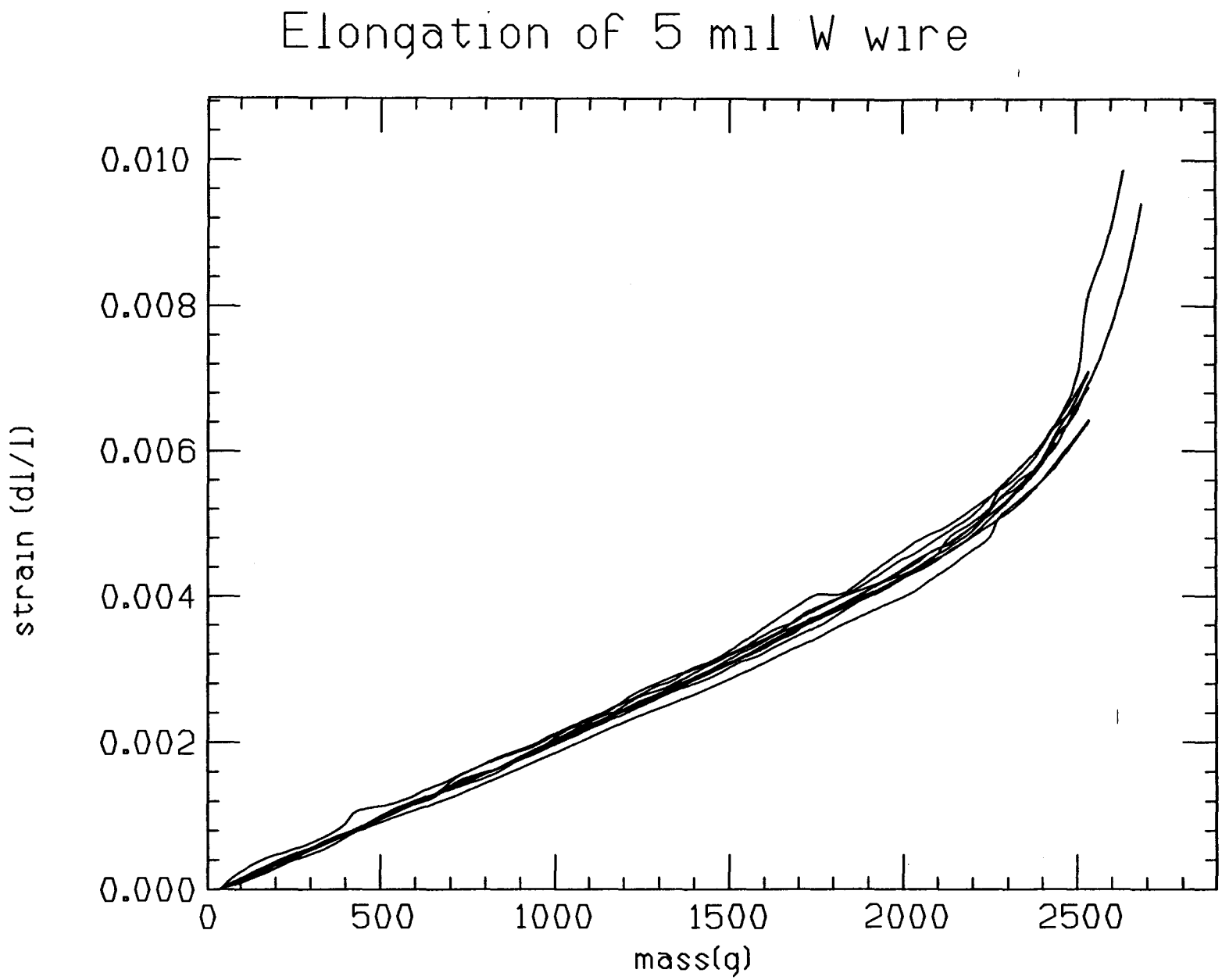
Elongation of 5 mil W wire
0.010
0.008
0.006
0.004
0.002
0.000
strain (dl/l)
0
500
1000
1500
2000
2500
mass(g)

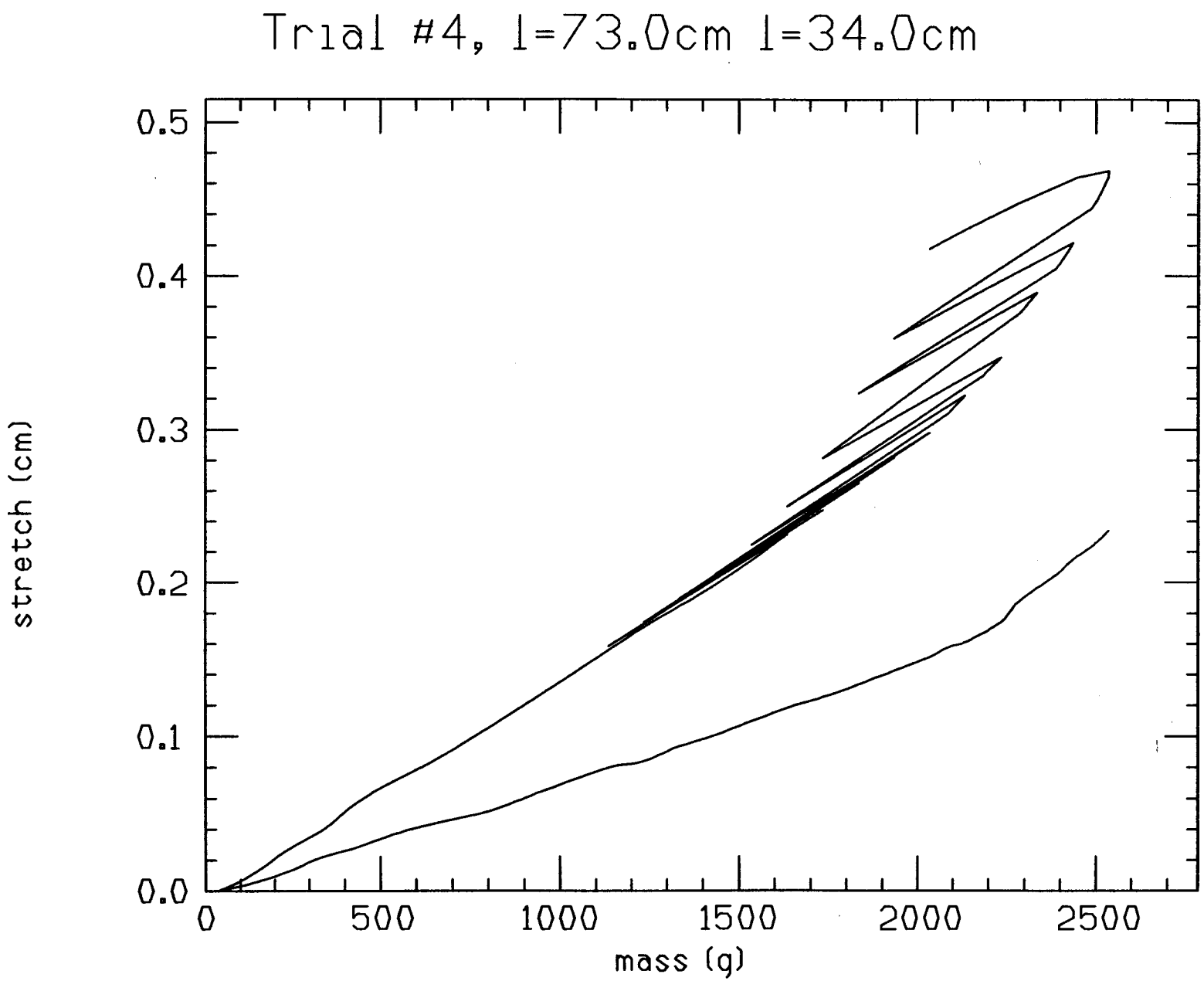
Trial #4, l=73.0cm l=34.0cm
0.5
0.4
0.3
0.2
0.1
0.0
stretch (cm)
0
500
1000
1500
2000
2500
mass (g)

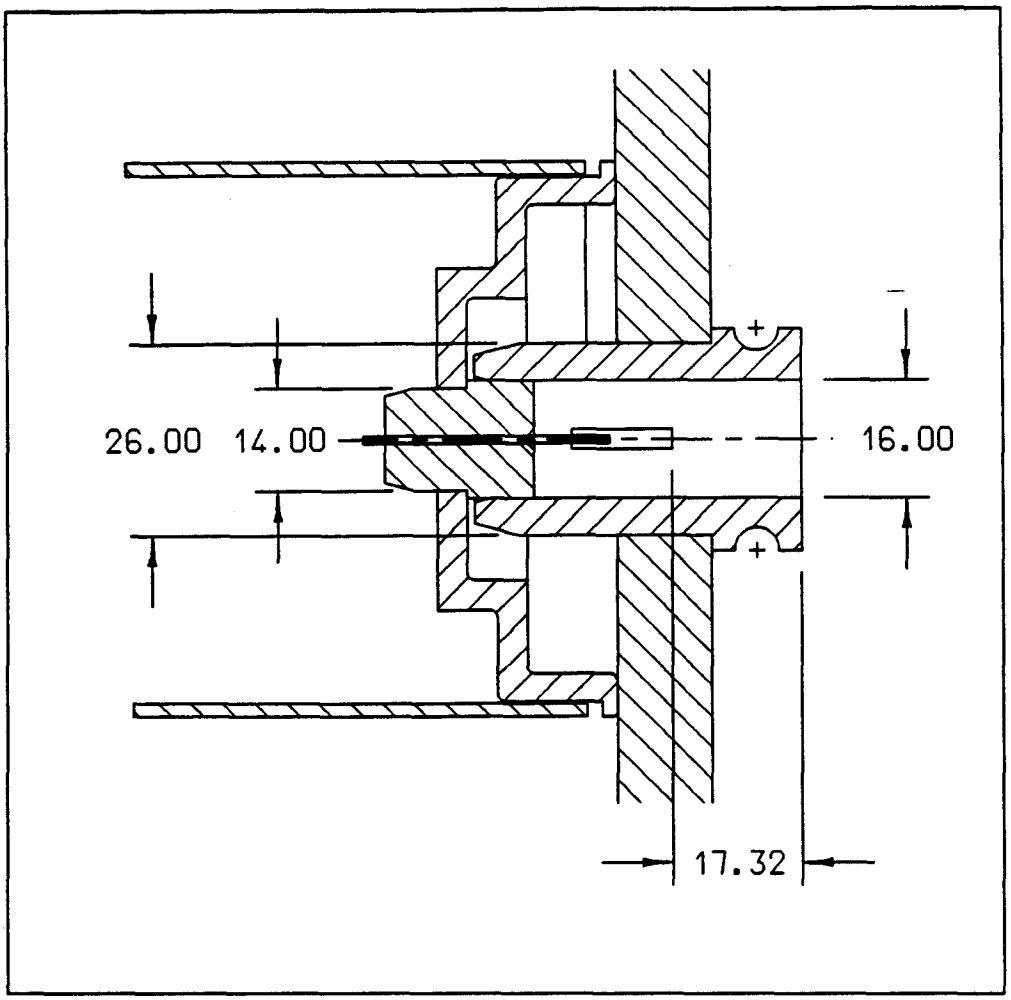

PRODUCED BY FF DRAWING FILENAME R4626032E
ON 12 / 12 / 91 AT 12 : 11 PLOTTED AT SCALE 1/1

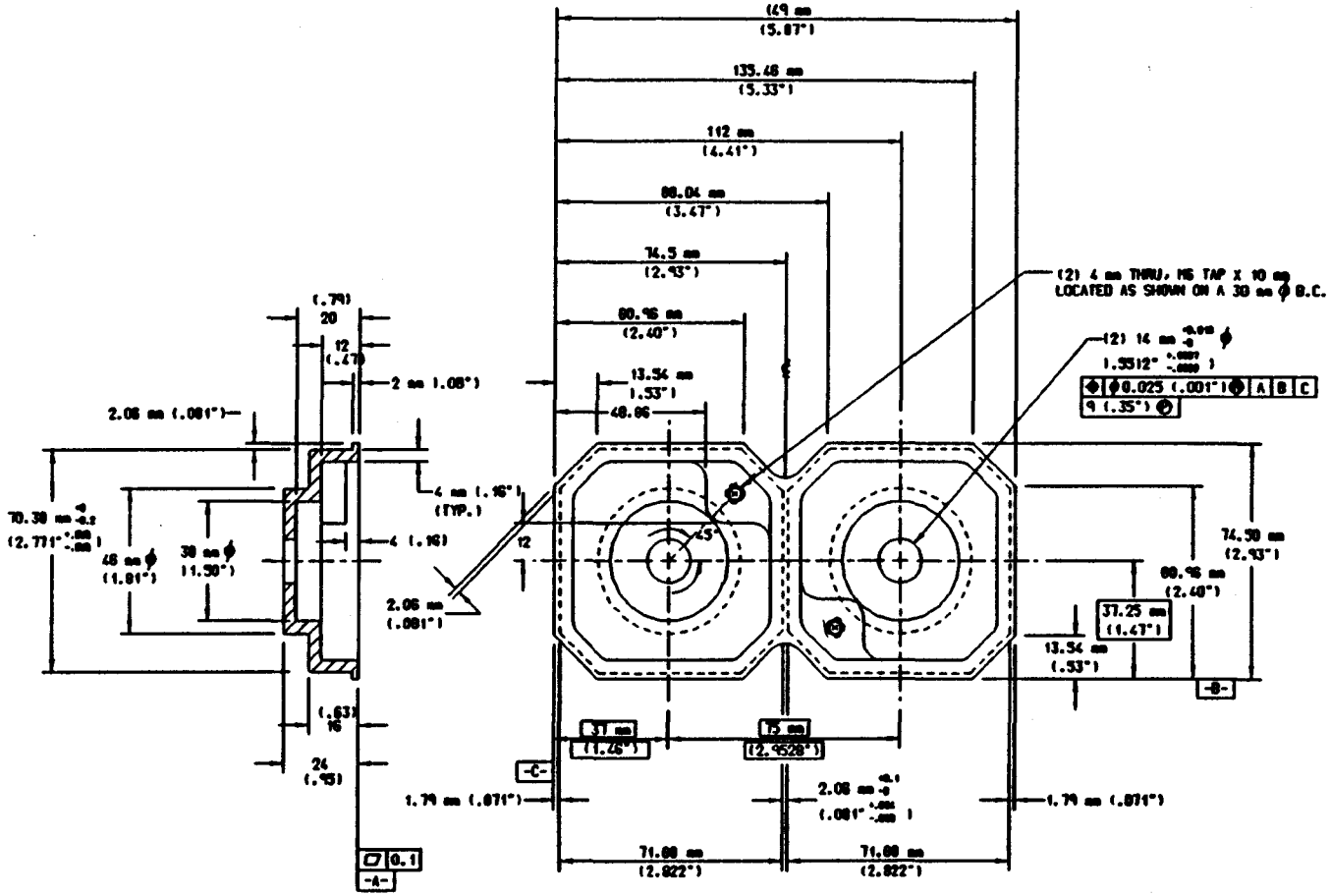

UNITS - mm(INCH)

REV	QTY	PART NO.	DESCRIPTION

DR. AMR	MAT'L DELRIN
CHK'D	SDC MUON SYSTEM DEVELOPEMENT
APPR'D	PROTOTYPE CHAMBER ASSEMBLY
MG. APPR.	END CAP

PHYSICAL SCIENCES LABORATORY
UNIVERSITY OF WISCONSIN

SCALE FULL | SHEET SIZE 4626E | DWG. NO. 4626C027
DATE 7-9-91

4626C027

SURFACE FINISH EXCEPT AS NOTED

TOLERANCES UNLESS OTHERWISE SPECIFIED
2 PLACE DECIMAL ±.005
3 PLACE DECIMAL ±.01
1 PLACE DEC., FRAC. ±1/32

CHANGE LETTER	CHG BY	REV BY	DATE	CHANGE

UNITS ARE INCHES UNLESS OTHERWISE SPECIFIED.
ANSI STANDARD Y14.5 APPLIES.

W FF DRAWING FILENAME R4626027C
/91 AT 16:43 PLOTTED AT SCALE 1/1

4626A025

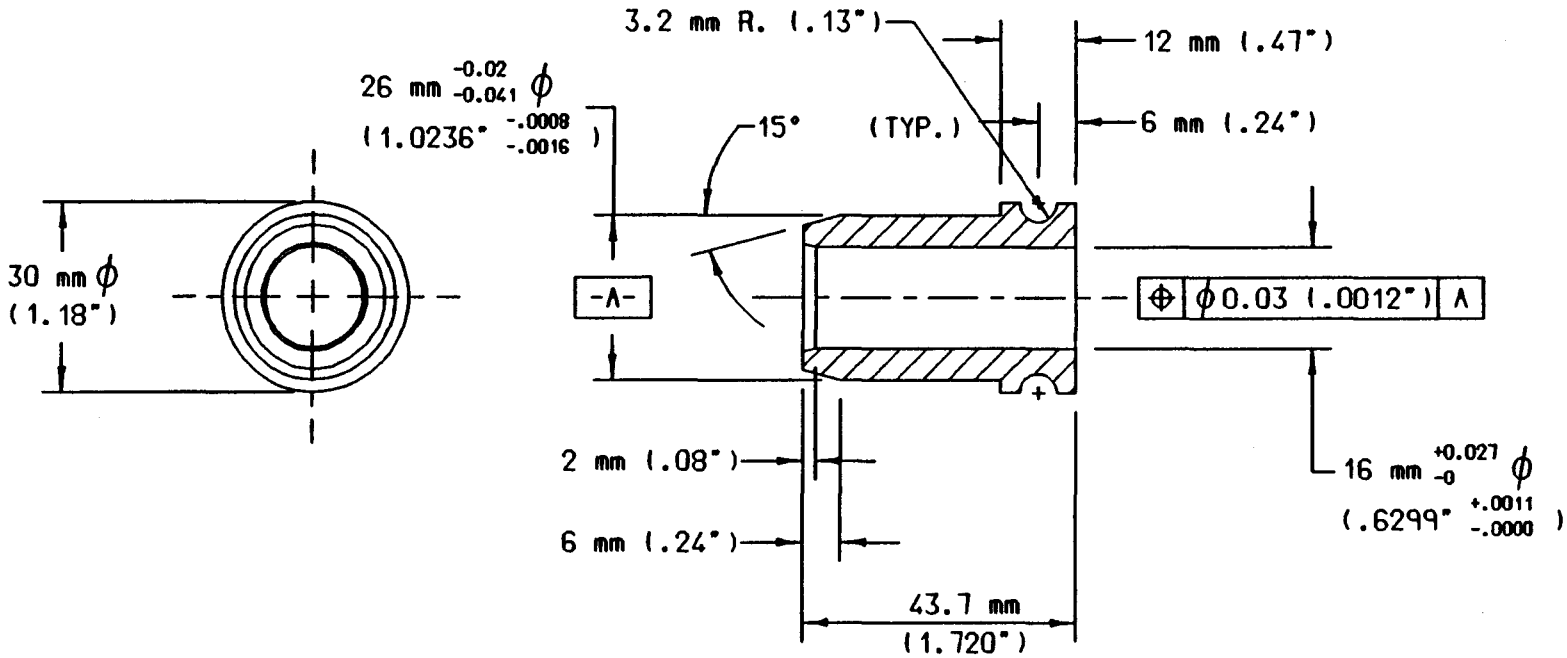

UNITS - mm(INCH)

UNITS ARE INCHES UNLESS OTHERWISE SPECIFIED. ANSI STANDARD Y14.5 APPLIES.		DR. AMR	KEY	Q'TY	PART NO.	DESCRIPTION
			MAT'L DELRIN			
	SURFACE FINISH EXCEPT AS NOTED:	CHK'D	SDC MUON SYSTEM DEVELOPEMENT			
		APPR'D	PROTOTYPE CHAMBER ASSEMBLY			
		NO. REQ. 68	LOCATOR PLUG			
	TOLERANCES UNLESS OTHERWISE SPECIFIED: 3 PLACE DECIMAL ±.005; 2 PLACE DECIMAL ±.01; 1 PLACE DEC., FRAC. ±1/32		PHYSICAL SCIENCES LABORATORY UNIVERSITY OF WISCONSIN (608)873-6651			
CHANGE LETTER	CHANGE		SCALE FULL	USED ON: 4626E	DWG. NO. 4626A025	
			DATE 7-9-91			

DRAWN BY PAFEC DOCS CAD V3.206B

PRODUCED BY FF ON 07/26/91 AT 16:42 DRAWING FILENAME R4626025A PLOTTED AT SCALE 1/1

4626A026

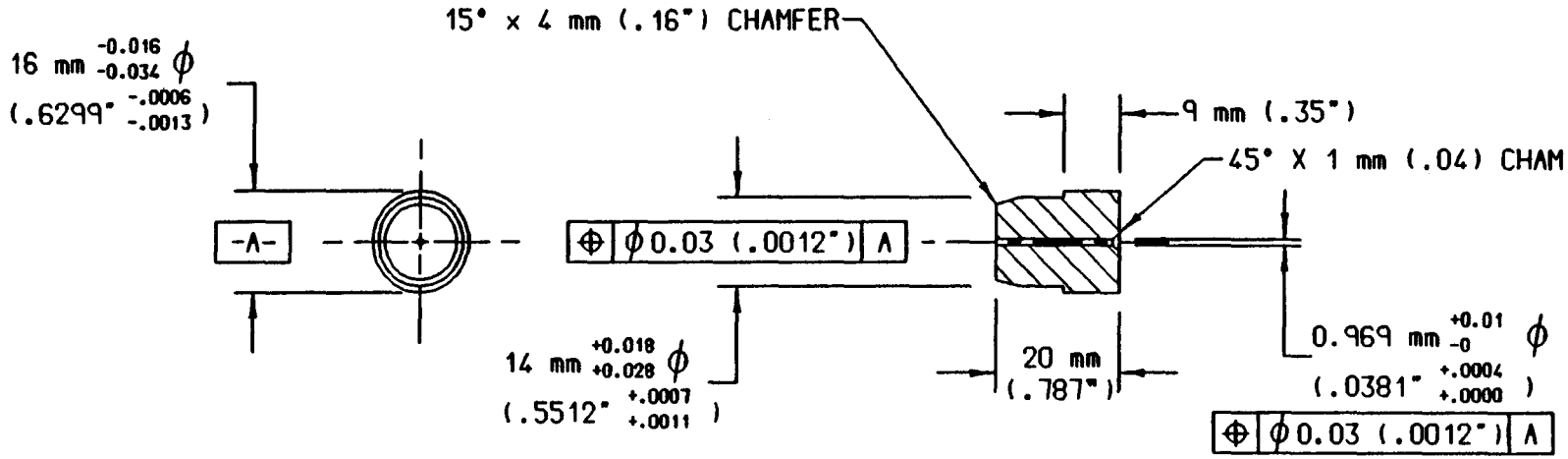

UNITS - mm(INCH)

UNITS ARE INCHES UNLESS OTHERWISE SPECIFIED. ANSI STANDARD Y14.5 APPLIES.			KEY	Q'TY	PART NO.	DESCRIPTION
		DR. AMR	MAT'L DELRIN			
		SURFACE FINISH EXCEPT AS NOTED: CHK'D	SDC MUON SYSTEM DEVELOPEMENT			
		APPR'D	PROTOTYPE CHAMBER ASSEMBLY			
		NO. REQ. 68	WIRE MOUNT			
		TOLERANCES UNLESS OTHERWISE SPECIFIED:	PHYSICAL SCIENCES LABORATORY UNIVERSITY OF WISCONSIN (608)873-6651			
		3 PLACE DECIMAL ±.005	SCALE FULL	USED ON:	DWG. NO.	
		2 PLACE DECIMAL ±.01				
CHANGE LETTER	CHANGE	1 PLACE DEC., FRAC. ±1/32	DATE 7-9-91	4626E	4626A026	

DRAWN BY PAFEC DOCS CAD V3.2068

FF DRAWING FILENAME R4626026A
/91 AT 16:42 PLOTTED AT SCALE 1/1

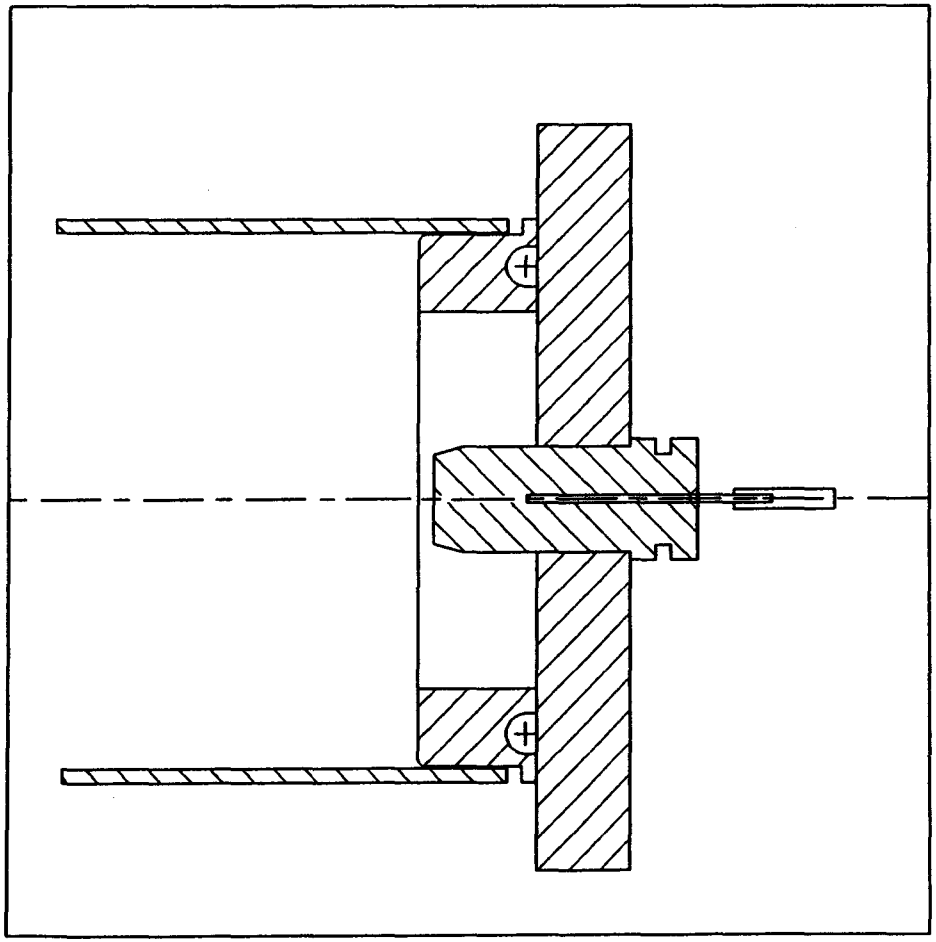

PRODUCED BY FF
ON 12 / 12 / 91 AT 12 : 12

DRAWING FILENAME R4626032E
PLOTTED AT SCALE 1/1

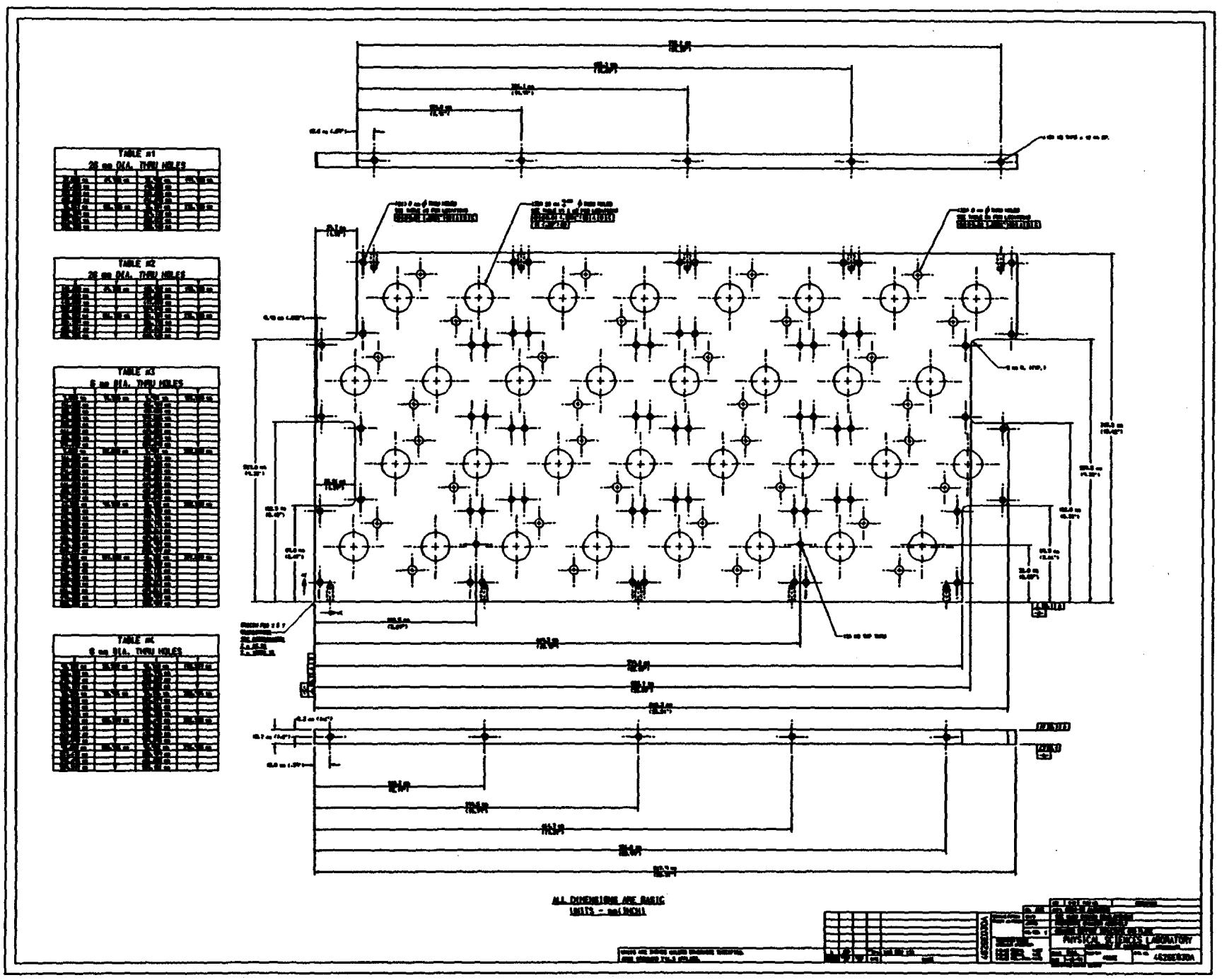

PRODUCED BY FF DRAWING FILENAME R4626030E
12 / 12 / 91 AT 12 : 17 PLOTTED AT SCALE 1/1

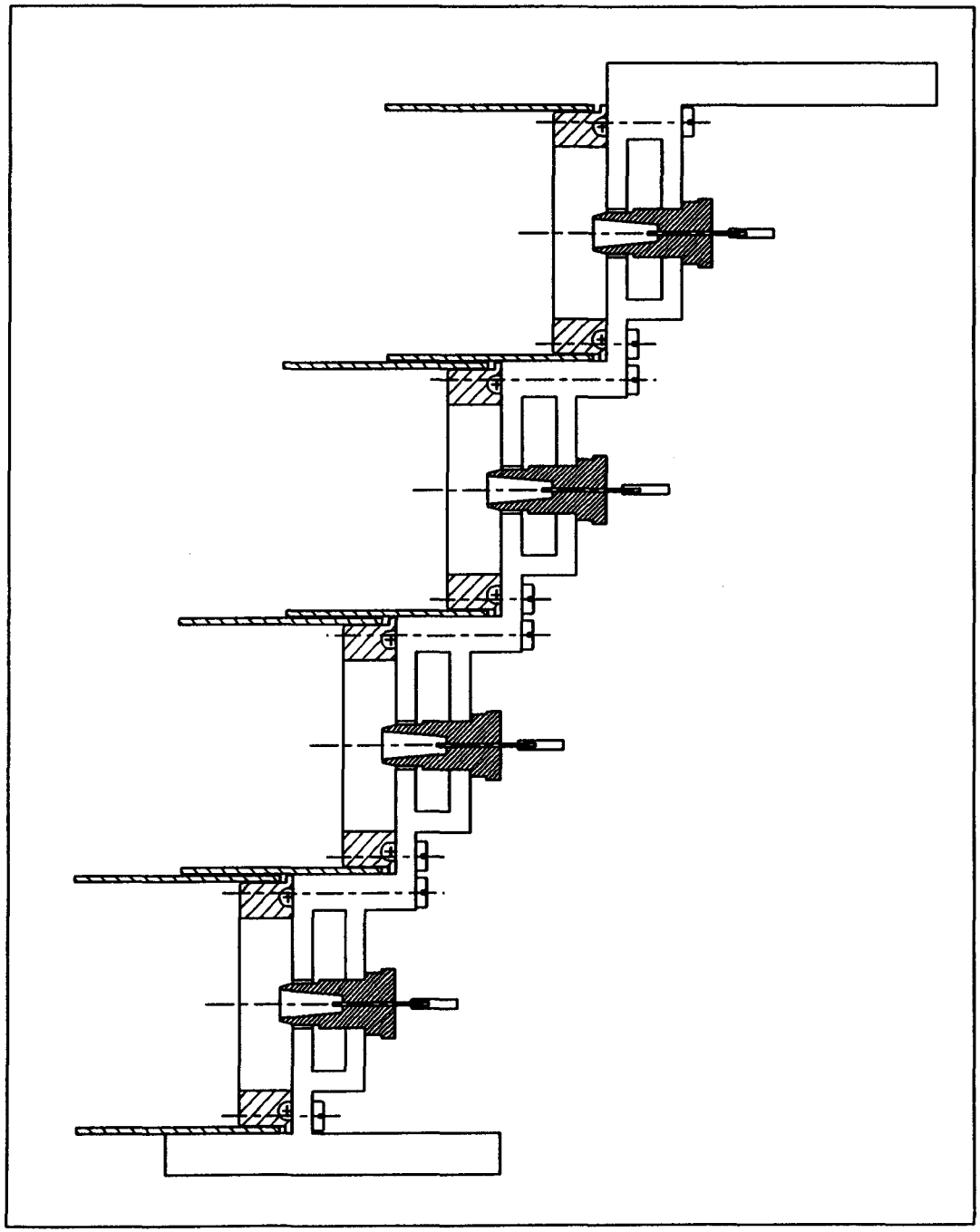

PRODUCED BY FF
ON 12 / 12 / 91 AT 12 : 14

DRAWING FILENAME R4626032E
PLOTTED AT SCALE 1/1

PSL meas.
27 Nov. '91

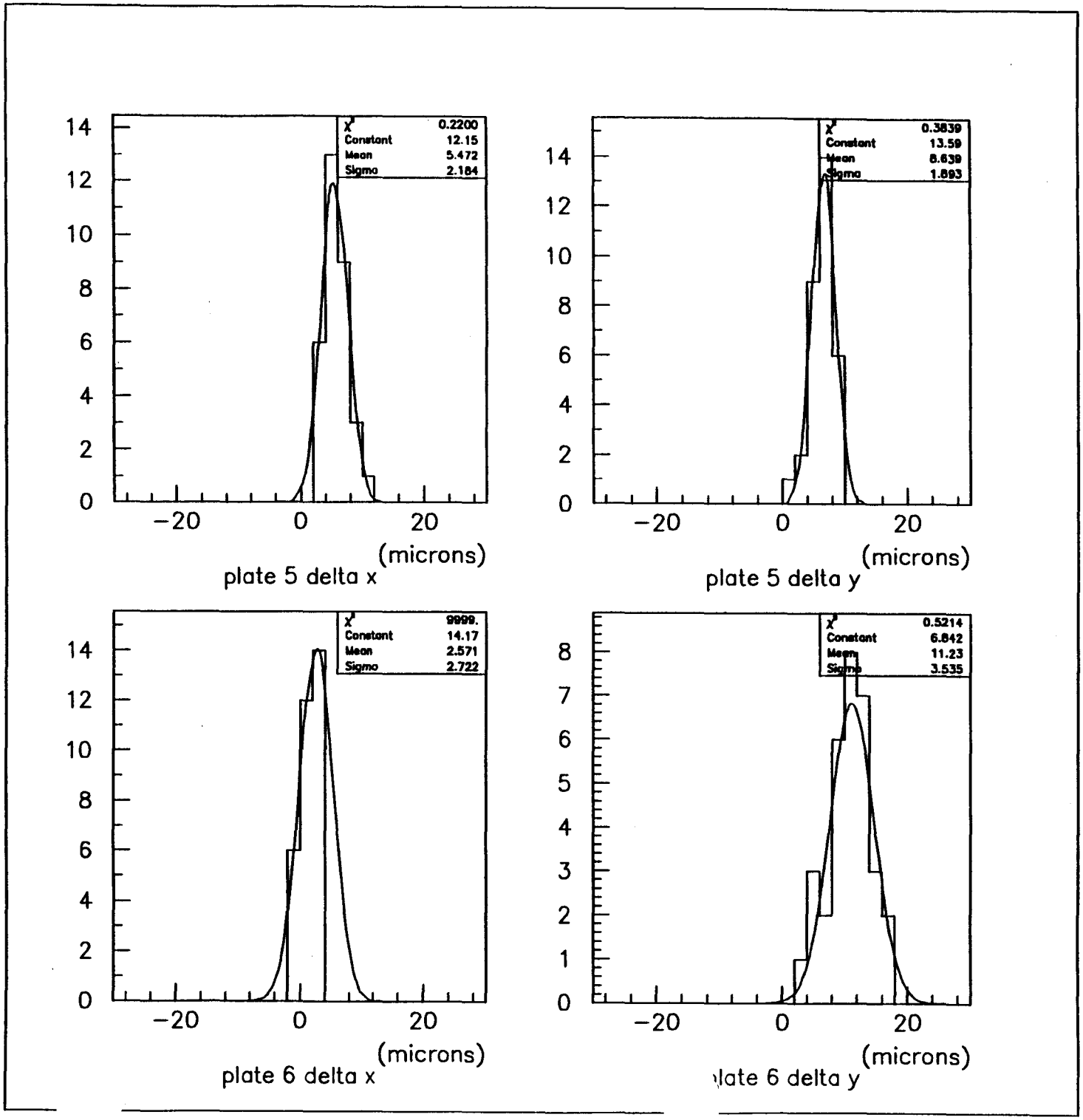

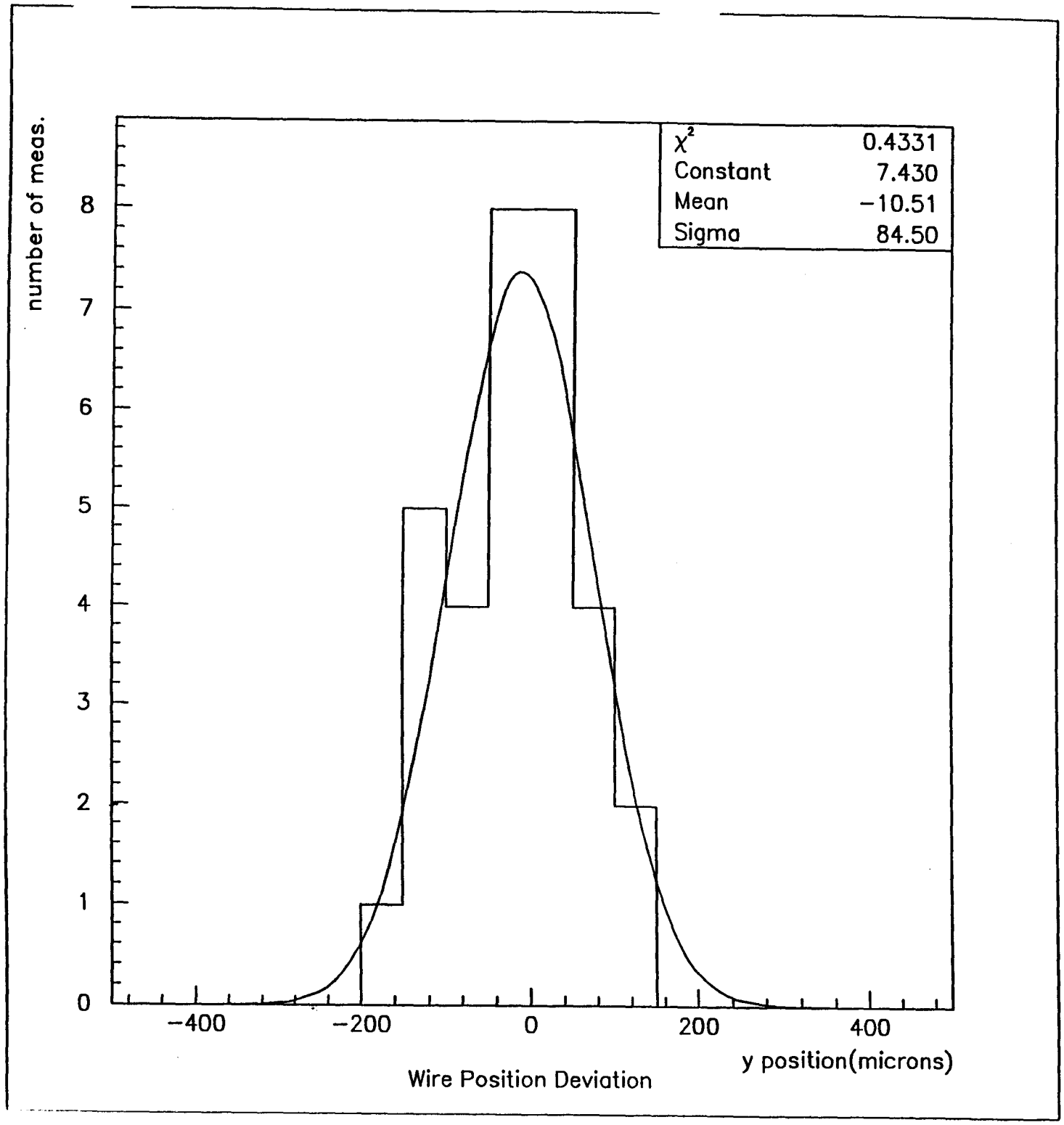
number of meas.
0
1
2
3
4
5
6
7
8
−400
−200
0
200
400
y position(microns)
Wire Position Deviation
χ²
0.4331
Constant
7.430
Mean
−10.51
Sigma
84.50

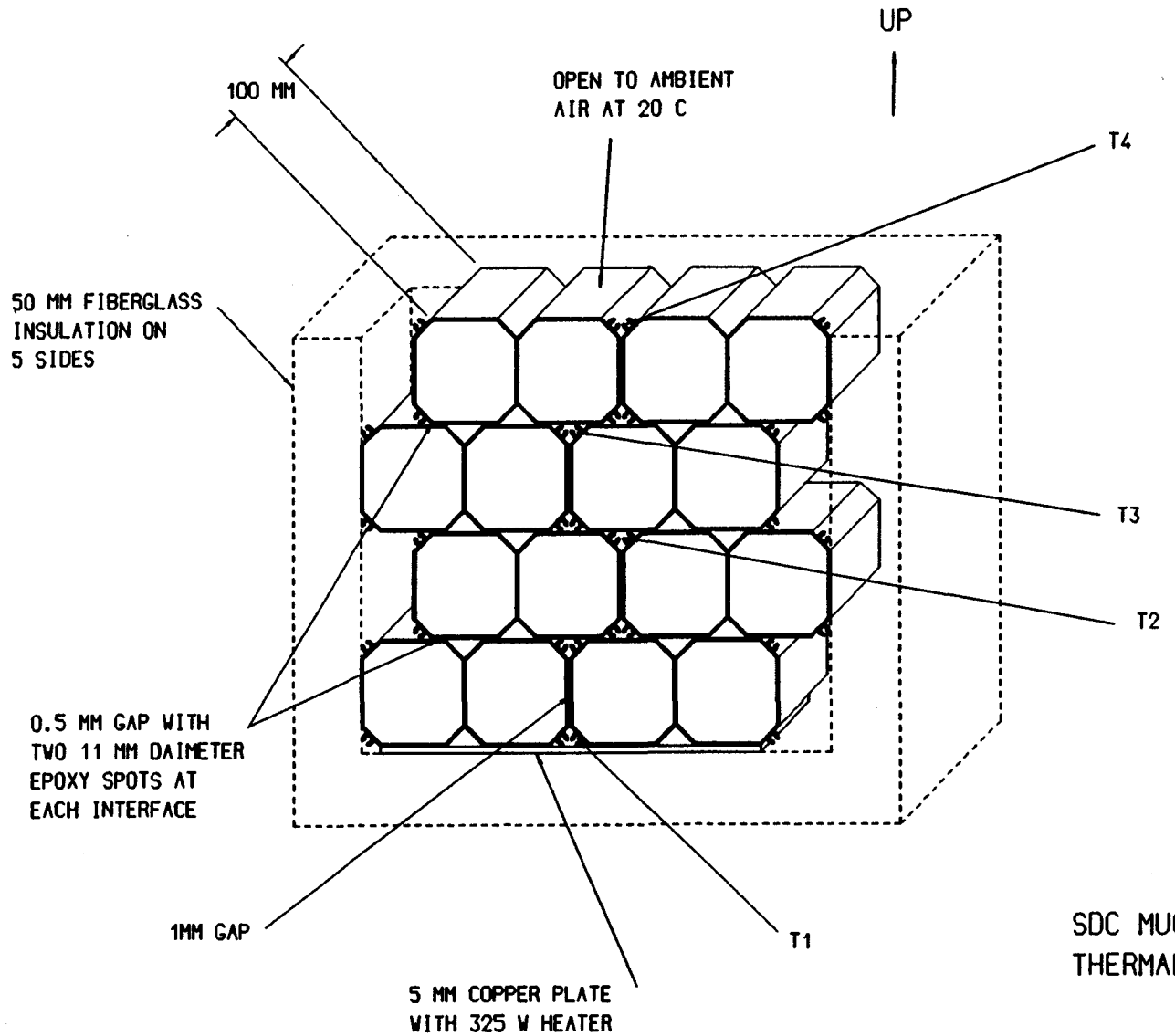

SDC MUON CHAMBER
THERMAL TEST SETUP

PRODUCED BY FF
2 / 12 / 91 AT 12 : 18

DRAWING FILENAME THERMAL
PLOTTED AT SCALE 1/1

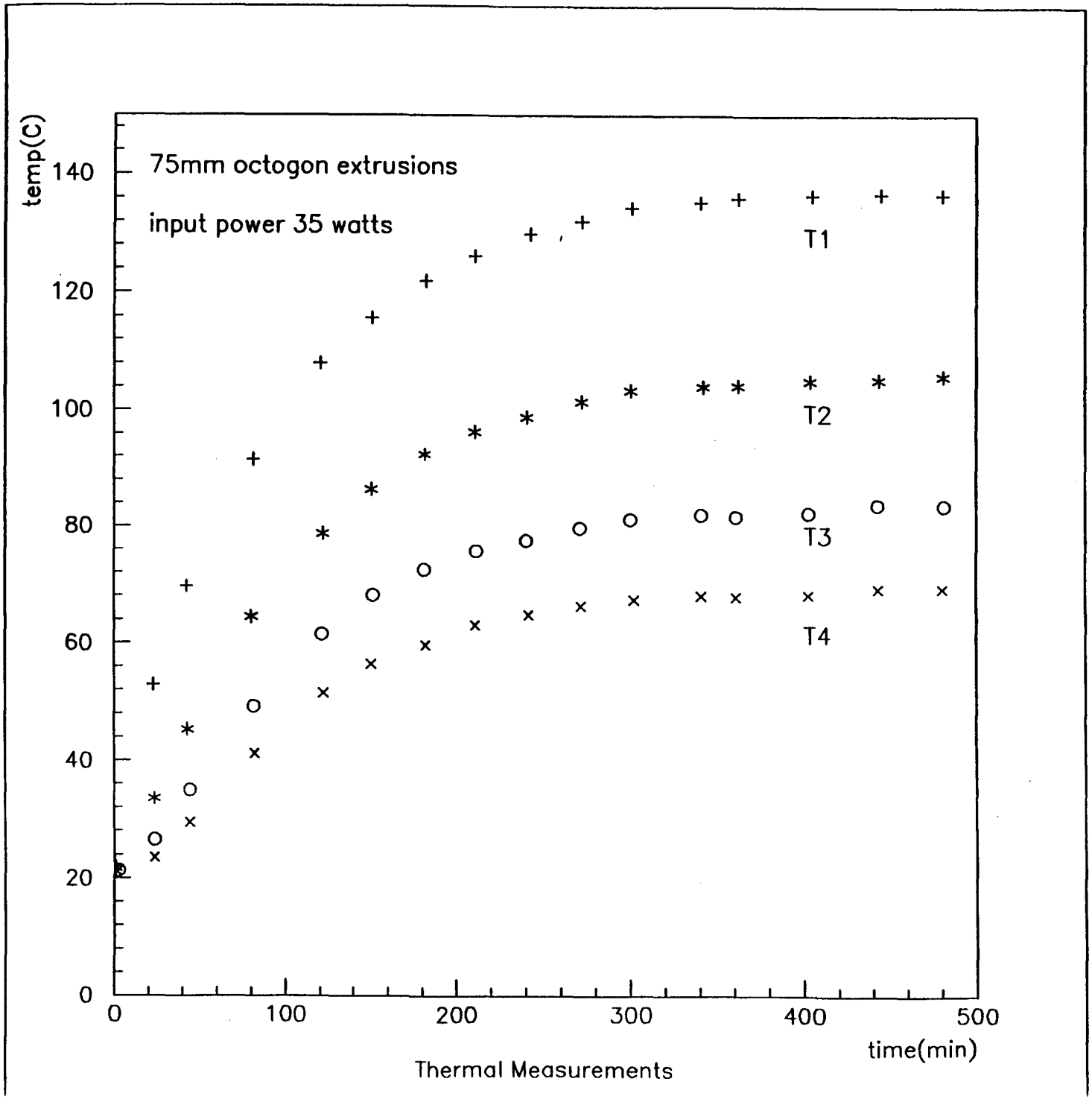
75mm octogon extrusions
input power 35 watts
temp(C)
140
120
100
80
60
40
20
0
0
100
200
300
400
500
time(min)
T1
T2
T3
T4
Thermal Measurements

Chapter 4

Supermodule Layout and Support Concept

4.1 Layout and Assembly

The entire surface of the iron toroid will be covered with drift tubes. Chamber modules are assembled in monolithic planes, and decks of monolithic planes into supermodules (BW1, BW2, and BW3) as illustrated in Figures 1.4-1.17. The dimensions and quantity of chambers of each type are given in Table 4.1. A number of special modules must be constructed to accomodate the cryostack and interferences with the toroid supports in the bottom octant but have not been separately itemized.

Each monolith is constructed from three or four muon modules. The endplates of the modules are crenellated to allow nesting of modules in a monolith and pinned together. It is possible to add single special tubes to the outside of a monolith to minimize the deadspace. Modules are assembled on a flat table and the endplates are pinned together with an alignment jig. It may be possible to simply glue monoliths together to form supermodules. We are exploring an alternate scheme in which 1/2" thick aluminum crossbraces (stringers) are glued to both the top and bottom surfaces of monoliths and used to pin monoliths into supermodules.

BW1 supermodules are mounted directly to the inner rail system on kinematic supports. BW2 and BW3 supermodules together with scintillator layers are premounted on a truss support structure to form a supertower which is mounted to the external rail system. The BW2 monoliths are mounted on the underside of the truss structure and BW3 monoliths on the top side. The scintillators are located to provide access to the phototubes from within the truss or outside the detector. Preliminary designs of the truss structure have been produced by Dave Eartly and company at Fermilab and some finite element analysis has been performed at PSL. In this chapter, some the details of the design considerations and tests are presented.

4.2 Barrel Truss Structure

A BW3 module has typical dimensions $9.0 \times 2.5 \times 0.3$ m^3 and weighs roughly 1.9 metric tons. The BW2 modules are $7.3 \times 2.5 \times 0.3$ m^3 and weigh 1.5 tons. The BW3 monolith is 9.0×7.5 m^2 and

may have a mass of 4700 kg. The scintillator unit mass is not well known but is assumed equal to that of a monolith.

The form of the truss will depend on support option chosen for the supermodules. Preliminary analysis of possible truss structures performed at PSL indicate that submillimeter maximum truss deflections are certainly attainable with a barrel truss freely loaded with supermodules without any use made of the rigidity of the modules themselves. Whether an entire truss may be supported on kinematic mounts from the rail system remains to be determined.

Example finite element calculations are illustrated in Figures 4.1 through 4.8 for a model truss structure constructed from weld 3 inch O.D. tubing. A steel structure is about a factor 2 stronger than aluminum but introduces a thermal expansion differential relative to aluminum modules. The maximum deflection of this first pass structure is 300 micron.

4.3 Supermodule Mounting Options

The shape of a horizontal beam of length L simply supported at fractional distances a and b from on end is given by

$$y = \frac{WL^4}{YI}[-\frac{x^4}{24} + \frac{R_a}{6}\theta(x-a)(x-a)^3 + \frac{R_b}{6}\theta(x-b)(X-b)^3 + c1x + c2] \tag{4.1}$$

$$R_a = \frac{b-1/2}{b-a} \ : \ R_b = -\frac{a-1/2}{b-a} \tag{4.2}$$

$$c1 = \frac{1}{b-a}[\frac{(b^4-a^4)}{24} - \frac{R_a}{6}(b-a)^3] \ ; \ c2 = \frac{a^4}{24} - c1 \times a \tag{4.3}$$

In these expressions, W is the weight per unit length, Y is the elastic modulus, I is the area moment of inertia, x is the fractional distance along the beam, θ denotes a Heaviside step function, and y(x) is the deflection. The range of beam shapes obtained for symmetrical supports are illustrated in Figure 4.9. The sag of the mass between the support points may be counteracted by the overhanging mass. As illustrated in Figure 4.10, as the supports are moved inboard, the ends first move up relative to the supports and then back down to zero at the 20 percent locations. The sag at the center of the beam is greatly reduced for this support configuration.

The sag goes like the fourth power of length and the inverse square of thickness. A single wire cell supported from the ends sags 5 mm for a length of about 5 m. A four layer honeycomb stack is about a factor of 9 stronger, roughly independent of wall thickness or cell size. A 4 layer module simply and quasicontinuously supported from the ends is measured to sag 5 mm for 9 meter length. This figure corresponds to a BW3 θ monolith with several supports from the truss to the module endplates. The shear stress developed in between layers appears well within adhesive specifications.

If θ and ϕ monoliths are continuously bonded, the rigidity of a supermodule is increased by a factor of two since the weight and thickness double and the sag is halved. The scintillator load, if not absorbed into the truss directly, could increase the total load by 50 percent. The few mm sag would have negligible effect on the θ tube operation. The distortion in the ϕ tube endplates could be measured or reduced by additional supports from the truss. For BW2 chambers, the problem is similar. The BW1 supermodules are shorter and the sag in this model may be expected to be a

factor 7.5 less than that of BW3 without the scintillator. It therefore appears that direct support from the endplates is a posible option.

The central sag may be reduced by a factor of 16 by moving the rails inboard to the 20 percent points. This strategy leads to negligible sag but implies a) a less direct connection between the endplates and support system, and b) load carrying capability by the monoliths. A support model under consideration is to assemble supermodules from θ and ϕ monoliths with stringers as described above and to support supermodules on 4 discrete kinematic mounts within the truss (BW2 and BW3) or on the rails (BW1).

A conservative estimate of the worst case sag is to consider a BW3 θ monolith with a ϕ monolith as dead weight. The sag for four "point" supports is estimated as the the sag for two continuous supports along the θ direction plus the sag for two continuous supports along the ϕ direction. The maximum sag of a BW3 top monolith supported in this way has been calculated to be 120 micron. If the load is transferred directly through the chamber, the same figure applies to θ and ϕ monoliths. Smaller figures obtain for BW1 or if shear is transfered between monoliths. At this level, thermal and assembly effects might be expected to dominate.

4.3.1 Extrusion crush test

The stringer support model places a BW3 supermodule load of order 15000 kg on four points on the chamber. If we assume .50 m wide stringers and effective area of $4 \times .25 = 1\ m^2$, we estimate a pressure of 1.5 kg per square cm. When the weight of a supermodule is carried through the Al extrusions there is a tendency for the extrusions to deform, very much like a circular extrusion. One method of local internal buttressing is to replace the air gaps between tubes locally with material to develop a local I-beam structure. This might be accomplished with special extrusions or with prism shaped stiffeners as illustrated in Figure 4.11. The measured deformation of a 100 mm length of extrusion loaded by a press equally on the two wire cells is shown in Figure 4.12. In this arrangement, a load of 500 lbs corresponds to the above pressure estimate and results in about 1.5 mm deformation. With an aluminum prism glued in the triangular region in the extrusion, the deformation at the estimated load is reduced to of order 200 micron.

4.4 Gas Handling System

A preliminary model gas handling system has been prepared by D. Eartly of Fermilab. The central system is estimated to have a gas volume of 72,000 cubic feet and a flow of 288 SCFH distributed in major manifolds which run parallel to the support rails and tie in a supermodule based distribution and monitoring system. A recirculating system including scrubbing and makeup mixing is warranted by virtue of the large volume.

The gas distribution system within a supermodule has not been specified. A system which feeds gas to each module with modules run in series is a possible model. We have begun to study a parallel gas flow system that might minimize the purging time during assembly. We can report preliminary tests of a flow in a prototype parallel piping system. In the prototype, gas enters and leaves each two cell extrusion by a 1/4 inch O.D. plastic pipe. A "paper punch" hole in the central wall at one end allows gas to flow into one tube and back the other in a single extrusion. Each pipe connects to a manifold by a 1/4 inch T. The manifold is formed by the T's connected

with 1/4 inch O.D. Ployflo tubing. The gas manifolding is shown in Figure 4.11. A mockup of the gas (Figure 4.12) system for 6 extrusions was prepared with the low impedance drift tubes omitted and 1/8 inch O.D. pressure taps inserted at each T. As shown in Figure 4.13, although the impedance appears to be the same in all paths, pressure differences of as much as a factor of four are observed. More detailed studies are required to ensure proper gas flow in all tubes in the final design.

4.5 Electronics

Our design philosophy goal is to make all active circuit elements accessible. Studies of the frontend electronics are underway by John Oliver at Harvard and trigger electronics is being designed by Jay Chapman at Michigan. Because the tube impedance is much larger than that of any small cable transmission line, if the analog signals are to be transported more than of order 1 meter, pulse transformers are required to avoid reflections. Commercial 80 MHz pulse transformers from Pulse Engineering survive a magnetic field of 200 Gauss so we do not expect toroid fringe fields to pose a difficulty. If the front-end cards are paved along the module surface, this complication might be avoided. However, it would appear cost effective to cluster the front ends for servicing.

We anticipate using amplifier-shaper-discriminator (ASD) circuits developed at the University of Pennsylvania. The circuits will likely be packaged in small cards supporting either 16 or 32 channels. By virtue of large scale integration, the card size will be determined by the connector size. The cards will be located on the accessible surface of the modules (inner surface of BW1 and BW3, outer surface of BW2).

Signals will be capacatively coupled from one end of each wire to a passive transformer to match the tube characteristic impedance to a transmission line. The signals may then transported to custom crates containing frontend and trigger electronics. High voltage may be distributed at either the near or far end of the tube through isolation resistors. A capacitively coupled resistive termination equal to the tube impedance is placed at the far end of each tube to avoid reflections. This termination may be place directly at the tube end and become inaccessible. Alternatively, signals at this end would be capacitive coupled (possibly again through transformers) to remote accessible termination cards.

4.6 Statistics

Barrel Chamber Layout - - Wisconsin option

29 November 1991

Barrel Toroid dimensions: half length = 14.016 m, radius = 6.750 m

Chamber sizes and counts

Wire direction	quantity	width(m)	length(m)	cells/ layer	layers	comment
BW1 (outer radius = 6.570 m; supermod = 5.440 x 7.51 msq)						
theta	48	2.50	5.44	33	4	3 chamb/supermod
spec. theta	20	1.78	5.44	23	4	2 cham/supermod octants 1,2,4,6,8
phi	48	1.73	7.51	23	4	3 cham/supermod
spec. phi	30	1.73	3.56	23	4	
BW2 (outer radius = 8.930 m; supermod = 7.320 x 7.383 msq)						
theta	80	2.50	7.32	33	4	3 cham/supermod
spec. theta	16	1.51	7.32	20	4	end supermods are slightly shorter
BW3 (outer radius = 10.960 m; supermod = 9.08 x 7.51 msq)						
theta	96	2.50	9.08	33	4	3 cham/supermod
phi(8.83m wide)	128	2.21	7.51	29	4	4 cham/supermod
stereo	128	1.97	7.26	26	2	10 deg wrt phi, 4 cham/supermod

Wire and Channel count

BW1 theta wires = 6336 + 1840 = 8176 (channel count identical)
phi wires = 4416 + 2760 = 7176 (channel count = 3588)

BW2 theta wires = 10560 + 1280 = 11840 (channel count identical)

BW3 theta wires = 12672 (channel count identical)
phi wires = 14848 (channel count = 7424)
stereo wires = 6656 (channel count = 3328)

totals: barrel wires = 61368

IW2

theta	48	.73	6.49	9	4
(ave)					
phi	16	5.59	2.18	74	4

IW3

theta	160	.59	7.76 (ave)	8	4

IW2 theta wires = 1728

```
IW2  phi   wires = 4736

IW3  theta wires = 5120

totals:   intermediate wires    = 11584
```

4.7 Figure Captions

Figure 4.1 Model truss structure of 3 inch tubing with 10 supports.

Figure 4.2 Model truss supporting modules from endplates around perimeter.

Figure 4.3 Deflections of loaded steel truss. The maximum deflection is 300 micron.

Figure 4.4 Same as Figure 4.3 with aluminum truss.

Figure 4.5 Endview of loaded aluminum truss, top octant.

Figure 4.6 Endview of loaded aluminum truss, 45 degree octant.

Figure 4.7 Endview of loaded aluminum truss, side octant.

Figure 4.8 Endview of loaded aluminum truss, 45 degree octant.

Figure 4.9 Beam shapes for various support locations.

Figure 4.10 Center and endplate location versus support posiiton.

Figure 4.11 Compression stiffener for 4 point kinematic support option.

Figure 4.12 Measured module deformation with and without prisms.

Figure 4.13 Test modules for measuring mechanical properties.

Figure 4.14 Prototype Gas Manifolding

Figure 4.15 Parallel Gas Flow Test Setup.

Figure 4.16 Variation of pressure with flow rate in test setup.

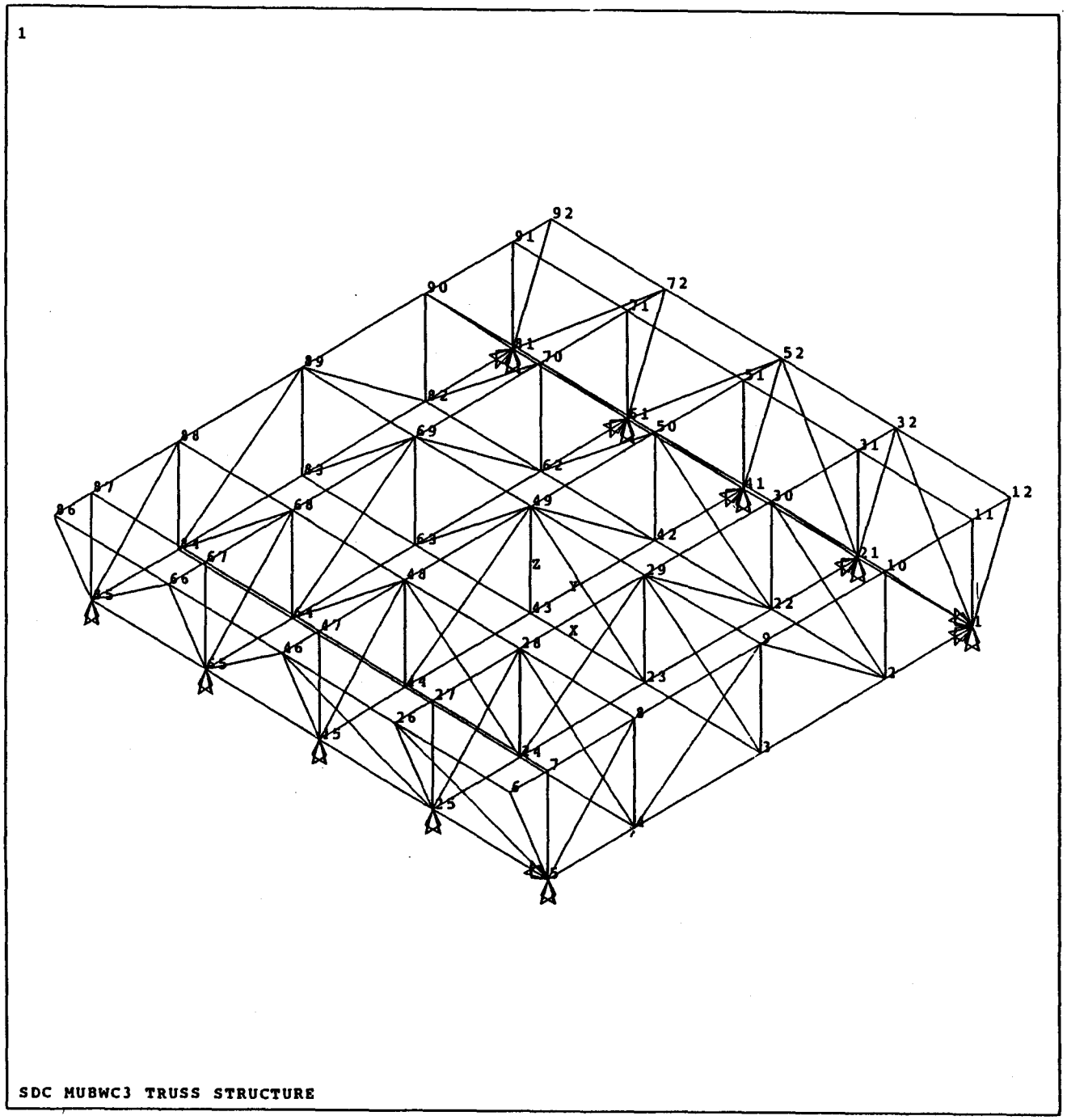

ANSYS 4.4A
MAY 21 1991
11:30:51
PLOT NO. 1
PREP7 ELEMENTS
TYPE NUM
TDIS

XV =1
YV =-1
ZV =1
DIST=6.503
ZF =0.7875
ANGZ=-60

DOF 547
WE · 160.5 rms
W(343 max

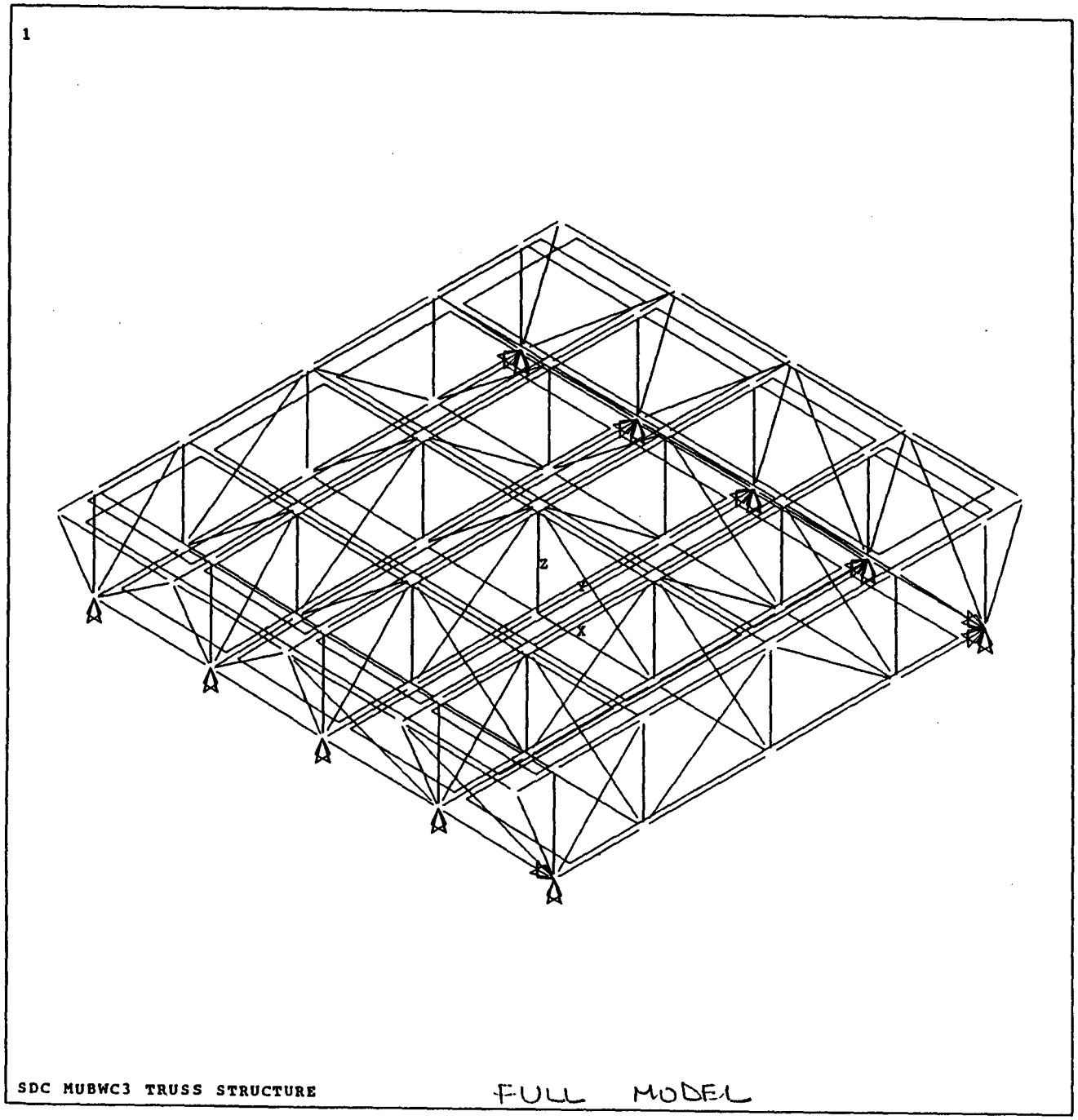

ANSYS 4.4A
MAY 21 1991
11:44:07
PLOT NO. 7
PREP7 ELEMENTS
TYPE NUM
TDIS

XV =1
YV =-1
ZV =1
DIST=6.503
ZF =0.7875
ANGZ=-60

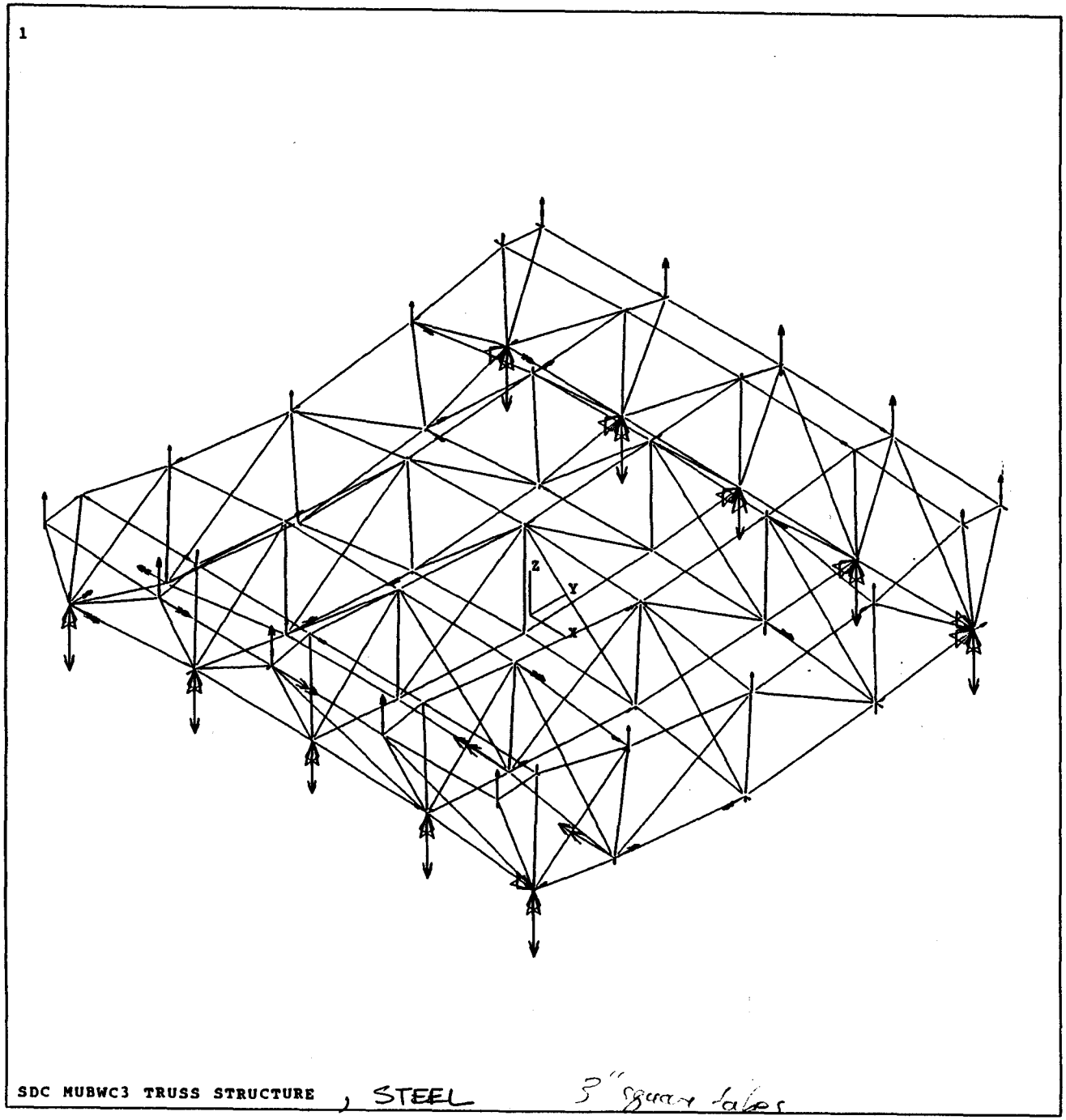

ANSYS 4.4A
MAY 21 1991
16:31:19
PLOT NO. 2
POST1 DISPL.
STEP=1
ITER=1
DMX =0.300E-03 3X10N
ERPC=0
TDIS
FORC
MOME

DSCA=2169
XV =1
YV =-1
ZV =1
DIST=6.503
ZF =0.7875
ANGZ=-60

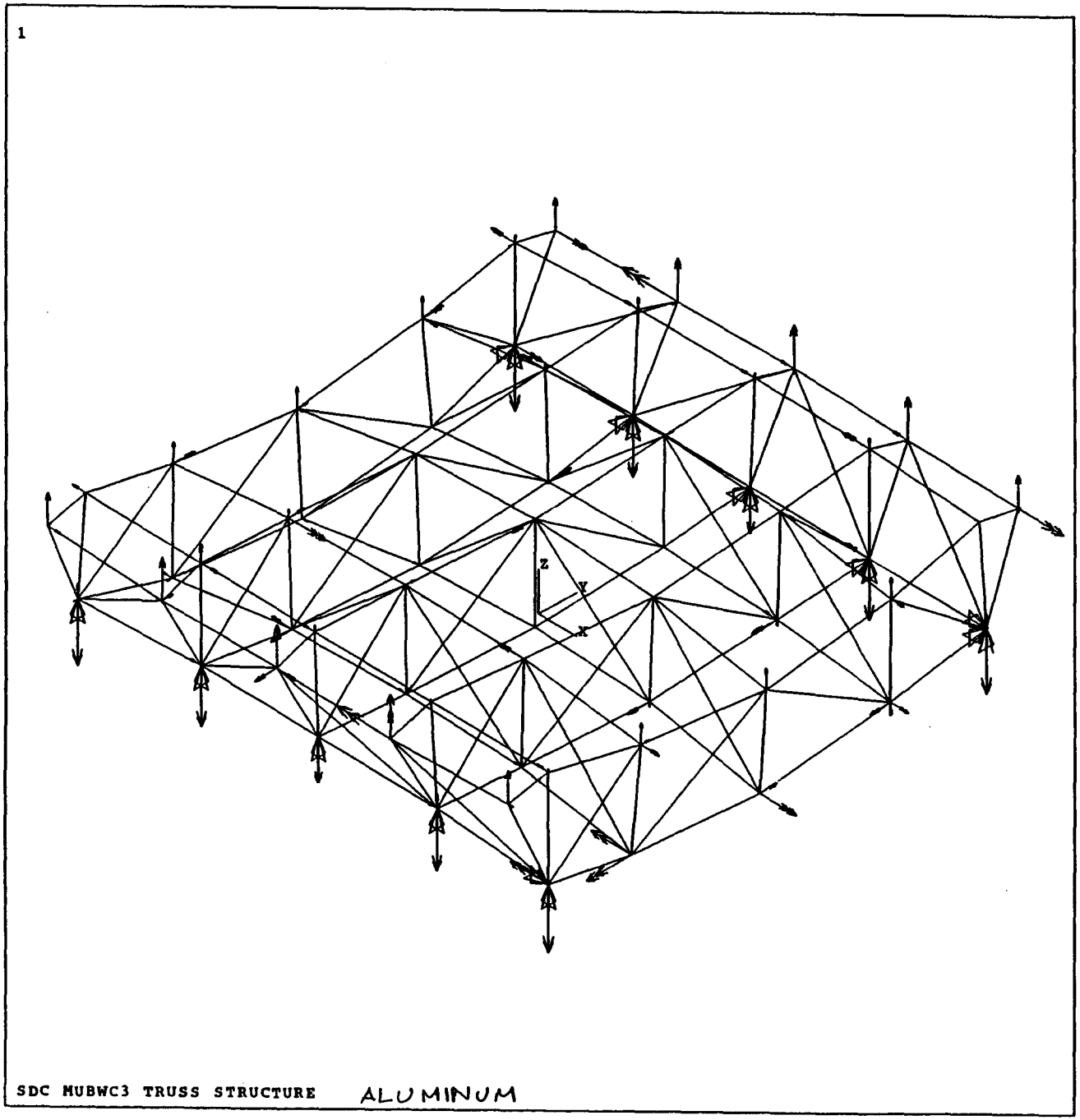

ANSYS 4.4A
MAY 28 1991
13:22:02
PLOT NO. 2
POST1 DISPL.
STEP=1
ITER=1
DMX =0.574E-03
ERPC=0
TDIS
FORC
MOME

DSCA=1134
XV =1
YV =-1
ZV =1
DIST=6.503
ZF =0.7875
ANGZ=-60

1

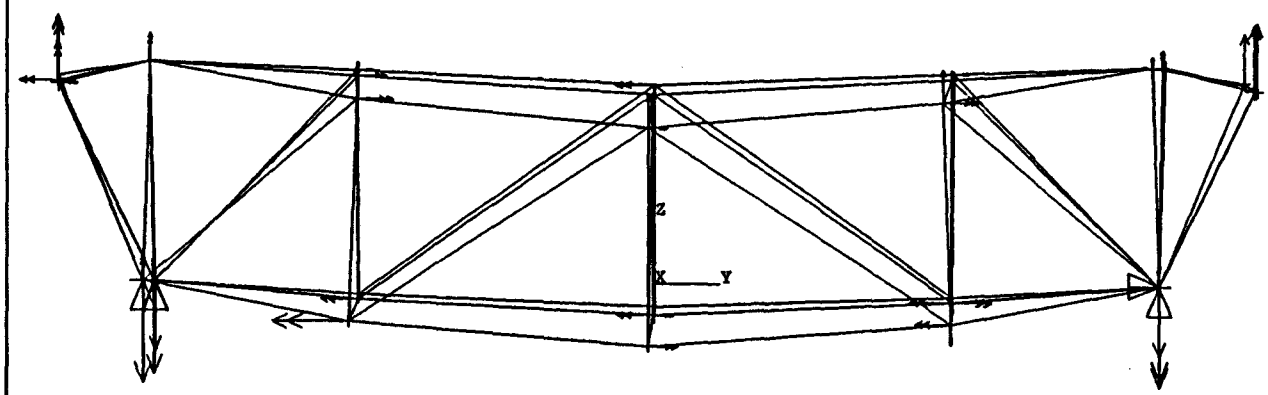

SDC MUBWC3 TRUSS STRUCTURE , ALUMINUM

ANSYS 4.4A
MAY 29 1991
16:47:42
PLOT NO. 9
POST1 DISPL.
STEP=1
ITER=1
DMX =0.574E-03
TDIS
FORC
MOME

DSCA=836.137
XV =1
DIST=4.796
ZF =0.7875
ANGZ=-90

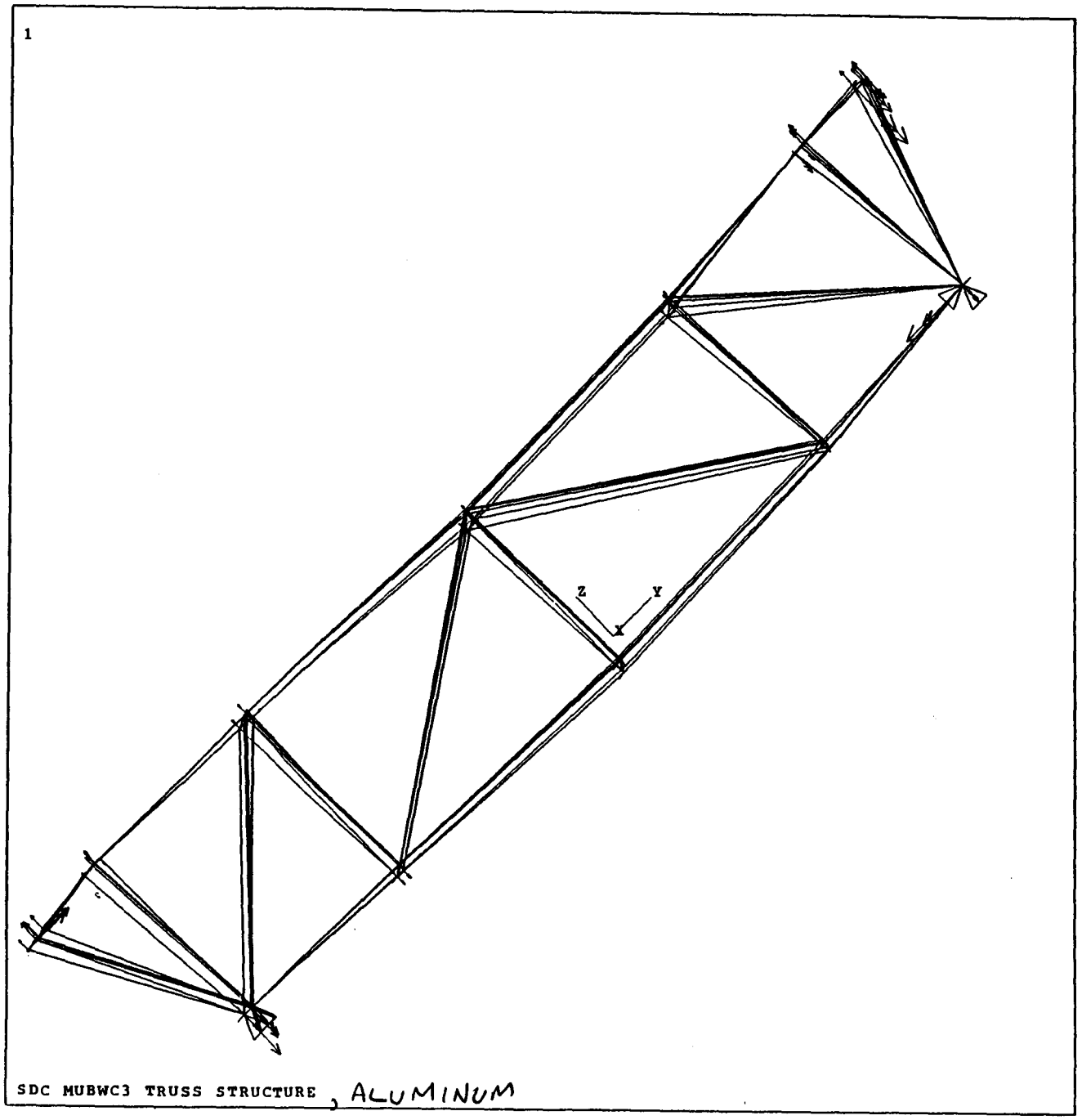

ANSYS 4.4A
MAY 29 1991
16:49:57
PLOT NO. 10
POST1 DISPL.
STEP=2
ITER=1
DMX =0.001135
TDIS
FORC
MOME

DSCA=352.912
XV =1
DIST=4.004
ZF =0.7875
ANGZ=-45

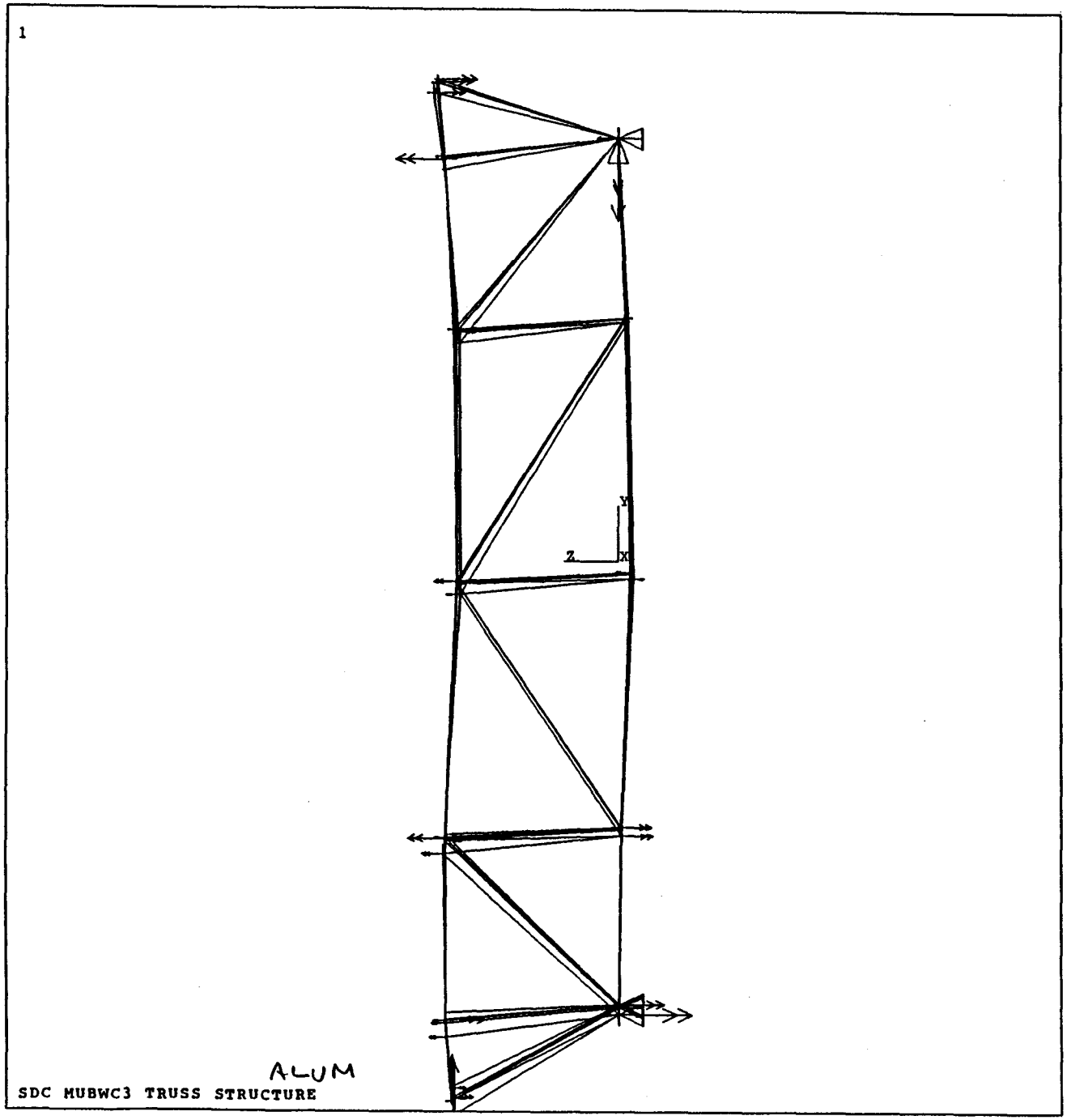

ANSYS 4.4A
MAY 29 1991
16:50:30
PLOT NO. 11
POST1 DISPL.
STEP=3
ITER=1
DMX =0.001519
TDIS
FORC
MOME

DSCA=315.653
XV =1
DIST=4.796
ZF =0.7875

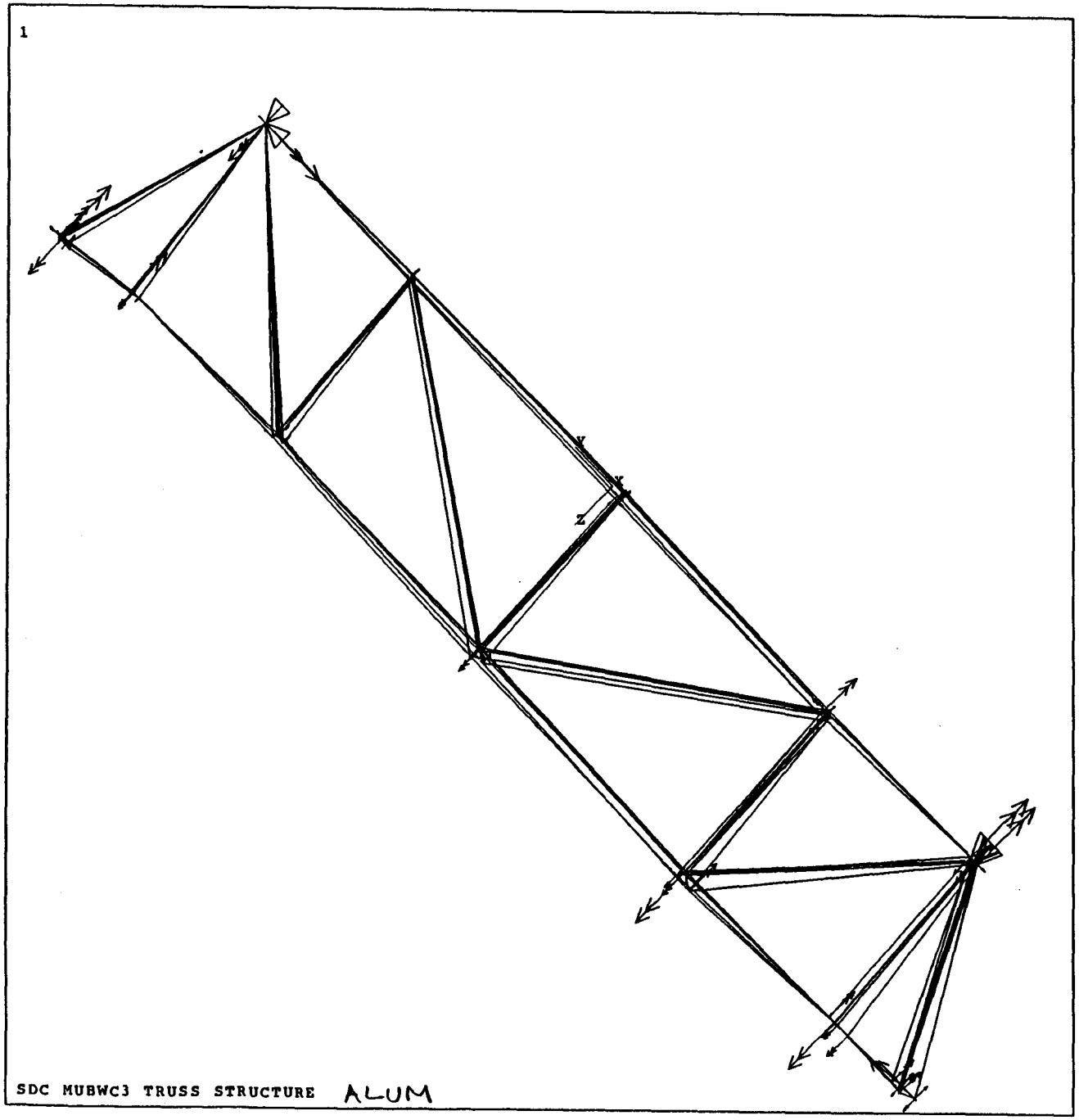

ANSYS 4.4A
MAY 29 1991
16:52:21
PLOT NO. 12
POST1 DISPL.
STEP=4
ITER=1
DMX =0.001027
TDIS
FORC
MOME

DSCA=389.993
XV =1
DIST=4.004
ZF =0.7875
ANGZ=45

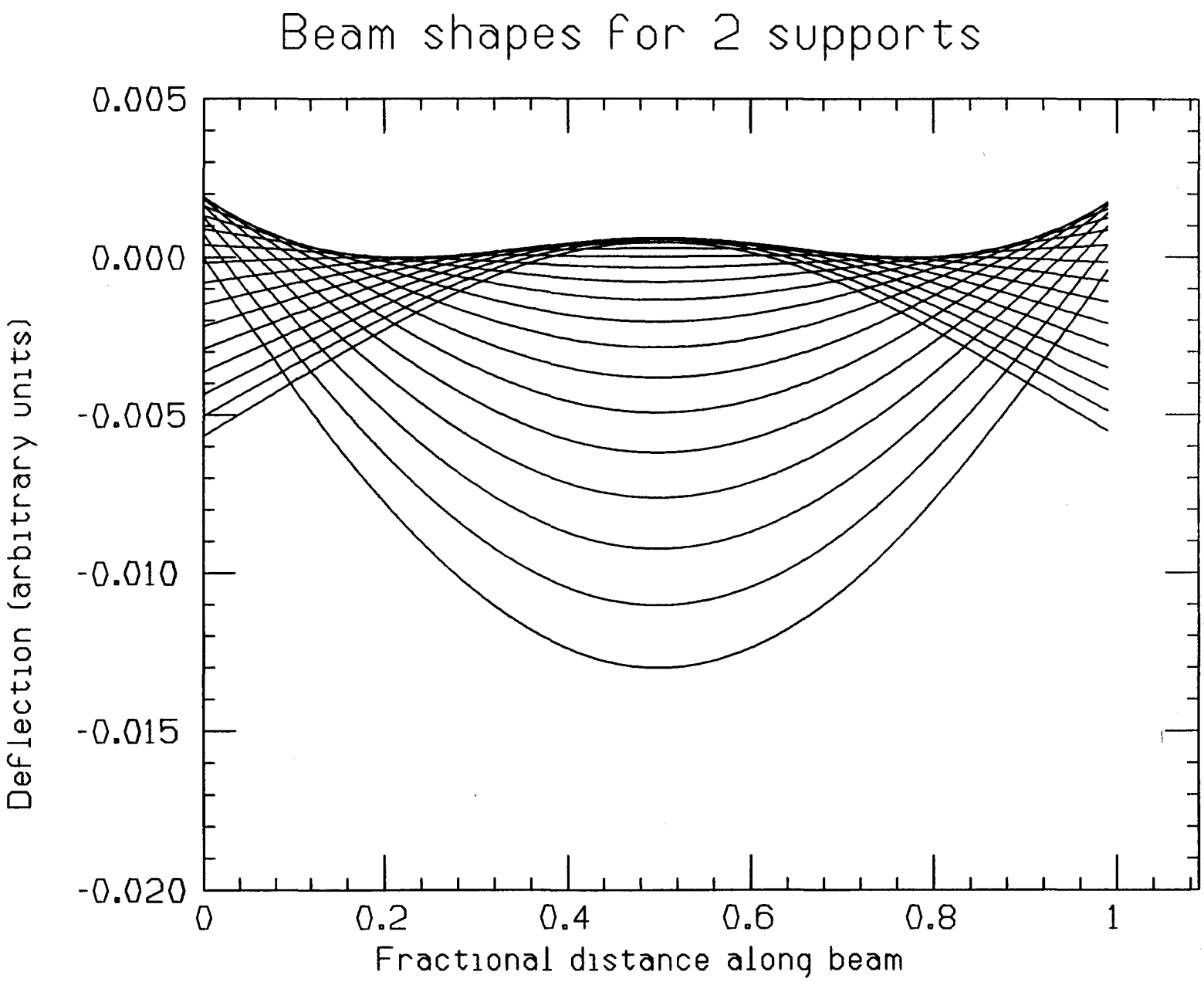
Beam shapes for 2 supports
0.005
0.000
-0.005
-0.010
-0.015
-0.020
Deflection (arbitrary units)
0
0.2
0.4
0.6
0.8
1
Fractional distance along beam

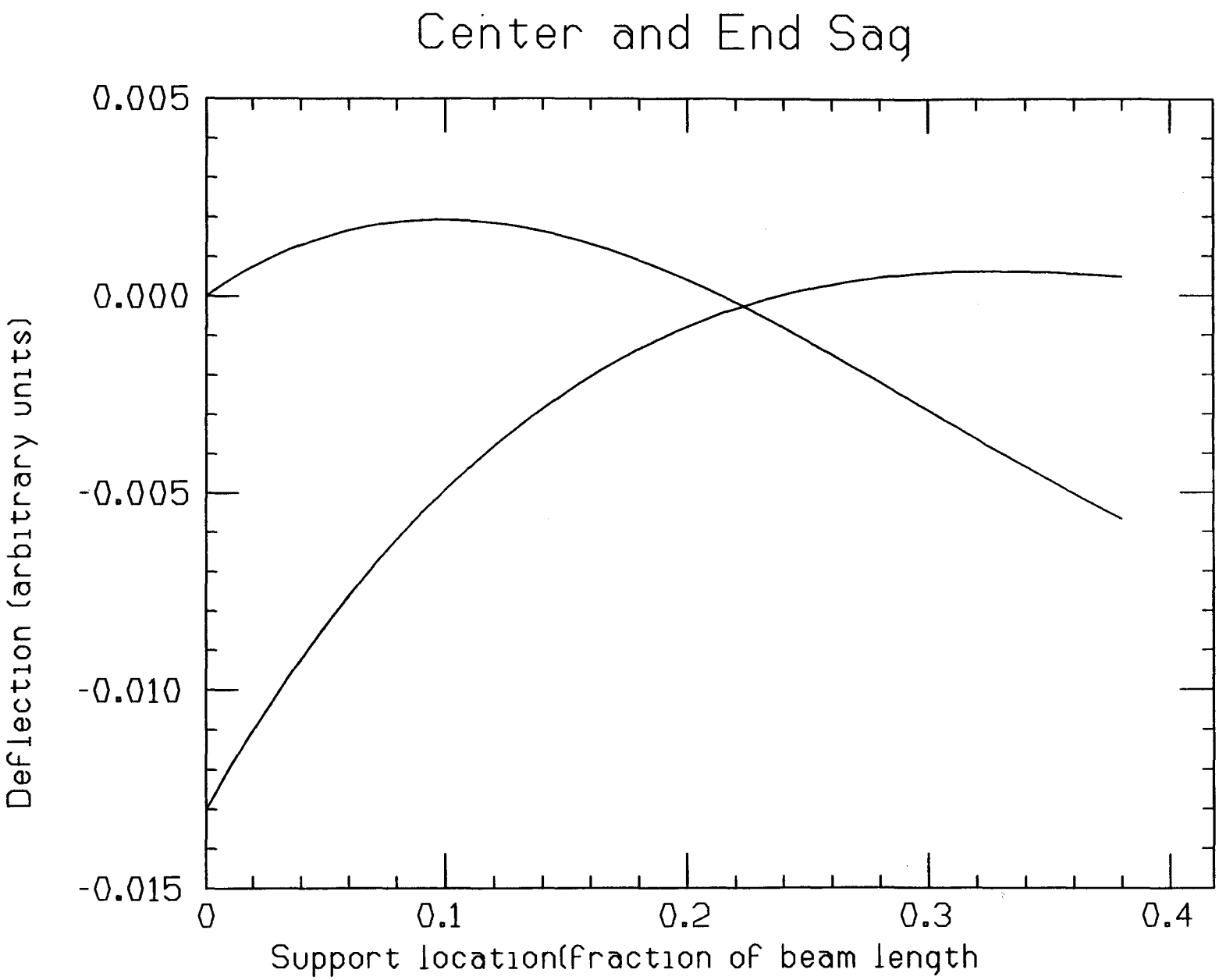
Center and End Sag
0.005
0.000
-0.005
-0.010
-0.015
Deflection (arbitrary units)
0
0.1
0.2
0.3
0.4
Support location(fraction of beam length

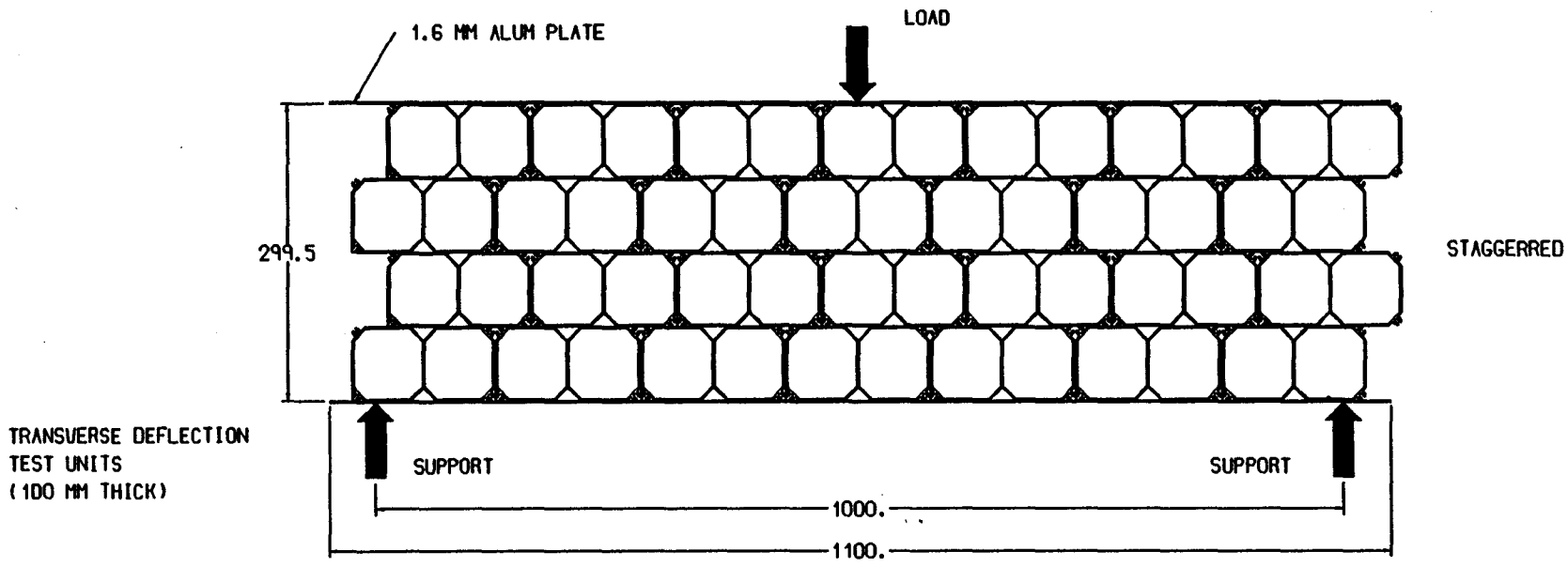

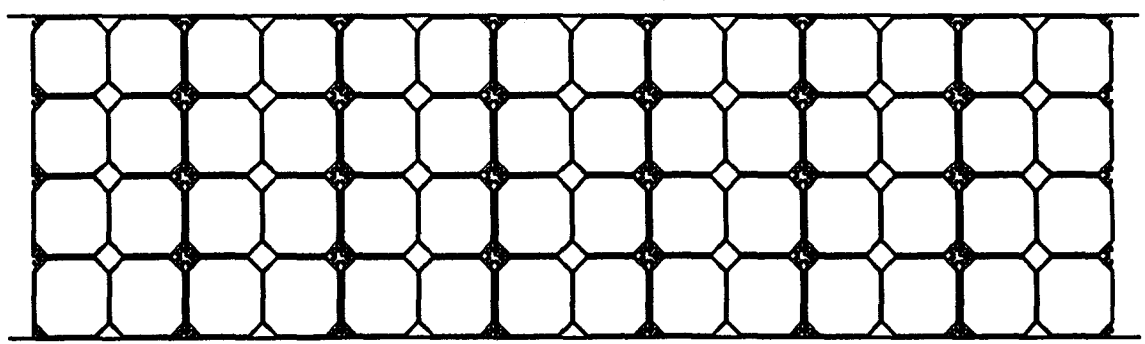

ALL DIMENSIONS ARE MM
11/26/91

'ODUCED BY FF
11/26/91 AT 14:55

DRAWING FILENAME DEFLECTION.DAT
PLOTTED AT SCALE 1/1

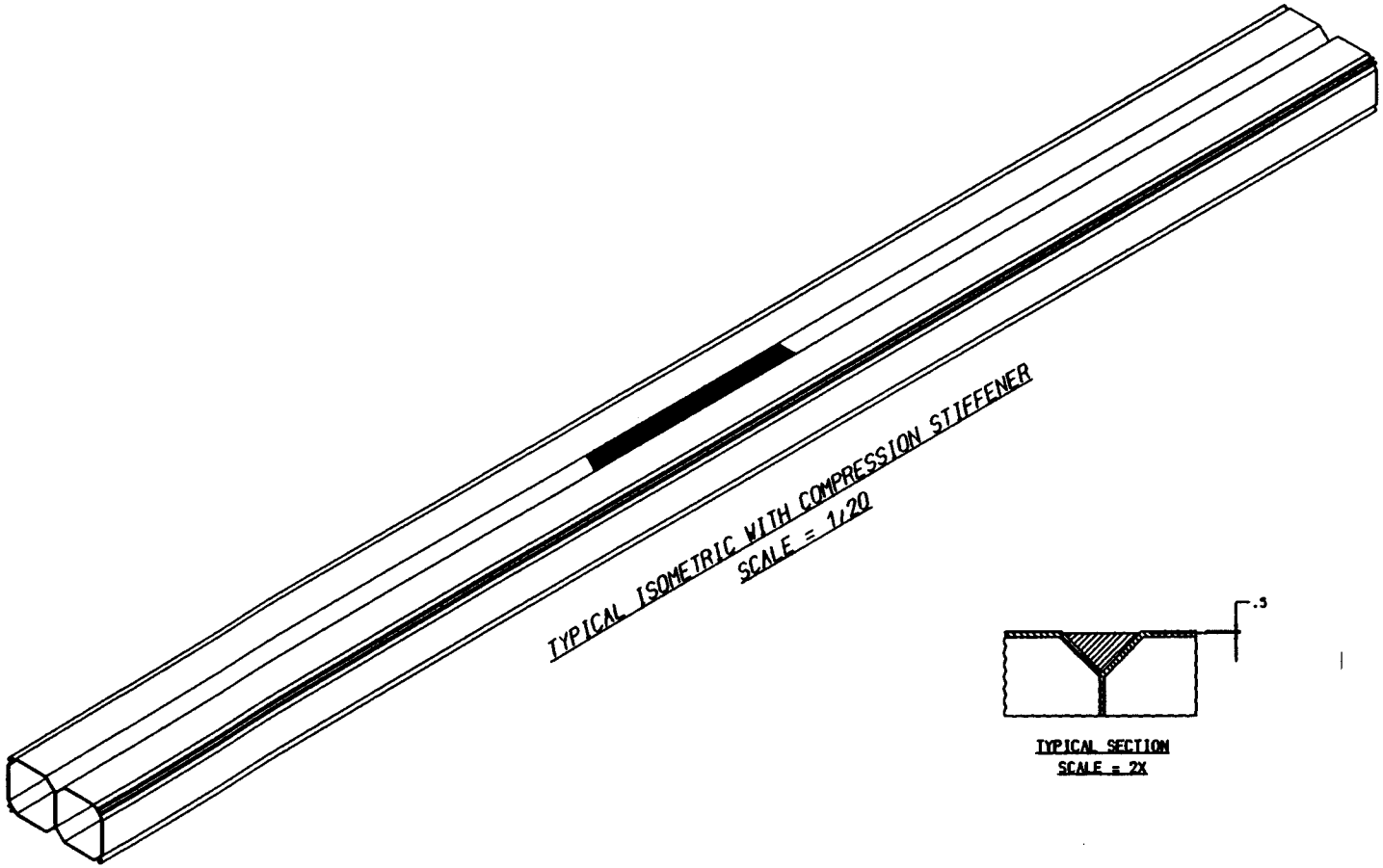

TYPICAL SECTION
SCALE = 2X

PHYSICAL SCIENCES LABORATORY

PRODUCED BY PIP DRAWING FILENAME SAT007E
ON 12 / 12 / 91 AT 12 : 48 PLOTTED AT SCALE 1/1

deflection = $\frac{d_A + d_B}{2}$

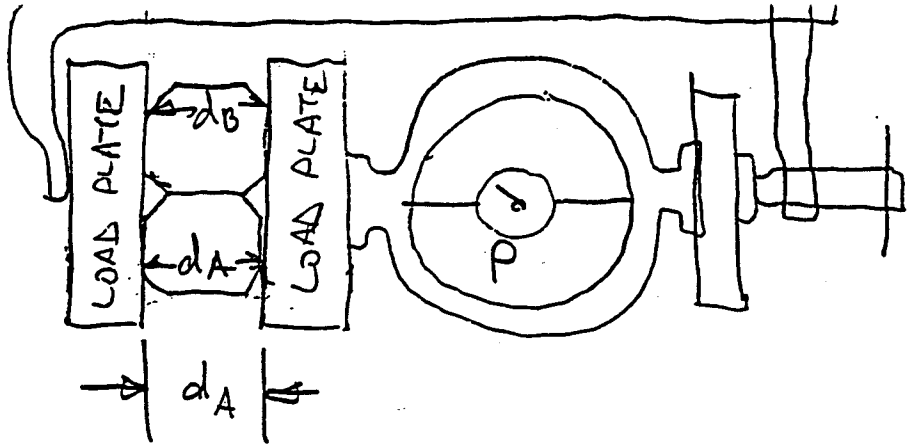

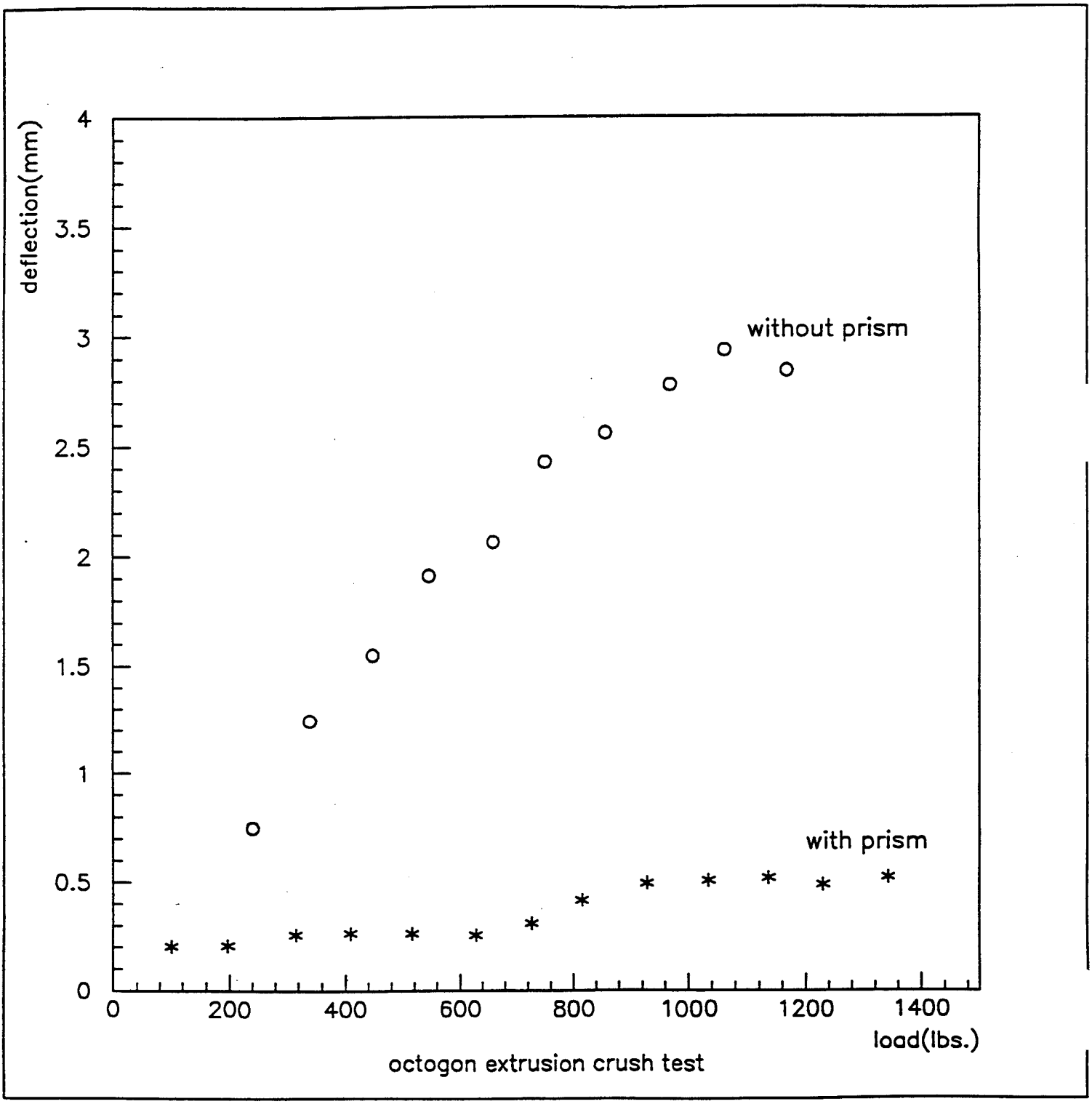

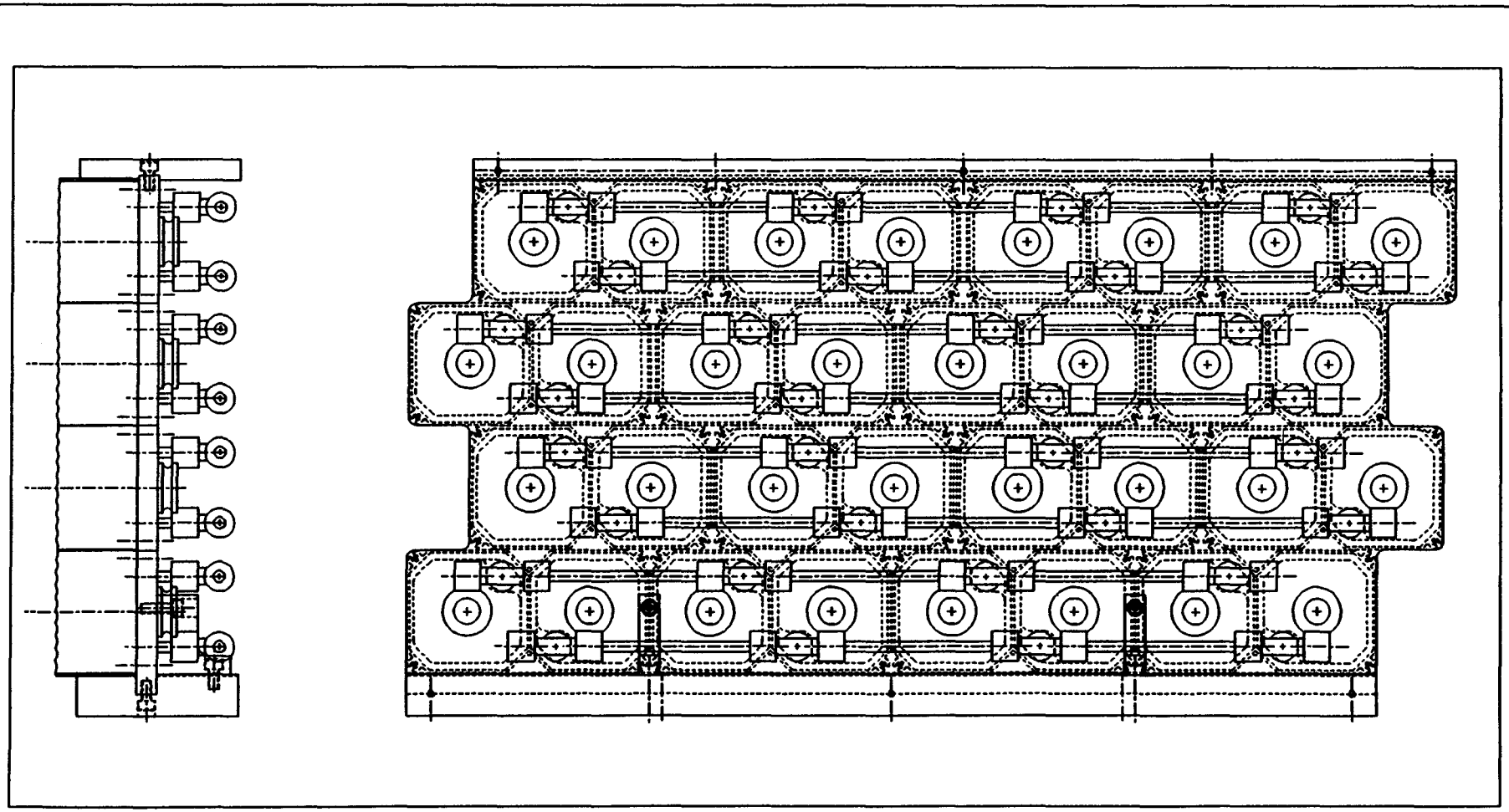

PRODUCED BY FF
ON 12 / 12 / 91 AT 12 : 26

DRAWING FILENAME R4626032E
PLOTTED AT SCALE 1/1

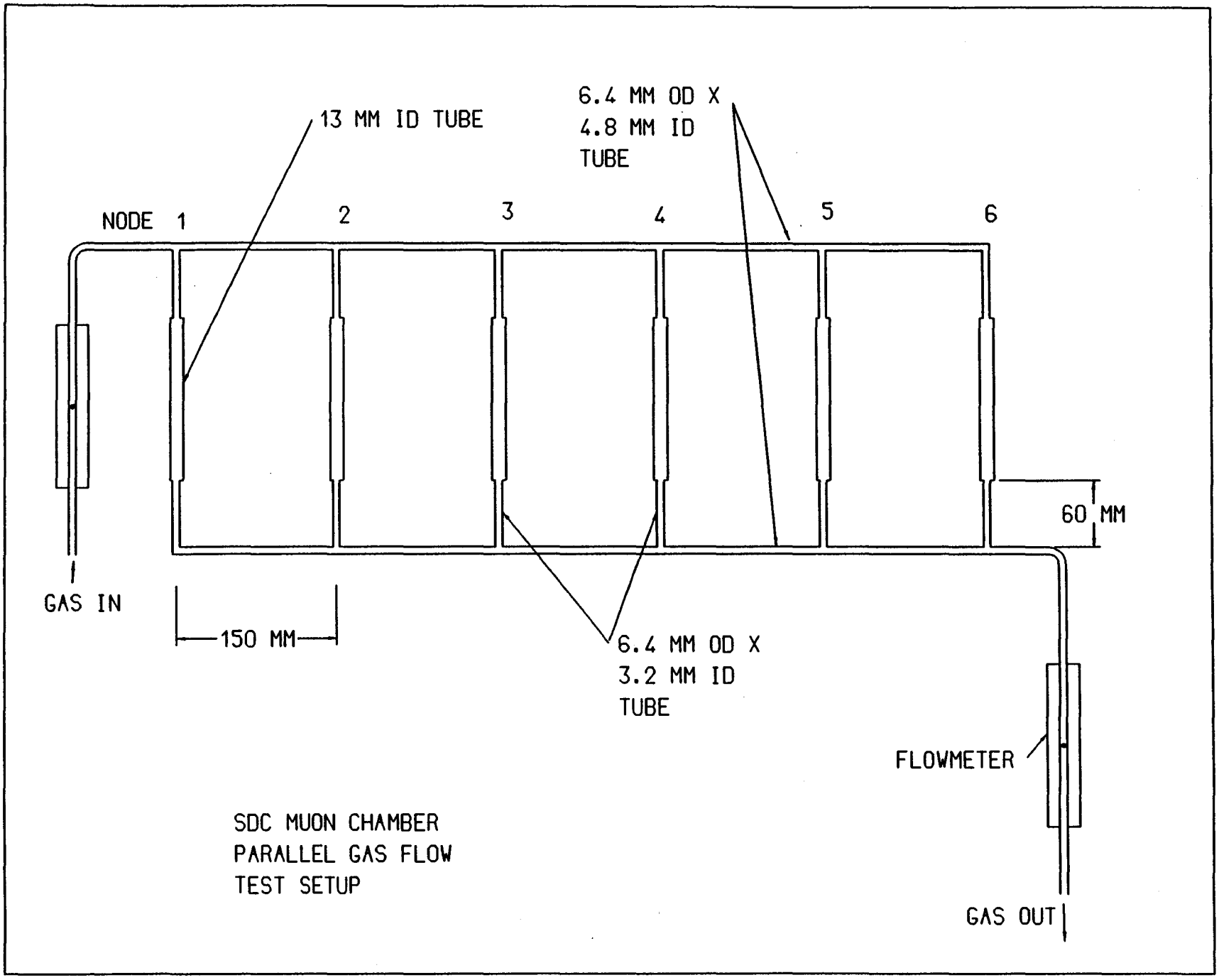

PRODUCED BY FF DRAWING FILENAME GAS.DAT
ON 11/21/91 AT 15:21 PLOTTED AT SCALE 1/1

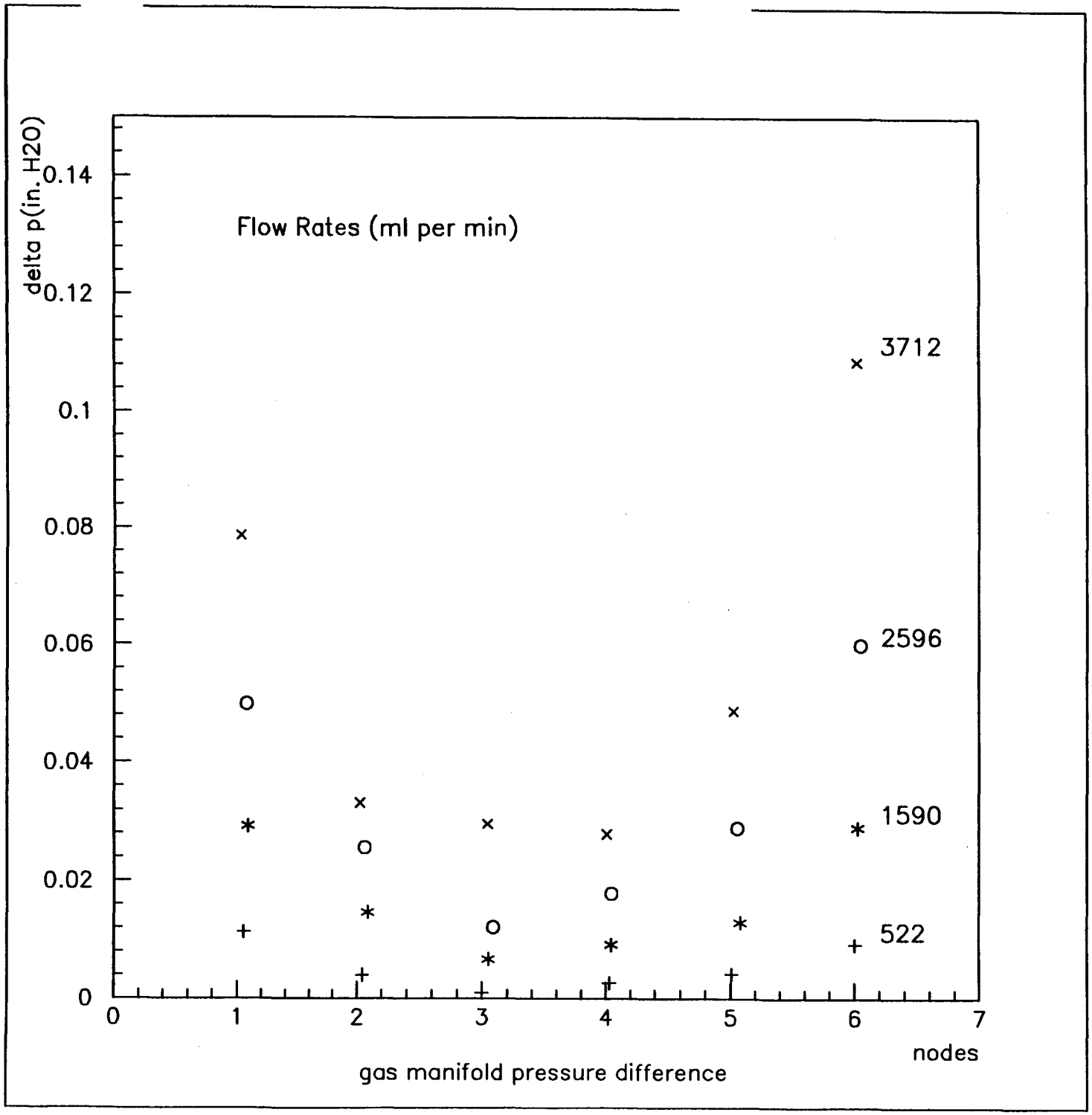
Flow Rates (ml per min)
delta p(in. H2O)
0.14
0.12
0.1
0.08
0.06
0.04
0.02
0
3712
2596
1590
522
0
1
2
3
4
5
6
7
nodes
gas manifold pressure difference

Chapter 5

Manufacturing Concepts

5.1 Overview

The philosophy of the manufacturing process is that as much as possible is purchased from industry and comes with well-defined tolerances. Since the number of parts will be large we can utilize (and afford) many automated cost-saving techniques requiring large capital investment, which are available in private industry. Thus building the muon system essentially involves specifying all the components and tolerances, assembling a set of parts and testing the final chambers.

The chambers will be built at a number of sites around the country, probably located at or near some of the universities and labs involved in the muon system. At these local sites the chamber structure will be constructed by gluing the extrusions together and mounting them on the endplates. In the sealed tube option, the extrusions are pre-strung. In the O-ring option, stringing is performed after assembly of the module. Once the wires have been checked the final assembly of gas and electrical manifolds will be done. The finished chamber will then undergo a series of tests for quality assurance.

The overall size of these chambers is roughly 2.5 meters by 7-9 meters. This is the largest size that can conveniently be transported by truck to the SSC site. The weight of these chambers varies from 1 ton to several tons depending on the size and number of layers. Each local site will need some storage space because we expect to ship "containers" which hold 6-8 chambers on each truck. There is likely to be a requirement that the chambers be shipped in a reasonable order so the SSC assembly goes rapidly.

The transportation to the SSC muon assembly building will be in climate-controlled trucks. While the exact specs are not yet available there is general agreement that the chambers should not be subjected to extremes of temperature (or shock) during the shipping process. We plan to use standard racks that can be easily loaded onto and off the truck. At the SSC site the chambers will be stored on the "narrow" footprint to maximize the storage space and to provide easy access to the ends for testing.

After the chambers are offloaded at SSC there will be some testing to ensure that no damage resulted from the shipping. These tests will probably not be as extensive as the testing at the local sites. The chambers will be assembled into monolith planes at one (or several) assembly stations in the muon assembly building. The assembled monoliths will be stored within the building, and

assembled into a supermodule by mounting them onto a truss. The inner muon supermodules BW1 do not mount on a truss and so the θ and ϕ planes will be attached and the kinematic supports mounted. The completed supermodule then moves to the alignment fixture for calibration.

5.2 Procurement

5.2.1 Aluminum extrusions

The aluminum extrusions will be fabricated in double cells. For the prototype the double cell resulted in a saving of 10% weight per cell and approximately $ 6.50 per 9m double extrusion (11%). The die cost for the double cell was $2700 vs. $1800 for the single cell.

The required tolerances are "half standard tolerances". Typically this means a tolerance of 0.5 mm on lengths and 0.25 mm on thicknesses. The bend must be less than 1/2° per meter with a maximum of 1 1/2o per extrusion. The extrusion lengths will be cut at the factory so no additional cutting or finishing is required at the local site. For the prototypes we specified a length tolerance of ±0.75 mm at 20o C. The lengths measured at Wisconsin were ± 2.0 mm, which is not satisfactory.

The surface finish of the extrusions is very important. Any oxide layer has the effect of insulating the chamber and decreasing the performance. Hence anodizing is clearly not acceptable. We had some prototype pieces put through an acid etch process and some allodyned. We were unable to measure any difference in the conductivity of the extrusions. Nonetheless, there is a feeling in the high energy community that allodyning is better. More work needs to be done in this area.

5.2.2 Plastics: endplugs, wire mounts, manifold plugs

The plastic endplugs for the prototype were machined from Delrin on a CNC machine. It is unlikely that volume production can give any cost reduction since we were dominated by the speed of the CNC machine. However, by injection molding we should be able to meet the necessary tolerances at a much cheaper price. Because the large startup costs, we have not used this process and have no prototype numbers. We plan to pursue this option.

Wire mounts were also machined from Delrin for the prototype. Injection molding looks appealing for production of these also. The gas manifold plugs were not needed for the prototype but will be needed to plug the ends of the endplate extrusion. These will also be injection molded and glued into place.

5.2.3 Endplates

The endplates for the prototype were machined from 1 2" aluminum at PSL on a Hermle CNC machine. Since the position of the machined holes determines the accuracy of wire placement, these locations are critical. The measured sigma of the deviations from design location was 13 microns. This result was at the limit of our ability to measure so it is possible that the plates are

even better. During the initial milling we discovered that the temperature of the plate during the machining is critical. If the piece heats up, the aluminum expands and the holes are mislocated. It is essential to maintain the temperature of the plate during machining within a few degrees.

For production we expect to extrude the aluminum endplates. The O-ring option stairstep endplate contains a void which we will use as the gas manifold. The inside hole will be sized to control the gas flow through the extrusions. Thus we need only provide plugs at the ends of the plates and a single feedthrough for each layer of each endplate. This decreases substantially the work necessary to distribute gas (feedthroughs, tubing, assembly) as well as decreasing the likelihood of leaks.

The endplate requires the following machining operations:

- 2 wire holes ($\sim$ 8 mm) per cell
- 4 screw holes (M5 clearance) per cell
- 8 threaded gas fitting holes per chamber
- 16 indentations (gas manifold plugs) per chamber
- 4 profiles (mating edges) per chamber
- threaded holes (??) as needed to secure the cover plates
- cleaning and deburring

Based on the prototype endplates we estimate the total for machining the endplates is 7.5 min/cell + 184 min/chamber.

5.2.4 Cover plates

Each chamber may be covered with a thin (1/16"??) aluminum plate as a secondary gas seal. These plates will be purchased precut from the manufacturer and attached to the endplates.

5.3 Chamber assembly

The chamber assembly will have a team of two people. The following operations will be performed:

- get extrusion from storage and glue endcaps (10 min/cell)
- place and clamp endplates into assembly station (60 min/chamber)
- insert O-ring, spread glue on extrusions, and mount on endplates (5 min/cell)
- move chamber to wiring station (30 min/chamber)
- install wires (6.5 min/cell)
- install manifold plugs (30 min/chamber)

- install gas manifold feedthroughs (30 min/chamber)
- install cover plates (30 min/chamber)
- install electronic termination and readout (?? min/chamber)

The estimated time to assemble one chamber is: 25/min per cell + 180 min per chamber. For a typical chamber 2.4 m wide there are 120 cells. The total time necessary to assemble such a chamber is 53 hours or 1.25 week for two people (106 man-hours).

5.4 Chamber Testing

Testing will be necessary at many stages to ensure quality control. At each chamber assembly site we need the following tests:

- structural size and rigidity
- wire tension and/or continuity
- gas leaks
- electrical continuity and noise suppression
- pulse test using source

5.5 Muon Assembly Building

The muon assembly building is planned to have 3000 m^2 of air- conditioned floor space. It will provide some room for storage of incoming chambers, assembly areas to build monolith planes and supermodules, an alignment fixture, and, possibly, storage for a few supermodules. There will be two cranes in the building, a 40-ton crane (hook height 12 m) for moving the completed supermodules, and a 10-ton crane (hook height 6 m) for moving individual chambers into and out of storage during the assembly process. Much of the building floor space is planned to be open so we have the flexibility to alter the usage patterns as our requirements change. An estimated volume of 12,000 cubic meter of forward, intermediate, and barrel muon chambers, trusses and counters is processed in this building.

Once the supermodules have been calibrated they will be moved to an adjacent temporary storage area which will be air-conditioned, but will not have a crane. The 40-ton supermodules will be moved using strato carriers (rubber-tired self-propelled gantry cranes). This temporary storage area is planned to have a capacity of 18 supermodules.

Since we must install 64 barrel and intermediate supermodules, our storage capacity will be only a small fraction of the total. In addition, we expect to provide some assembly and storage area for the forward chamber system. Hence we must plan to build and install supermodules using "just-in-time" techniques. As a result we will need relatively constant access to the assembly hall. A preliminary analysis of the assembly process within this building by Martin Marietta indicates

that the octagon tube design can complete all supermodule assembly within two years using two assembly areas. The current schedule for the muon assembly building shows the final design specifications are due in Jan. '92 and we get occupancy in Jan. '94.

5.6 Schedule

A full-size prototype supermodule will be designed and constructed Feb. '92 to Jan. '94. During '94 it will be tested and evaluated, and any necessary design changes will be made. The local sites will be setup during '94. Production begins in Jan. '95 and continues until Jan. '98. Assembly of supermodules begins Jan. '96 and ends Jan. '99. Hall installation begins Jan. '97 and ends Mar. '99. Since the intermediate planes will be the last to be installed, they will also be last in the production string.